CAPITAL UNIVERSITY OF SCIENCE AND
TECHNOLOGY, ISLAMABAD

Numerical Investigation of Flow-Induced Noise Reduction in TPMS-Based Silencers

by

Junaid Majeed

A thesis submitted in partial fulfillment for the
degree of Master of Science

in the

Faculty of Engineering
Department of Mechanical Engineering

2026

Copyright © 2026 by Junaid Majeed

All rights reserved. No part of this thesis may be reproduced, distributed, or transmitted in any form or by any means, including photocopying, recording, or other electronic or mechanical methods, by any information storage and retrieval system without the prior written permission of the author.

CERTIFICATE OF APPROVAL

Numerical Investigation of Flow-Induced Noise Reduction in TPMS-Based Silencers

by

Juniad Majeed

(MME233002)

THESIS EXAMINING COMMITTEE

S. No.	Examiner	Name	Organization
(a)	External Examiner	Dr. Naseem Ahmad	IST, Islamabad
(b)	Internal Examiner	Dr. M. Mahabat Khan	CUST, Islamabad

Dr. Shummaila Rasheed
Thesis Supervisor
May, 2026

Dr. M. Mahabat Khan
Head
Dept. of Mechanical Engineering
May, 2026

Dr. Imtiaz Ahmad Taj
Dean
Faculty of Engineering
May, 2026

Author's Declaration

I, **Junaid Majeed** hereby state that my MS thesis titled "**Numerical Investigation of Flow-Induced Noise Reduction in TPMS-Based Silencers**" is my own work and has not been submitted previously by me for taking any degree from Capital University of Science and Technology, Islamabad or anywhere else in the country/abroad.

At any time if my statement is found to be incorrect even after my graduation, the University has the right to withdraw my MS Degree.

(Junaid Majeed)

Registration No: MME233002

Plagiarism Undertaking

I solemnly declare that research work presented in this thesis titled "**Numerical Investigation of Flow-Induced Noise Reduction in TPMS-Based Silencers**" is solely my research work with no significant contribution from any other person. Small contribution/help wherever taken has been duly acknowledged and that complete thesis has been written by me.

I understand the zero tolerance policy of the HEC and Capital University of Science and Technology towards plagiarism. Therefore, I as an author of the above titled thesis declare that no portion of my thesis has been plagiarized and any material used as reference is properly referred/cited.

I undertake that if I am found guilty of any formal plagiarism in the above titled thesis even after award of MS Degree, the University reserves the right to withdraw/revoke my MS degree and that HEC and the University have the right to publish my name on the HEC/University website on which names of students are placed who submitted plagiarized work.

(Junaid Majeed)

Registration No: MME233002

Acknowledgement

All praise and gratitude are for **Allah Almighty**, whose countless blessings, mercy, and guidance gave me the strength, patience, and courage to complete this thesis. Without His will, nothing is possible. I also send heartfelt salutations and peace upon the beloved **Prophet Muhammad (PBUH)**, whose life and teachings are a source of light and inspiration for me.

I owe my deepest gratitude to my **family**, whose prayers, love, and encouragement have always been my greatest strength. In particular, my heartful gratitude to my Wife **Misbah Fatima** for her untiring support, constant motivation, and belief in me throughout this journey. Her care and sacrifices have truly been a foundation for my success.

I am deeply grateful to my esteemed supervisor, **Dr. Shummaila Rasheed**, whose outstanding mentorship and unwavering support have guided me at every stage of this research. Her thoughtful insights, valuable suggestions, and constant encouragement have not only strengthened the quality of this study but also enhanced my confidence throughout the entire process. Her dedication, patience, and commitment to my academic growth have been truly inspiring, and this work would not have been possible without her exceptional guidance.

I would also like to extend my sincere appreciation to my friends, **Muhammad Noman Shahid** and **Muhammad Usman Shahid**, for their invaluable technical assistance and academic support throughout the research. At every step during my project their collaborative spirit, reliability, and continuous encouragement brought a significant and positive impact. Lastly, I would like to acknowledge my Brother **Dr. Meraj Majeed** for his encouragement, meaningful discussions, and companionship during the course of this work. To all of you, I remain forever grateful.

(Junaid Majeed)

Abstract

The increasing demand for efficient noise control in industrial, automotive, and aerospace applications has led to the exploration of novel sound-absorbing materials. This thesis investigates the acoustic performance of porous silencers with geometries based on triply periodic minimal surfaces (TPMS), specifically focusing on Gyroid, Diamond, and Primitive structures. A comprehensive numerical study is conducted using the Ffowcs Williams–Hawkings (FW–H) acoustic model to assess both pneumatic and acoustic characteristics. The study aims to evaluate the influence of TPMS geometry on pressure drop, velocity distribution, turbulence generation, and sound attenuation across different frequency ranges.

The results indicate that the Gyroid structure provides the most efficient performance, achieving approximately 15–25% lower pressure drop compared to the Primitive structure while maintaining effective broadband noise attenuation. The Diamond structure demonstrates a balanced trade-off, with moderate pressure losses and consistent noise reduction across mid-frequency ranges (500–2000 Hz). In contrast, the Primitive structure shows strong attenuation in high-frequency ranges but results in higher pressure drops (up to 30% increase) and reduced efficiency at low frequencies (< 500 Hz).

Analysis of velocity and pressure contours reveals that smoother flow pathways in Gyroid structures reduce turbulence intensity, leading to improved acoustic performance. Additionally, Sound Pressure Level (SPL) analysis shows a reduction of up to 10–15 dB in mid-to-high frequency ranges for optimized TPMS configurations. The study also highlights the influence of receiver placement, with variations of up to 5 dB observed depending on measurement location.

Keywords: TPMS structures, Flow-induced noise, Acoustic attenuation, Ffowcs Williams–Hawkings (FW-H), Pneumatic silencers, Sound Pressure Level (SPL)

Contents

List of Figures

List of Tables

Abbreviations

3D	Three Dimensional
AC	Acoustic
ACA	Acoustic Absorbing
AM	Additive Manufacturing
ASTM	American Society for Testing and Materials
BCC	Body-Centered Cubic
CFD	Computational Fluid Dynamics
DLP	Direct Laser Printing
DMLS	Direct Metal Laser Sintering
HVAC	Heating, Ventilation, and Air Conditioning
IIoT	Industrial Internet of Things
ISO	International Organization for Standardization
NIOSH	National Institute for Occupational Safety and Health
OSHA	Occupational Safety and Health Administration
Pa	Pascal
RANS	Reynolds-Averaged Navier–Stokes
SLA	Stereolithography
SLS	Selective Laser Sintering
TPMS	Triply Periodic Minimal Surface

Symbols

μ	Dynamic viscosity	kg/(m·s)
ρ	Fluid density	kg/m^3
$\mathbf{u}$	Fluid velocity	m/s
Δp	Pressure drop	Pa
$\rho\mathbf{u}'\mathbf{u}'$	Reynolds stresses	–
L	Characteristic length / model length	m
Re	Reynolds number	–
R	Specific gas constant	J/(kg·K)
T	Absolute temperature	K

Chapter 1

Introduction

1.1 Background

Compressed air systems are widely utilized in industrial manufacturing environments for operating machines and tools. However, pneumatic devices inherently generate substantial noise due to the release of high-pressure air through exhaust ports [1]. Additional noise can also result from air leaks in the system [2]. Apart from mechanical sounds, especially from percussive devices, the main source of unwanted acoustic emissions is pneumatic noise caused by turbulent air flow in the working elements. When pressurized air (typically 6–8 bar) is rapidly discharged to atmospheric conditions, transient pneumatic noise is produced [3], which may appear either as intermittent or impulsive bursts depending on their duration [4].

This pneumatic noise originates from transient choked air flow with significant pressure differentials, leading to the formation of shock waves at the junction between the source and the exhaust tube [3, 5]. The exhaust process generally consists of sonic and subsonic regions, separated by a critical pressure ratio. During the sonic phase, the flow produces intense roaring noise due to high pressure and flow rates [5]. According to Lighthill's theory, pneumatic noise results from monopole, dipole, and quadrupole acoustic sources corresponding to mass flow variations, boundary interactions, and turbulence, respectively [6, 7] the resulting

impulse noise often reaches sound levels of 96–120 dBA [8, 9], and may even approach 130 dBA [10].

European Directive 2003/10/EC limits noise exposure in an 8-hour working period to 85 dB, with 80 dB serving as a warning threshold [11]. Prolonged exposure above these levels can cause serious health issues, including hearing damage, fatigue, concentration difficulties, and cardiovascular strain. Each 1 dB increase beyond the threshold can reduce safe working time by approximately 100 minutes [12]. For instance, exposure to 90 dB noise should not exceed 2.5 hours.

Given the health risks and operational inefficiencies caused by high noise levels, effective noise reduction strategies are essential in pneumatic industries. Noise mitigation methods are typically classified as passive or active [13–15] , with the most common approach being the use of mufflers. There are four main categories of mufflers: expansion chambers, sintered bronze silencers, porous-diffusion types, and perforated panel silencers [16]. Daggerhart and Berger [17] observed that commercial silencers could reduce muzzle noise to 85–95 dB, with porous plastic mufflers achieving reductions from 120 to 90 dBA at 8bar. Zhao et al. [10] used expansion-chamber mufflers with sound-absorbing fiber and valve control, reducing noise from 115 to 82 dB, although at the cost of a longer exhaust process. Similarly, Li et al. [5] applied Ergun's equation to model porous bronze silencers, achieving noise reductions of about 15 dBA in the 1–10 kHz range. Other designs, such as perforated mufflers, reduced intermittent noise to below 85 dBA [16].

Alternative approaches include optimizing nozzle geometry, which Ivanov [9] demonstrated could lower noise to 82 dBA, and controlling valve openings to regulate pressure variation, as proposed by Li and Zhao [3], who achieved reductions of 2–4 dBA on average and up to 11 dB for peak noise. Nevertheless, these solutions generally fail to reduce overall noise below 80 dB and often overlook the distributed nature of pneumatic noise sources in industrial plants.

Silencers are devices used to reduce noise by either dissipating or reflecting sound energy while allowing fluid flow. Conventional silencers are often made of perforated tubes and fibrous materials. However, these designs can have limitations such as

clogging, limited design flexibility, or poor balance between noise reduction and flow performance. Recent advancements in additive manufacturing and computational design have enabled the development of porous silencers based on Triply periodic minimal surface geometries. These structures, such as Gyroid, Diamond, and Primitive types, provide high surface area, structural integrity, and controllable porosity. Such features make them promising candidates for acoustic attenuation with controlled pressure drop.

1.2 Exposure Limits and Occupational Standards

Occupational exposure standards set guidance for permitted noise levels and durations at the workplace. Two commonly referenced authorities are NIOSH (US Centers for Disease Control and Prevention — National Institute for Occupational Safety and Health) and OSHA (Occupational Safety and Health Administration) [18].

i. NIOSH Recommended Exposure Limit (REL): 85 dB(A) as an 8-hour time-weighted average (TWA). NIOSH uses a 3 dB exchange rate, meaning that with every 3 dB increase the allowed exposure time halves. For example, at 88 dB the recommended exposure time is approximately 4 hours.

ii. OSHA Permissible Exposure Limit (PEL): 90 dB(A) as an 8-hour TWA (with a 5 dB exchange rate historically used in enforcement examples and calculations). OSHA sets regulatory requirements including hearing conservation programs when levels exceed specified action levels. The precise application and enforcement of these standards is covered in OSHA documents.

In many industrial settings (compressors, pneumatic tools, blowers), equipment can emit sound levels above these limits. Installing effective silencers reduces worker exposure, reduces the need for costly PPE programs, and helps meet regulatory compliance.

1.3 Acoustics

1.3.1 Sound Level Measurement

In measuring sound levels, instruments are used which resemble the human ear in sensitivity to noise composed of varying frequencies [19]. The instruments measure the "A-weighted sound level" in units called dB (A) [20]. Workplace noise measurements indicated the combined sound levels of tool noise from a number of sources (machinery and materials handling) and background noise. Typical sound level shown in Fig 1.1.

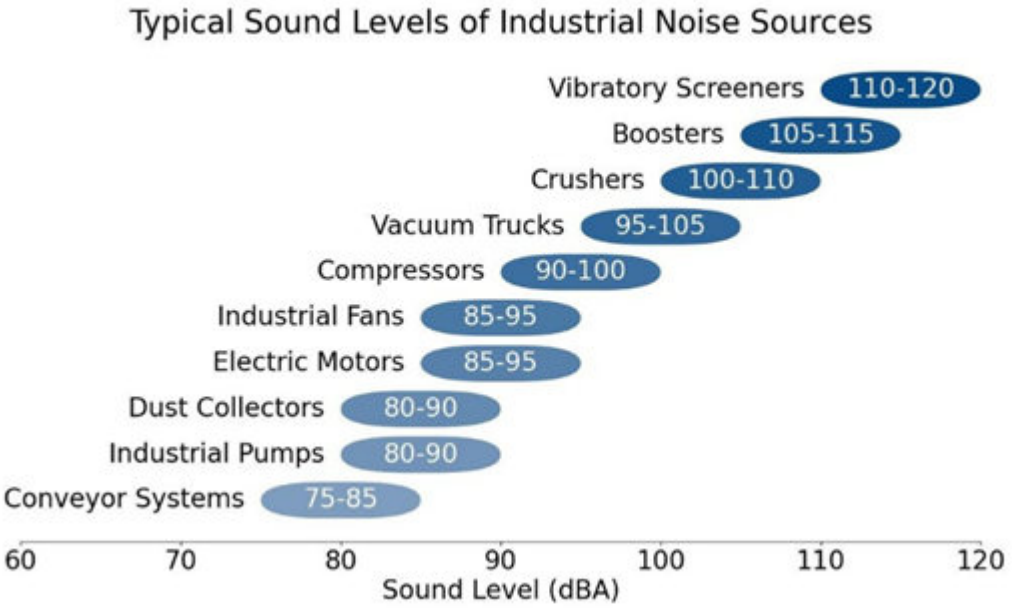

FIGURE 1.1: Typical Sound Levels of Industrial Noise Source [21]

1.3.2 Decibel Scales

i. **A scale:** It is used for industrial noise measurement. It measures middle and higher frequencies of the audible range which can easily be heard by human ear. Therefore, in order for the sound level meter to mimic the response of the human ear, an A-weighting filter is incorporated in the meter. The A-weighting filter de-emphasizes the low frequencies produced.

ii. **B scale:** It is used for middle range between 55 and 85dB.

iii. **C scale:** C-weighting filter influences only the highest and lowest frequencies and provides an almost flat response. Peak noise levels are measured using the C-weighting filter and expressed as dB(C).

1.4 Economic Impact of Occupational Hearing Loss in Industrial Workers

Occupational noise-induced hearing loss (NIHL) remains one of the most common work-related health conditions globally, particularly affecting industrial laborers exposed to high levels of noise over extended periods. According to the U.S. Bureau of Labor Statistics, approximately 14,500 hearing loss cases were reported in private industry in 2019 as shown in figure 1.2, with the majority (about 75.9%) occurring in the manufacturing sector, highlighting the significant prevalence of NIHL among industrial workers. More broadly, exposure to hazardous occupational noise affects an estimated 30 million workers in the United States, with approximately 22 million exposed to noise levels exceeding recommended safety limits ($\geq$ 85 dBA), which are sufficient to cause irreversible hearing damage over time [22].

Number of Hearing Loss Illness cases in selected manufacturing Private Industries are shown in figure 1.3. In the United States, workers' compensation claims for occupational hearing loss disability amount to an estimated $242 million annually, based on disability settlements recorded by national compensation systems. Additional evidence indicates that average annual workers' compensation costs specifically associated with occupational hearing loss claims range between $49 million and $67 million, according to multi-state analyses of the U.S. workforce.

Overall, occupational hearing loss among industrial workers is both highly prevalent and economically burdensome. Direct annual costs from workers' compensation claims alone can reach hundreds of millions of dollars, while broader societal costs accounting for lost productivity, healthcare expenditures, and reduced quality of

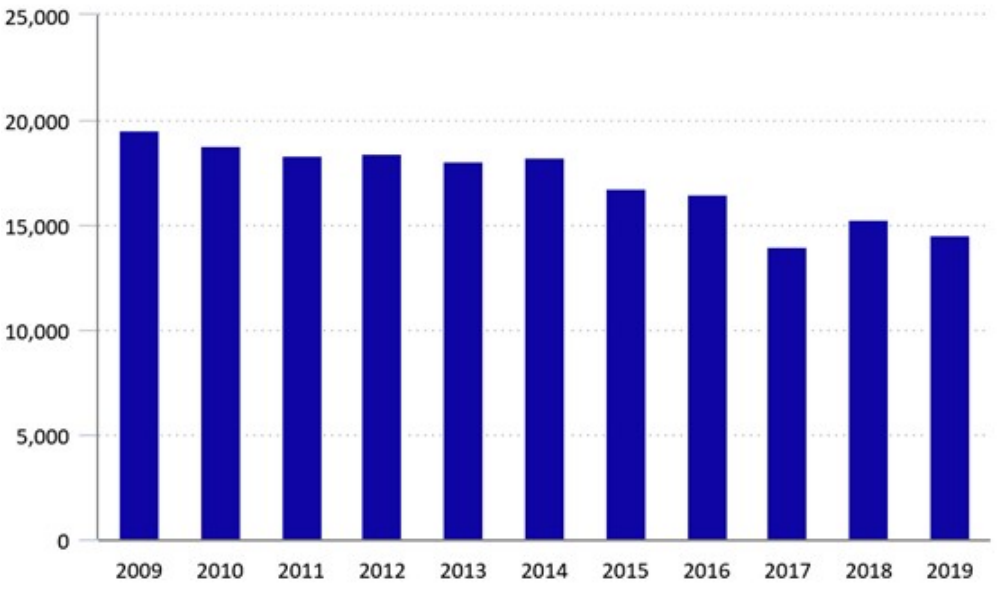

FIGURE 1.2: Number of Hearing Loss Illness Cases in Private Industry, 2009-19

life, extend into the hundreds of billions of dollars globally. These figures underscore the critical importance of effective noise control strategies and hearing protection interventions in industrial environments to reduce both the incidence and economic impact of noise-induced hearing loss (NIHL).

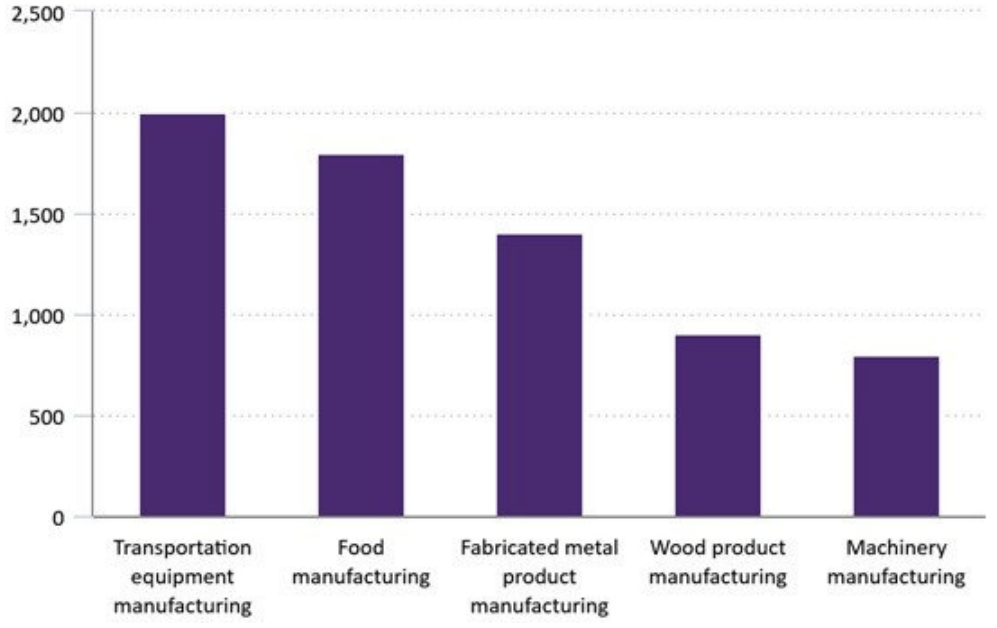

FIGURE 1.3: Number of Hearing Loss Illness cases in selected Manufacturing Private Industries

1.5 Pneumatic Systems in Industries

Pneumatic systems are widely used in industrial settings due to their efficiency, reliability, and safety in transferring and controlling energy through compressed air or gases, line Diagram of basic industrial Pneumatic System is shown in Figure 1.4. The fundamental principle behind pneumatic systems is the conversion of compressed air pressure into mechanical motion, which drives actuators, valves, and other components to perform various industrial tasks such as clamping, lifting, and automation of manufacturing processes. The simplicity of pneumatic systems, combined with their ability to operate in hazardous or explosive environments where electrical systems might pose risks, makes them a preferred choice in many industries. Typical industrial applications of pneumatic systems include automation and robotics, where pneumatic cylinders and valves are integral to welding, assembly, and packaging operations. They also play a crucial role in material handling, particularly in pneumatic conveying systems used to transport bulk materials such as powders, grains, biomass, and industrial dust particles. Optimizing these pneumatic conveying systems for pressure regulation and flow control has been a focus area, as it directly affects energy efficiency and operational costs. Pneumatic systems are also extensively employed in manufacturing processes like machining and stamping, where precise control of actuators ensures accuracy and repeatability [23].

Recent research and industrial developments on pneumatic systems revolve around enhancing energy efficiency and system intelligence. Studies highlight that pneumatic systems traditionally suffer from low energy utilization, with considerable wastage of compressed air. Advances now focus on optimizing pressure regulation to reduce energy consumption by up to 40%-75%, which not only lowers operating costs but also reduces greenhouse gas emissions, especially in regions dependent on thermal power. Alongside energy savings, condition monitoring using artificial intelligence techniques such as neural networks is gaining traction for predictive maintenance, fault detection, and improved system reliability, limiting downtime and enhancing safety [25]. Further technological progress includes innovations in pneumatic components like pilot valves and actuator designs aimed at improving

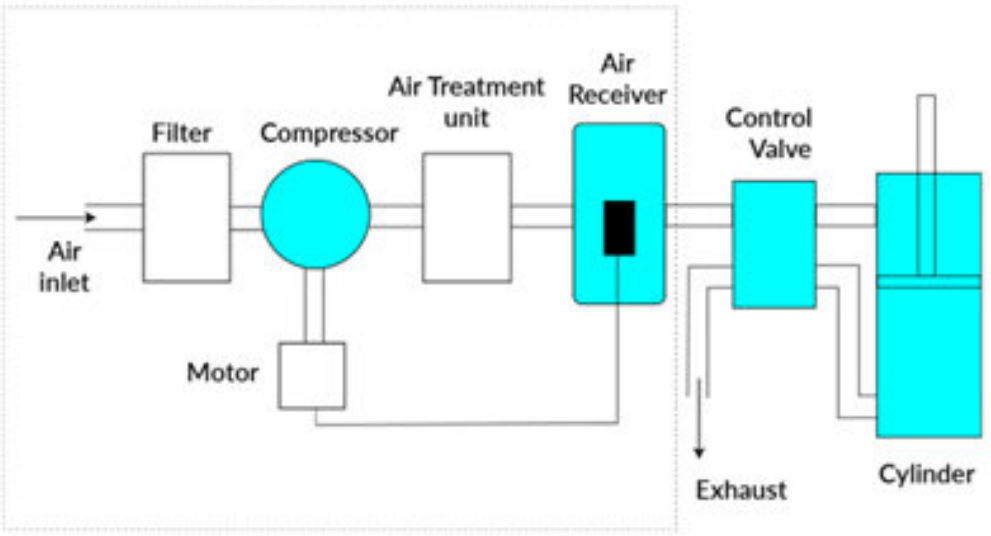

FIGURE 1.4: Diagram of an industrial pneumatic system [24]

flow characteristics, reducing noise, and enhancing durability. Soft pneumatic actuators and novel pumping mechanisms demonstrate increased operational frequencies, noise reduction, and improved pressure modulation, widening the applications of pneumatics in human-centered and robotic systems. The integration of AI and Industrial Internet of Things (IIoT) frameworks is also emerging, enabling real-time monitoring, advanced control algorithms, and smart diagnostics that align with Industry 4.0 trends [26]. In summary, pneumatic systems remain a critical technology in modern industry, valued for their robustness, safety, and adaptability. Current and future research is focused on making these systems more energy-efficient, intelligent, and environmentally sustainable, leveraging advances in AI and sensor technologies to meet the demands of increasingly automated and interconnected industrial environments.

1.6 Compressors

Compressors are mechanical devices that increase the pressure of a gas by reducing its volume, and they play a vital role in various industrial applications ranging from manufacturing to HVAC systems, oil and gas, power generation, and refrigeration.

Main Types of compressors used in industries are shown in Figure 1.5. The fundamental principle of a compressor is based on thermodynamics, where mechanical energy is converted into pneumatic energy by compressing air or gas, thereby increasing its pressure and kinetic energy. Compressors are commonly classified based on their working mechanism into two main categories: positive displacement compressors and dynamic compressors. Positive displacement compressors include reciprocating and rotary types, while dynamic compressors include centrifugal and axial flow types [27].

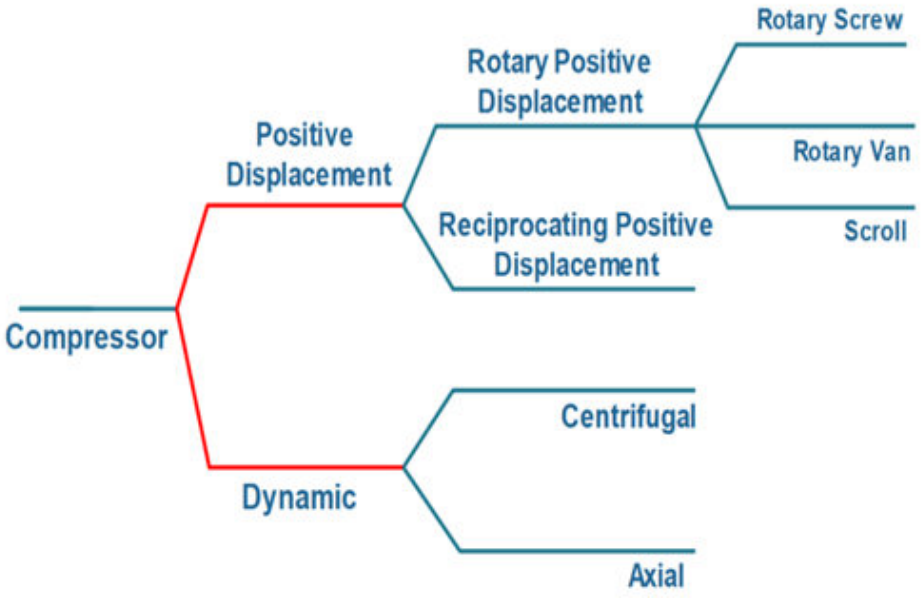

FIGURE 1.5: Types of Compressors [28]

Positive displacement compressors function by trapping a fixed volume of air or gas and reducing its volume through mechanical movement. Reciprocating compressors, which are one of the oldest and most widely used types, use pistons driven by a crankshaft to deliver gases at high pressure. Generally these are the loudest type, often exceeding 85 dB(A), which requires hearing protection. They generate high noise and vibration. These compressors are typically used in applications requiring high pressure and relatively low flow rates. Rotary compressors, on the other hand, such as screw and vane compressors, are more suitable for continuous-duty industrial operations due to their smoother flow, lower vibration, and quieter operation [29]. Screw compressors use two helical rotors to compress gas, offering

high efficiency and durability in oil and gas processing, manufacturing, and large-scale pneumatic systems. Screw compressors Known for "low noise" operation compared to pistons, with many models featuring sound-dampening enclosures.

Dynamic compressors differ from positive displacement types in that they use rotating impellers to impart velocity to the gas, which is then converted into pressure. Centrifugal compressors are widely used in industries requiring large volumes of gas at moderate pressures, such as chemical plants, refineries, and air separation units. These compressors are known for their compact design, high reliability, and ability to handle large flow capacities with minimal maintenance. Centrifugal Compressors Often quieter overall than positive displacement types but produce high-pitched noise. Axial compressors, while more common in jet engines and gas turbines, offer extremely high flow rates and are optimized for aerospace and power generation applications.

The selection of a compressor depends on various factors such as required pressure, flow rate, gas type, application environment, energy efficiency, and cost. Energy efficiency is a critical consideration in modern compressor systems, as compressors can account for up to 10% of a manufacturing facility's total energy consumption. The data for compressors are presented in the figure 1.6 in the form of normalized octave band SPLs at a distance of 0.9 m. According to a study published in the International Journal of Energy Research, the implementation of variable speed drives (VSDs), proper maintenance, and leak detection can improve compressor energy efficiency by 20% to 30%. Additionally, heat recovery systems can capture waste heat generated during compression and repurpose it for space heating or preheating feedwater, further enhancing energy savings.

In terms of environmental considerations, compressors that handle hazardous gases must comply with strict safety and emission standards. Oil-free compressors are often used in sensitive environments such as food and pharmaceutical industries to avoid contamination. Noise and vibration control is another important factor, especially in urban or indoor applications. Advanced compressor technologies now incorporate digital controls, sensors, and IoT-enabled monitoring systems to optimize performance, predict failures, and reduce downtime.

Octave frequency band (Hz)	Sound pressure level (dB) Air compressor power (kW)		
	0.75-1.5	2-6	7-50
31	82	87	92
63	81	84	87
125	81	84	87
250	80	83	86
500	83	86	89
1000	86	89	92
2000	86	89	92
4000	84	87	90
8000	81	84	87
Overall	93	96	99
A-weighted	91	94	97

FIGURE 1.6: The standard sound pressure levels in dB at (0.9-m) distance for air compressors [30]

The global compressor market continues to evolve with technological advancements aimed at increasing energy efficiency, reducing emissions, and improving automation. Innovations such as magnetic bearing centrifugal compressors, oil-free scroll compressors, and high-efficiency screw compressors are becoming increasingly prevalent. These developments align with the growing demand for sustainable industrial solutions and regulatory pressures to minimize environmental impact. Research and development in materials, pneumatics, and thermal management are also contributing to the next generation of high-performance compressors.

1.7 Pneumatic Silencers and Mufflers

The Branches classification tree of Silencers is shown in figure 1.7. Pneumatic silencers are specialized devices used to attenuate the noise generated when compressed air or other gases are vented from pneumatic systems. When air at elevated pressure is released through exhaust ports, valves or actuators, the rapid expansion

and turbulent flow create impulse and broadband noise sources. For example, it is noted that "the sudden exhaust process of the air expanding from the typical gauge pressure of 6–8 bar to the level of atmospheric pressure generates transient pneumatic noise" in pneumatic tools and machines [31]. To protect worker hearing, meet industrial noise limits, and improve operational comfort, such silencing is often essential in pneumatic power systems.

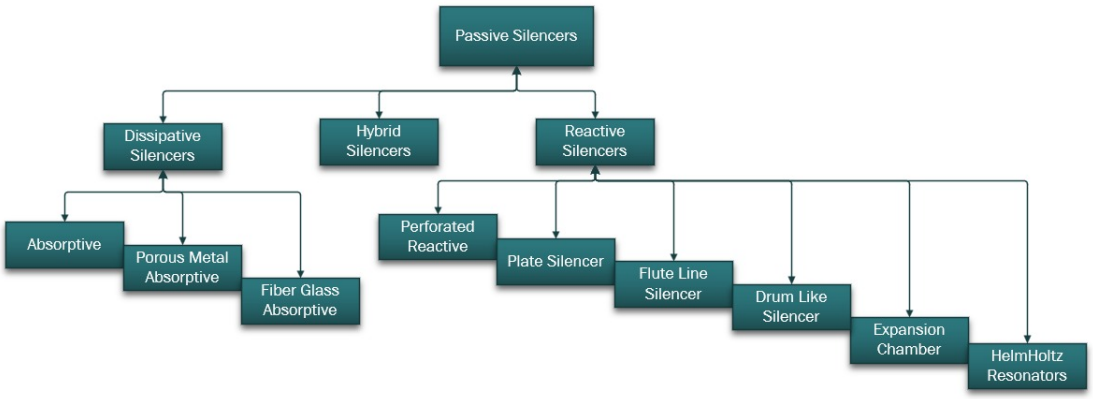

FIGURE 1.7: Classification Tree of Silencer

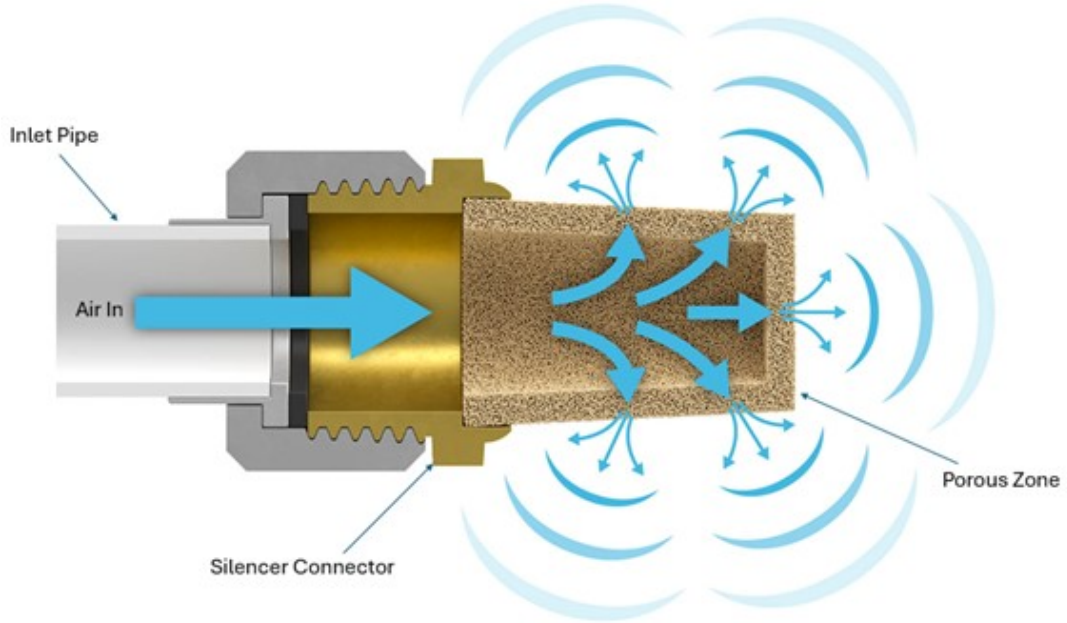

FIGURE 1.8: Pneumatic Silencer [32]

A Pneumatic silencer consist at a porous area, connector and a inlet pipe as shown in Figure 1.8. Common core components include porous or sintered materials (e.g., sintered bronze, sintered plastic, porous polyethylene) that act to dissipate acoustic

energy by breaking high velocity jets into smaller flows, reducing turbulence and thus sound generation. The device may also include expansion chambers and tube elements designed to reduce pressure drop and attenuate specific frequency bands. For instance, a study described three kinds of muffler types using metal sintered porous inlet plus expansion cones and spiral tubes, showing that the combined configuration (porous + expansion) achieved superior acoustic transmission loss [33].

Material selection and geometry are key. Porous plastic silencers such as those made by POREX® using porous polyethylene, are designed to balance noise reduction with acceptable back pressure while offering advantages of low weight, corrosion resistance and cost efficiency. Sintered metal silencers (bronze, stainless steel) offer higher durability, higher temperature/pressure tolerance and often serve in demanding industrial environments. For example, one manufacturer advertises sintered bronze silencers that "reduce noise by more than 15dB, and are installed on exhaust ports of pneumatic tools" with pore sizes, material options and pressure ratings tailored to the application. According to a product datasheet for porous plastic silencers, sound pressure levels for some models at 6bar/1m distance reached 81-84 dBA depending on size.

Functionally, the silencer accomplishes two primary goals: (1) sudden deceleration and turbulence of the exiting air, thereby lowering noise, and (2) to filter or diffuse the exhaust air, reducing contaminants and controlling flow behavior. For instance, a blog on industrial efficiency states: "A pneumatic silencer reduces the noise generated by compressed air or gas exiting pneumatic systems. Besides noise reduction, these silencers also filter contaminants from the exhaust air, ensuring compliance with environmental standards". The filtration function is especially important when the exhaust passes into sensitive environments or when system cleanliness is a concern.

From a performance standpoint, studies have shown significant noise reduction when using well designed silencers. One experimental analysis found that when a "biomimetic silencer" (with polyurethane foam and slit structures mimicking shark gills) was applied to a pneumatic device exhaust, more than 10% improvement

in noise reduction compared with a general pneumatic silencer was achieved [34]. Another study showed using an expanded collecting system (rather than a simple muffler) reduced sound pressure level (SPL) of a pneumatic screwdriver from 87dB(A) to 80dB(A) in a production setting[33]. These results highlight that silencer design (porosity, flow path, expansion volume) can have measurable impact on workplace noise levels.

However, there are design trade offs and challenges. One of the main considerations is back pressure: adding a silencer introduces resistance to flow which can affect pneumatic actuator performance, exhaust timing, and system efficiency. Designers must balance between effective noise attenuation and minimal impact on system operation. Moreover, diesel type or pulse type exhausts generate wideband and impulse noise; achieving attenuation across all frequencies is non trivial. The pneumatic noise generated by turbulent jets and rapid expansions is more difficult to suppress at low frequencies. Indeed, one review observed that despite many attempts, noise levels below 80dB in production plant settings remain elusive for many current solutions [35]. In addition, space constraints, maintenance (e.g., clogging of porous elements) and cost are practical issues.

In recent research and development, attention has turned toward hybrid porous expansion designs and optimization using computational methods (e.g., FEM, genetic algorithms) for muffler geometry. The aforementioned simulation study on metal sintered porous plus spiral tube plus expansion cones found that combining dissipative (porous) and reactive (expansion/geometry) elements produced superior attenuation in constrained spaces [36].

1.8 Additive Manufacturing Technology

Additive manufacturing (AM), often referred to as 3D printing, is a group of technologies that fabricate three dimensional parts by depositing or fusing material layer by layer, following a digital model as shown in figure 1.9. Unlike traditional subtractive manufacturing which removes material via machining, casting or forging

AM builds parts from the ground up, enabling significant design freedom, complex geometries, and often reduced waste of material. The transformative nature of AM lies in its ability to produce structures that were previously impossible or prohibitively expensive using conventional manufacturing means [37].

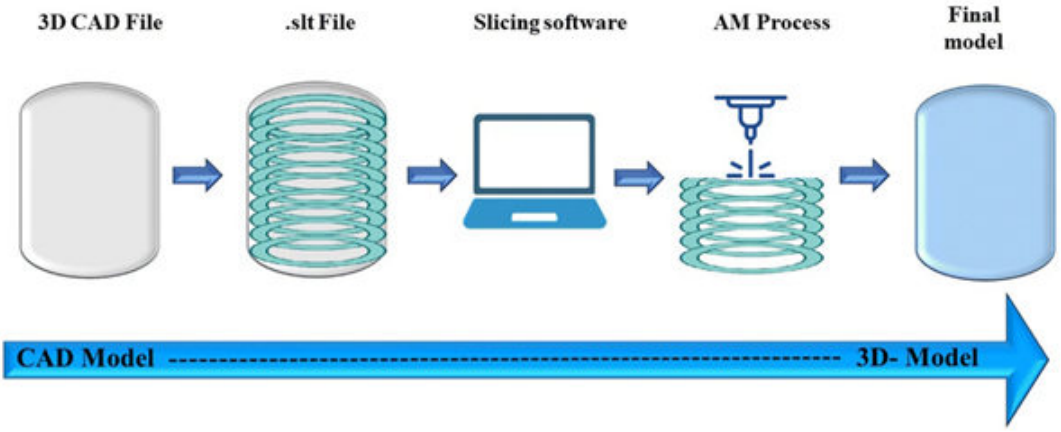

FIGURE 1.9: Basic Steps for Additive Manufacturing [38]

One of the major advantages of AM is design flexibility: internal channels, lattice structures, functional gradients, and topology optimized shapes can be created directly and integrated into parts, opening possibilities for lightweighting, part consolidation (reducing assemblies), customized or patient specific components, and rapid iterations or prototyping. For instance, the automotive and aerospace industries leverage AM to create lightweight, complex brackets or conformal cooling channels that would be difficult or impossible to machine [39]. Furthermore, the layer by layer nature of AM can reduce waste compared to subtractive methods, especially for high-value materials like titanium alloys, and enable shorter lead times from concept to production. Main processes of AM is shown in figure 1.10.

Despite these benefits, there are several important challenges in additive manufacturing. Material options, process reliability, repeatability, surface finish, anisotropy of mechanical properties, residual stresses, defect formation (e.g., porosity, lack of fusion) and post processing overhead remain active concerns. For metal AM in particular, the literature points out that although many processes are mature, "there is still a need of a robust understanding of processes, challenges, and application specific needs" when scaling to production environments [40]. In addition,

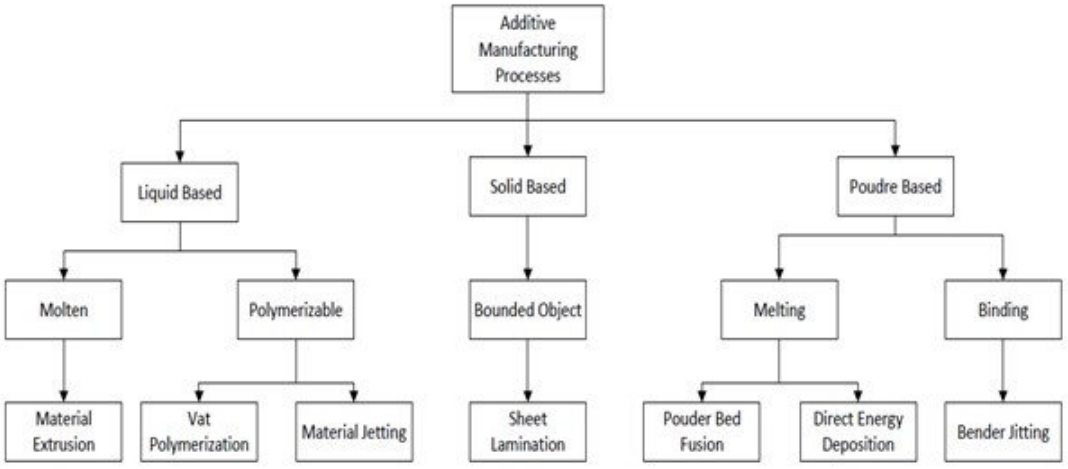

FIGURE 1.10: Additive Manufacturing Technology

printing speed, build volume constraints, cost of AM machines and feedstock, and certification/qualification in regulated industries are barriers to widespread adoption.

Another dimension of AM's evolving role is the expansion in materials and applications beyond polymers and metals into ceramics, composites, bio materials, and even concrete and food printing. The convergence of AM with design for additive manufacturing, topology optimization, lattice/truss structures, and hybridization (combining AM with subtractive or formative methods) is shaping next generation manufacturing strategies. Moreover, sustainability considerations are becoming more prominent: researchers are investigating energy consumption, material reuse/recycling, and life-cycle impacts of AM compared to traditional manufacturing routes.

1.9 Lattice Structures

Lattice structures are architected or cellular materials composed of repeating unit cells that form a periodic or semi periodic network in three dimensional space. These structures enable a unique combination of low weight, high specific strength, tailored mechanical properties (such as stiffness, energy absorption, and

deformation behavior) and design freedom, particularly when produced via additive manufacturing (AM) technologies.

In the AM context, use of lattice structures offers significant advantages: the ability to produce complex internal geometries (which would be very difficult or impossible by conventional subtractive or formative processes), to tune structural parameters such as cell topology, relative density, strut thickness and unit cell size, and to integrate multi functionality (e.g., load bearing plus heat transfer plus acoustic damping).

Design of lattice structures begins with defining a unit cell topology, which is then replicated throughout a volume (uniformly or graded). The replication may follow a grid or conform to a curved boundary. Key parameters include relative density (ratio of lattice mass to solid mass), strut or wall thickness, unit-cell size, connectivity, and orientation. Manufacture via AM introduces further considerations: minimum feature sizes, surface roughness, build direction effects, residual stresses, and anisotropy of properties.

Lattice structures have found applications in aerospace (lightweight panels, structural brackets), automotive (energy absorption and crashworthiness zones), biomedical implants (porous scaffolds promoting bone in-growth), and heat exchangers (via high surface area designs). Their ability to absorb energy, tailor stiffness and mimic natural architectures (e.g., cancellous bone) makes them desirable in many advanced engineering fields.

1.9.1 Strut or Beam Based Lattice Structures

Strut or beam-based lattice structures are one of the most commonly used types of cellular materials, consisting of slender members, or "struts," connected at nodes, forming truss-like networks as shown in figure 1.11. These structures are often referred to as trusses or frameworks and are widely utilized due to their simplicity and versatility. The most common unit-cell topologies for strut-based lattices include body-centered cubic (BCC), face-centered cubic (FCC), octet truss,

and Kelvin cells. These lattices are characterized by the repeated arrangement of struts that provide a network for transferring forces across the structure. A key characteristic of these lattice structures is their ability to offer high strength-to-weight ratios, making them ideal for applications requiring lightweight but robust components, such as aerospace and automotive industries. For example, BCC and FCC lattices are widely used in lightweight structural components because of their superior mechanical properties and ease of manufacturing using additive manufacturing (AM) technologies.

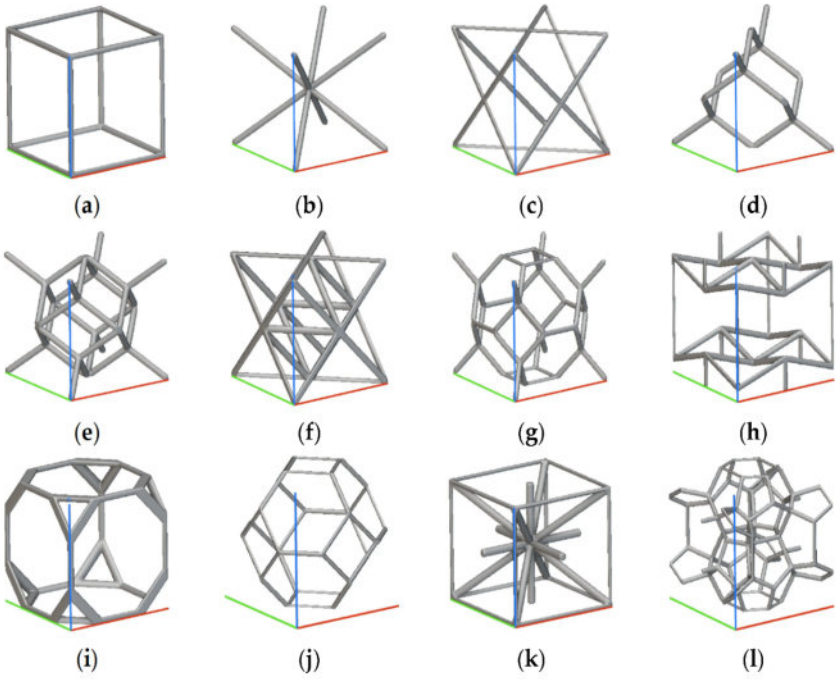

FIGURE 1.11: Strut/Beam Lattice (generated with nTop and the colored lines show the 3D reference system useful for comparison): (a) Simple Cubic Cell; (b) Body Centered Cubic Cell; (c) Face Centered Cubic Cell; (d) Diamond Cell; (e) Fluorite Cell; (f) Octet Cell; (g) Truncated Octahedron Cell; (h) Re-entrant Cell; (i) Truncated Cube Cell; (j) Kelvin Cell; (k) Iso Truss Cell; (l) Weaire–Phelan Cell [41]

Strut-based lattices exhibit mechanical behavior that can be well described by cellular material models, such as the Gibson-Ashby model, which links relative density to stiffness and strength. The mechanical performance of these lattices is heavily influenced by key design parameters such as relative density, strut thickness, and unit-cell size. As relative density increases, both strength and stiffness improve, but so does the weight of the structure. The deformation mechanism of strut lattices

is typically dominated by either bending or stretching, depending on the design. Bending-dominated lattices tend to be more flexible, while stretching-dominated lattices are stiffer and more efficient in carrying loads. The ability to tune these structures by adjusting the relative density and strut thickness makes them suitable for a range of applications, from energy absorption systems to lightweight structural elements. However, one of the challenges associated with strut-based lattices is the anisotropic nature of their mechanical properties, meaning the properties may vary depending on the orientation of the structure. This is especially pronounced when using additive manufacturing, where the build direction can affect the material's mechanical behavior [42].

1.10 Triply Periodic Minimal Surface Structures

Triply Periodic Minimal Surface (TPMS) structures are advanced lattice architectures defined by continuous, smooth periodic surfaces that divide space into two interpenetrating volumes as shown in figure 1.12. These surfaces are a type of minimal surface, meaning they have zero mean curvature at every point on the surface. TPMS lattices are characterized by their highly symmetric and isotropic properties, which make them particularly valuable for applications requiring uniform mechanical behavior in all directions. TPMS structures can be designed with various unit-cell types, such as Gyroid, Diamond, Neovius, and Schwarz Primitive, each offering unique mechanical and fluidic properties. These lattices are often used in applications where high surface area, isotropy, and efficient load distribution are important. For instance, TPMS structures are gaining popularity in fields like biomedical implants, heat exchangers, and filtration systems due to their ability to provide optimal balance between strength, stiffness, and energy absorption while maintaining a lightweight structure.

One of the key advantages of TPMS lattices is their geometric symmetry and isotropy. The continuous, smooth surfaces of TPMS lattices lead to uniform mechanical properties in all directions, unlike traditional strut-based lattices that can exhibit directional dependence of properties. This makes TPMS lattices ideal

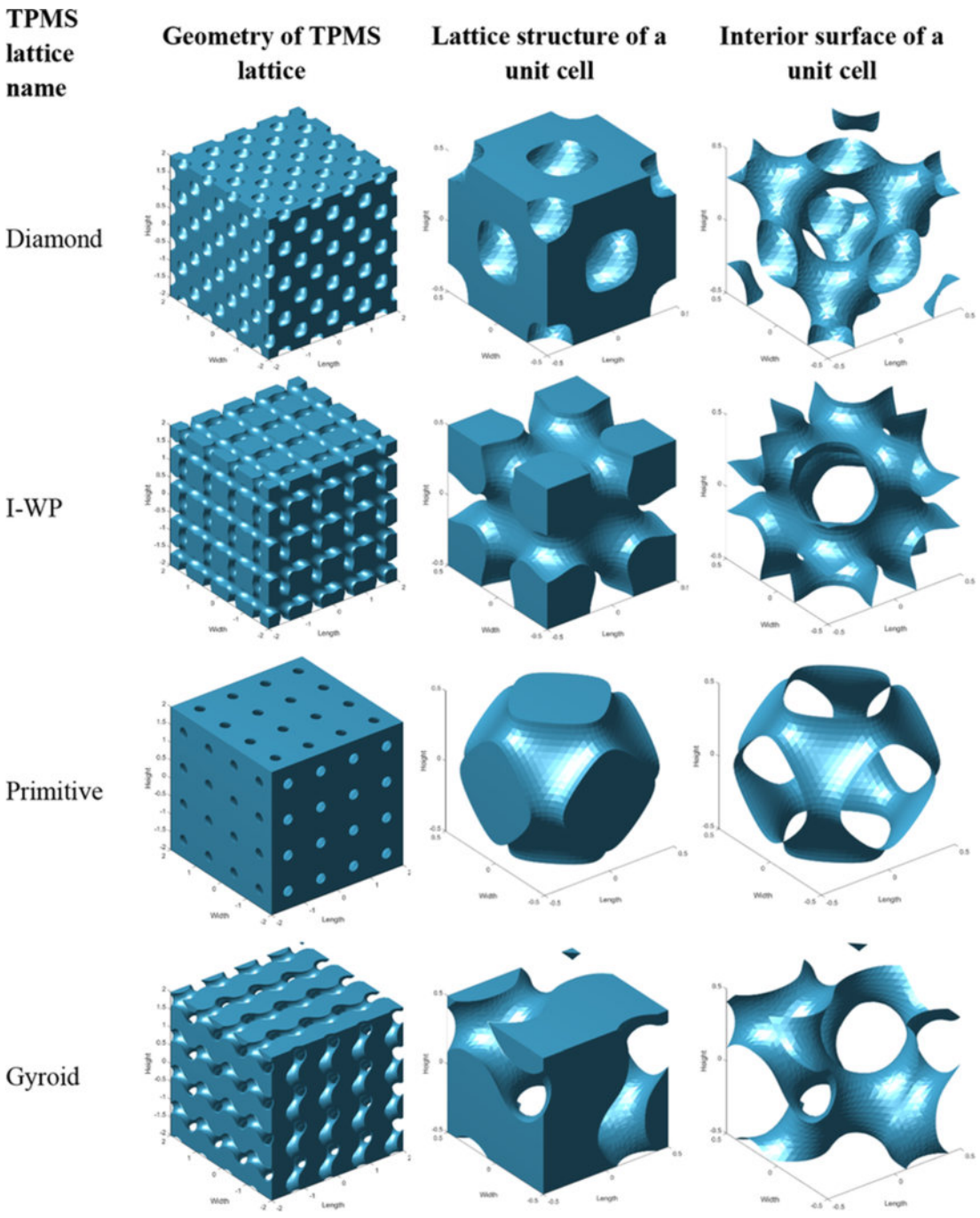

FIGURE 1.12: TPMS Structures [43]

for applications where multidirectional load-bearing capability is required, such as in aerospace or automotive structural components. Additionally, TPMS lattices offer an extremely high specific surface area, which is beneficial in applications such as heat exchange or fluid filtration, where a large surface area is needed for efficient thermal or fluid transfer. The high surface area also contributes to the acoustic properties of TPMS lattices, making them an ideal choice for noise reduction applications, such as in porous silencers.

Another advantage of TPMS lattices is their ability to optimize mechanical performance without sacrificing structural integrity. Studies have shown that sheet-based TPMS structures, such as the Gyroid, exhibit superior compressive strength and energy absorption capabilities compared to traditional strut-based lattices at the same relative density. This is due to the nature of the TPMS structure, where the smooth, interconnected surface allows for more efficient load distribution and energy dissipation. Furthermore, TPMS lattices can be designed with a range of relative densities and geometries, allowing for the fine-tuning of properties like stiffness, damping, and flow resistance.

From a manufacturing perspective, TPMS lattices are well-suited for additive manufacturing due to their smooth, continuous geometry, often requiring minimal support structures. Techniques like SLS and DMLS can produce these complex lattices, though fine details may pose printability challenges. Optimizing TPMS structures involves balancing print resolution, material properties, and mechanical performance, enabling customized designs for aerospace, automotive, medical, and energy applications [44].

1.11 Flow of Gas Through Conventional Silencers and their Limitations

The flow of gas through conventional silencers is typically characterized by complex interactions involving turbulence generation, flow separation, and energy dissipation mechanisms, which are primarily responsible for acoustic attenuation. In reactive silencers, the exhaust gas passes through a series of expansion chambers and perforated ducts, where abrupt changes in cross-sectional area induce pressure wave reflections and interference effects, leading to noise reduction. However, these sudden expansions and contractions often result in significant flow separation and recirculation zones, causing increased pressure losses and reduced flow efficiency. In dissipative silencers, the gas flows through porous or fibrous materials, where acoustic energy is converted into heat through viscous and thermal losses. While

these silencers are effective at attenuating high-frequency noise, they tend to exhibit poor performance at low frequencies and may suffer from material degradation over time under high-temperature or high-velocity conditions. Hybrid silencers attempt to combine both reactive and dissipative mechanisms; however, they still face challenges in achieving an optimal balance between noise attenuation and pressure drop. Additionally, conventional silencer designs often rely on simplified geometries, which limit their ability to control flow distribution and turbulence intensity effectively. As a result, excessive turbulence and non-uniform velocity fields can lead to inefficient acoustic performance and increased aerodynamic losses. These shortcomings highlight the need for advanced structural designs, such as TPMS-based geometries, which can provide smoother flow pathways, enhanced surface interaction, and improved control over both flow and acoustic characteristics.

1.12 Problem Statement

In many industrial applications, such as pneumatic systems and exhaust management, controlling noise levels while maintaining efficient fluid flow is a significant challenge. Porous silencers are commonly used to mitigate the noise produced by high-velocity gas flows; however, their effectiveness is heavily dependent on the internal pore structure and flow characteristics. Traditional silencer designs often fail to optimize both noise reduction and flow performance, leading to inefficient designs that either compromise acoustic attenuation or increase pressure drop.

Triply Periodic Minimal Surface (TPMS)-based porous structures, such as Gyroid, Diamond, and Primitive, have shown promise in offering high surface area and unique geometric properties that can potentially enhance the performance of porous silencers. However, there is a lack of comprehensive numerical studies that systematically compare these TPMS structures in terms of their acoustic and fluidic performance in transient flow conditions. Existing models fail to address the complex transient interactions between flow and acoustic waves in such intricate porous geometries, limiting the ability to design highly efficient and optimized porous silencers. This thesis seeks to fill this gap by conducting a

numerical investigation using Transient Reynolds-Averaged Navier-Stokes (RANS) simulations in ANSYS Fluent to assess and compare the performance of Gyroid, Diamond, and Primitive TPMS-based porous silencer designs. The aim is to evaluate the noise reduction efficiency, pressure drop, and flow dynamics for each pore structure, providing valuable insights for the optimization of porous silencer designs in various industrial applications.

1.13 Research Objectives

The primary objective of this thesis is to numerically investigate the flow and acoustic performance of porous pneumatic silencers incorporating triply periodic minimal surface (TPMS) structures. To achieve this aim, the following specific objectives are defined:

i. To design and develop three-dimensional geometric models of porous silencers based on Gyroid, Diamond, and Primitive TPMS pore structures, ensuring identical external dimensions and comparable porosity same as market Pneumatic silencer.

ii. To perform high Computational Fluid Dynamics (CFD) simulations using ANSYS Fluent by applying the Transient Reynolds-Averaged Navier–Stokes (RANS) approach to accurately capture unsteady flow behavior inside the porous silencer configurations.

iii. To analyze the internal flow characteristics of each TPMS-based silencer by examining pressure, velocity, temperature, and streamline contours, with the aim of understanding flow resistance, vortex formation, and energy dissipation mechanisms.

iv. To predict the acoustic performance of each silencer configuration using the Ffowcs Williams–Hawkings (FW-H) acoustic model, enabling the computation of far-field sound pressure levels generated by turbulent flow structures.

v. To assess the A-weighted Sound Pressure Level (A-weighted SPL) across octave bands for Gyroid, Diamond, and Primitive structures, providing a human-hearing-relevant comparison of acoustic attenuation performance.

1.14 Thesis Structure

This thesis is organized into five chapters.

Chapter 1: Introduction The introductory chapter provides the background, objectives, and significance of the study, laying the foundation for the research. Chapter 2: Literature Review This chapter reviews the existing literature on silencers, focusing on the principles of noise attenuation, types of silencers, and the role of porous structures in sound absorption. It also examines previous studies on the modeling and simulation of porous silencers, highlighting gaps in knowledge that this research aims to address. Chapter 3: Methodology The methodology chapter outlines the modeling and simulation techniques used in the study. It describes the numerical methods employed to simulate the behavior of porous silencers under transient flow conditions and explains the selection of materials and pore structures. This chapter also details the computational tools and software used for the simulations. Chapter 4: Results and Discussion This chapter presents the results of the simulations, including the sound attenuation performance and pressure drop for each of the porous structures under various conditions. The results are analyzed and discussed in terms of their implications for silencer design and performance. and Chapter 5: Conclusions and Recommendations The final chapter summarizes the key findings of the research, discusses their practical implications, and offers recommendations for future research and potential improvements in silencer design.

Chapter 2

Literature Review

2.1 Introduction of Metamaterials

Research in acoustic absorption has traditionally focused on conventional materials and methods. However, there is a growing interest in metamaterials, artificially engineered structures with unique topological properties that do not violate the laws of physics. The concept of metamaterials emerged in the field of electromagnetics in 1968, when physicist Veselago identified that materials with negative dielectric characteristics and permeability differed from typical materials that possess positive properties. Metamaterials are categorized into thermal, acoustic, electromagnetic, and mechanical types based on their modified physical properties. Unlike naturally occurring materials, metamaterials are designed to achieve specific functionalities or multiple functions (i.e., multifunctional).

For acoustic applications, these materials must meet several functional criteria, including a high absorption coefficient over a broad frequency range, cost-efficiency, structural integrity, lightweight properties, and flame resistance. Acoustic metamaterials (AC-Meta) are a subset of metamaterials designed to manipulate acoustic waves. These structures, typically composed of cellular arrays, can influence sound waves on the sub-wavelength scale. AC-Meta materials exhibit a wide range of densities and bulk moduli, both critical properties for sound wave propagation. Over the past two decades, AC-Meta has gained significant attention, with researchers

exploring their complex features that can enable unusual functions. The increasing interest in metamaterials is evident from the vast number of publications available: over 25,000 articles related to "Metamaterials" and over 1,500 articles focusing on "Acoustic Metamaterials" on Scopus.

Acoustic metamaterials are known for their negative density, anisotropic mass properties, and negative elastic modulus. These materials are often created by combining two or more substances with different densities and bulk moduli. AC-Meta has shown exceptional performance in acoustics, providing remarkable sound manipulation capabilities across a broad frequency range. Their ability to surpass conventional materials in controlling sound has led to significant advancements in noise control and absorption techniques. These materials are specifically engineered to meet precise functional requirements, such as targeting specific frequency ranges, achieving high sound absorption coefficients, and maintaining structural integrity in diverse environmental conditions. Furthermore, they offer tunability, enabling customization for applications that require precise acoustic adjustments. Their versatility and effectiveness across a wide frequency spectrum make them a promising area for future research and development in acoustic technology, particularly in optimizing the balance between absorption, reflection, and durability [45].

Figure 2.1 illustrates the number of publications related to 'Metamaterials and Acoustic Metamaterials' over the past decade, highlighting the growing interest among researchers in exploring the wide-ranging applications of Acoustic Metamaterials (AC Meta). However, the broader use of AC-Meta is constrained by significant challenges in fabrication, especially when it comes to producing complex structures. In recent years, additive manufacturing (AM) has become a prominent technique for creating 3D metamaterials with intricate designs [47]. Moreover, noise sources span a broad spectrum of frequencies, making it difficult to manage noise using a single type of absorber. Acoustic absorbers, however, can be tailored to address specific frequency ranges, making customization a crucial aspect of their design and development. As a result, the development of acoustic absorbers should prioritize flexibility in fine-tuning their performance across various frequency bands to achieve optimal sound absorption. AM provides several advantages, offering

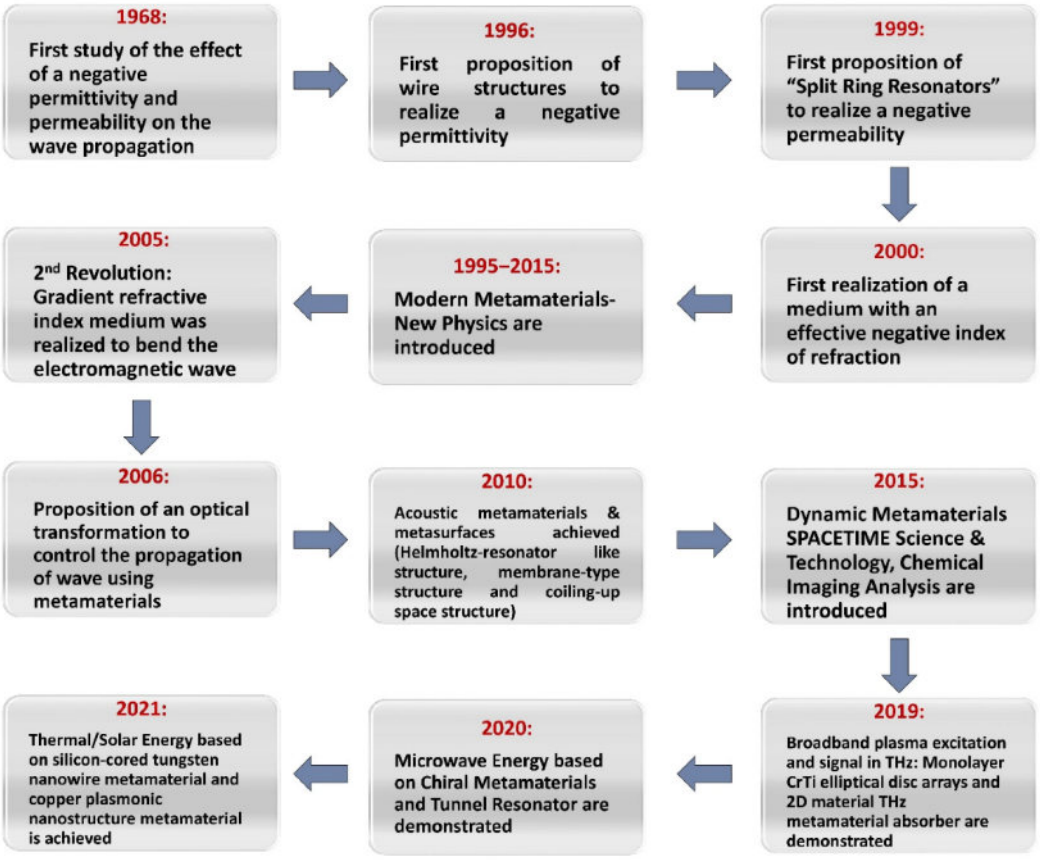

FIGURE 2.1: Schematic depicting the evolution of the field of metamaterials over the years, from 1968 to nowadays [46]

flexibility to optimize both process and product parameters, which is essential for such customization [48].

2.2 Types of Acoustic Absorbing Metamaterial

Acoustic absorbing metamaterials (ACA-Meta) can be generally divided into three categories based on their structural features: perforated, slotted, and cellular. If a structure incorporates more than two of these geometries, it is referred to as a hybrid ACA-Meta. The classification of ACA-Meta is illustrated in the Figure 2.2. Traditionally, configurations like perforated, slotted, and cellular structures were considered separate from metamaterials. However, their characterization changes significantly when they are created using additive manufacturing (AM) techniques. AM allows for intricate modifications to these structures, resulting in substantial improvements in their performance compared to traditional materials

and designs. This transformative effect has led to the reclassification of such structures as metamaterials. By utilizing AM, these materials acquire unique properties that directly influence their physical characteristics. This shift challenges the conventional classification of these structures, highlighting the role of advanced manufacturing techniques in shaping their behavior and justifying their recognition as metamaterials.

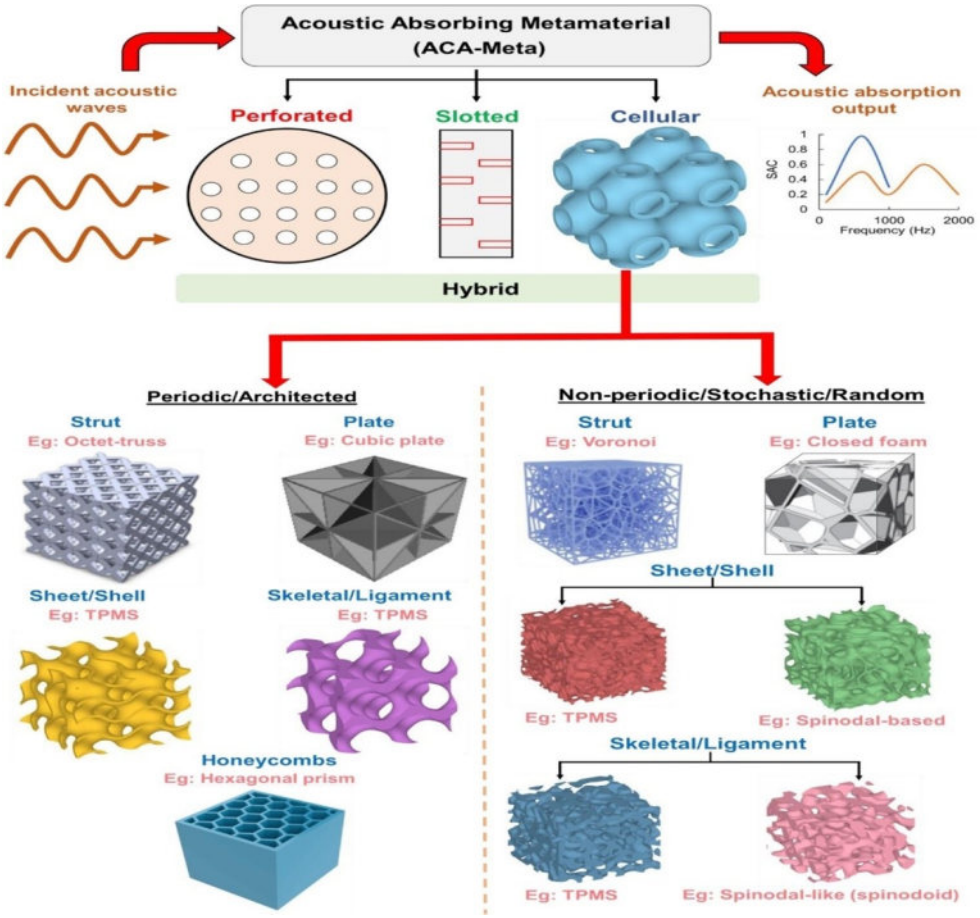

FIGURE 2.2: Acoustic Meta Materials [49]

2.2.1 Perforated ACA-Meta

Perforated Acoustic Absorbing Metamaterials (ACA-Meta) consist of panels with numerous perforations and have been utilized by researchers to enhance the acoustic environment of buildings [43]. These materials are recyclable, non-flammable, and environmentally friendly acoustic absorbers. They absorb sound through viscous friction in small holes, typically spaced away from a rigid surface. The efficiency of

these absorbers is maximized when the acoustic particle velocity within the pores is at its highest. Perforated ACA-Meta is effective at absorbing sound in the mid and high-frequency ranges but has limited effectiveness at lower frequencies [50]. The perforations in micro-perforated panels (MPP) generally have diameters of less than 1 mm, and the surface area of the panel made up of micro-perforated pores is typically between 1% and 2% of the total area. MPP absorbers have been successfully used in various applications, such as construction machinery, architectural rooms, and exhaust systems. They are suitable for use in interior wall barriers, windscreens, fluorescent light covers, sunshades, and column covers. To achieve optimal sound absorption, an air gap must be maintained between the perforated ACA-Meta and a rigid wall. While first-generation perforated panels were made of metal with circular laser-cut perforations, second-generation panels are more cost-effective as they are produced through etching, cutting, shearing, or grinding. In the current generation, these panels are fabricated and fine-tuned using advanced technologies like additive manufacturing (AM).

2.2.2 Slotted ACA-Meta

Slotted Acoustic Absorbing Metamaterials (ACA-Meta) are structures that feature slots rather than circular perforations, functioning similarly to perforated ACA-Meta. These structures can include resonators and coiled designs such as Hilbert, fractal, labyrinthine, spiral, and helix. When a sound wave passes through the slotted ACA-Meta, it travels along the extended path of the slots, which is much longer than the physical dimensions of the structure. This helps reduce the sound intensity by slowing the wave and decreasing its strength due to the frictional resistance at the air channel wall interface. For slotted absorbers, 3D printing offers flexibility, enabling design freedom, customization, and fast manufacturing. It is generally more resource-efficient than traditional subtractive manufacturing methods, reducing material waste and providing a more sustainable production approach. Additionally, 3D printing is scalable, making it suitable for both small- and large-scale production, while also lowering manufacturing costs, making the creation of custom slotted absorbers more affordable.

2.2.3 Cellular ACA-Meta

Cellular structures have gained significant attention due to their lightweight, high strength, energy absorption, and vibration damping capabilities. The term "Cellular Structure" was first introduced by Gibson and Ashby, who considered it to encompass materials like foams and honeycombs. These materials possess a wide range of topological features, structural characteristics, and length scales, such as improved vibration absorption, a high strength-to-weight ratio, and structural control over breakdown and length distribution. Thanks to their exceptional properties, cellular structures are commonly used in fields like aerospace, bioengineering, robotics, and other technological sectors. The application of additive manufacturing (AM) has accelerated the development of these structures. Additionally, cellular structures have demonstrated outstanding acoustic properties.

Cellular Acoustic Absorbing Metamaterials (ACA-Meta) can be classified as either periodic or non-periodic based on their periodicity. Periodic cellular ACA-Meta can be further categorized into strut, plate, sheet/shell, skeletal/ligament, and honeycomb structures. In contrast, non-periodic structures, like spinodal topologies, are added without the inclusion of honeycombs. Periodic strut-based structures feature a network of prismatic struts connected at vertices, forming a truss-like framework that effectively distributes load, making them ideal for applications requiring a high strength-to-weight ratio [51]. These include geometries such as octet-truss, face-centered cube, body-centered cube, Kelvin cells, and others connected by struts. Non-periodic trusses, such as those based on Voronoi diagrams, utilize seed-based spatial divisions where points in each cell are closer to the seed point that generated them, resulting in cells that form convex polygons without holes in 3D and line segments dividing the space in 2D. These cells are defined by their characteristic of being hole-free convex polygons in both dimensions [52].

Periodic plate-based structures consist of plates regularly placed between trusses, providing distinct mechanical properties, while non-periodic plate-based structures, such as closed-cell and quasi-random foams, lack regularity. TPMS-based structures: gyroid, Neovius, primitive, and diamond can be created by thickening minimal

surfaces for sheet-based lattices or solidifying enclosed volumes for skeletal-based lattices. Non-periodic TPMS are generated by introducing randomness via control points and sub-domains. Spinodal structures are non-periodic, bi-continuous cellular designs resembling early-stage diffusion-driven phase separation, modeled using Gaussian random fields based on the Cahn-Hilliard equation; these are classified as spinodal-based (sheet) or spinodoid (skeletal). Periodic honeycomb structures feature uniform unit cells, including tetrahedrons, triangular prisms, and hexagonal prisms [53, 54].

2.2.4 Hybrid ACA-Meta

In the broad exploration of perforated, slotted, and cellular acoustic metamaterials, hybrid ACA-Meta emerge as a blend of two or more configurations. This combination seeks to leverage the benefits of various structures to create a synergistic effect.

2.3 AM Techniques for Acoustic Metamaterials

Traditional methods such as casting, molding, machining, and laser cutting have been widely used for manufacturing acoustic absorbers, but they come with several limitations, especially in terms of customization, design control, and achieving high internal porosity [55]. For instance, Daniel et al. (2018, 2020) used compression molding to produce PLA-based absorbers reinforced with kenaf and coconut fibers, but encountered difficulties in adjusting these materials for specific acoustic performance [56, 57]. Likewise, Daeipour et al. (2017) and Jayamani et al. (2014) created absorbers reinforced with natural fibers like wood, rice straw, and kenaf, which performed well but lacked flexibility in adjusting their properties. These methods often involve intricate and time-consuming steps such as fiber preparation, blending, and perforation. Given these constraints, additive manufacturing (AM) offers a promising alternative, providing greater design flexibility, customization,

and the potential to address many challenges associated with conventional techniques, particularly in producing absorbers with tailored acoustic properties across various frequency ranges [58, 59].

Furthermore, additive manufacturing (AM) technologies offer more controlled parameters and a stronger interaction between material properties and process variables, enabling the creation and optimization of complex designs. This method, commonly referred to as 3D printing, involves layering materials to construct three-dimensional objects and is utilized across various industries, including automotive, biomedical, and aerospace. Additive manufacturing is categorized into multistep and single-step techniques, with further subdivisions according to the ISO/ASTM 59000:2021 standard [60].

2.3.1 Vat Photopolymerization

The vat photopolymerization technique involves exposing a light-curable resin, stored in a vat, to visible or ultraviolet light. This curing light initiates a polymerization reaction that either forms polymer chains or crosslinks them, resulting in a solid resin. Once the process is complete, it is irreversible, and the resin cannot return to its liquid state. A sliced STL file is used to create successive resin layers. Two curing methods, stereolithography (SLA) and digital light processing (DLP) (as shown in Figure 2.3), are commonly employed in photopolymerization. In SLA, a platform is submerged in a resin-filled tank, and a laser beam traces the building area, curing the resin according to the STL file. The platform is then moved along the z-axis, and the curing process is repeated layer by layer until the 3D object is complete. In contrast, DLP uses a digital light projector to reflect a laser source instead of a mirror during the curing process, and the projector's resolution impacts the accuracy of the printed parts.

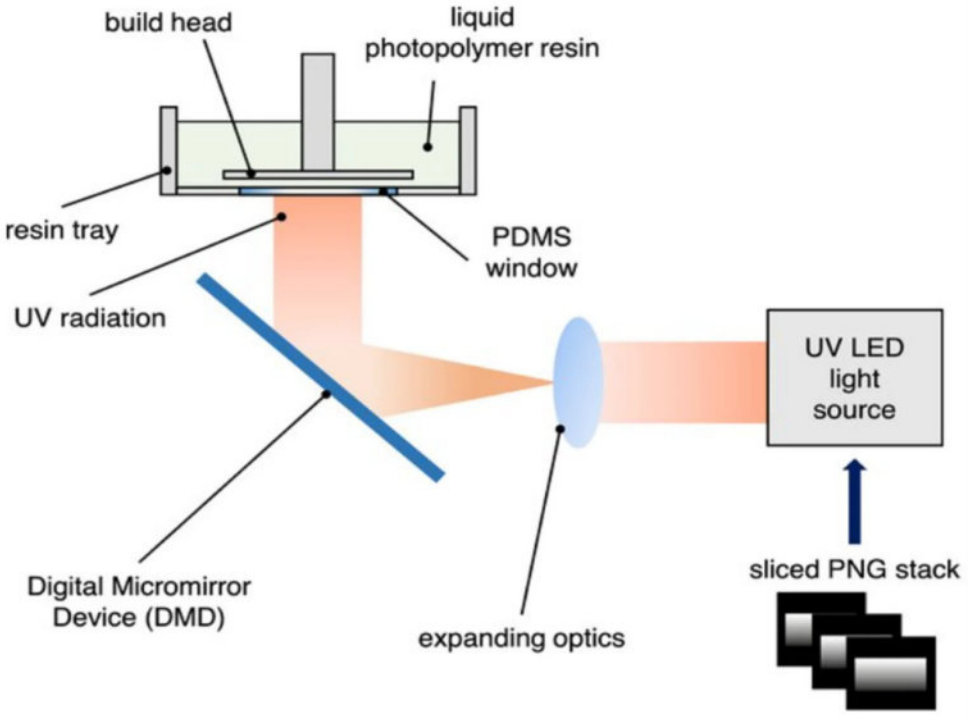

FIGURE 2.3: Principle of Digital Light Processing (DLP) [61]

2.3.2 Stereolithography

Stereolithography (SLA) as shown in figure 2.4, was found to be particularly effective for creating periodic shapes, making it ideal for prototypes and advanced acoustic modeling of porous materials. However, SLA 3D printers may create materials with periodic networks of pores that are more substantial than traditional acoustic foams. In contrast, affordable conventional 3D-printing equipment, including SLA and other AM technologies, cannot enhance these characteristics, especially when using powder-based materials like laser sintering, laser melting, or binder jetting, which may result in microporosity in the 3D-printed skeleton. This microporosity leads to beneficial double porosity, which significantly improves sound absorption by affecting how sound waves travel through these materials. Additionally, a study thoroughly analyzes the 3D printing of structured acoustic absorbent materials using DLP and SLA at microscopic scales. The design involves a periodic network of interconnected resonant chambers with cubes containing spherical interior cavities linked by cylindrical holes. Variations in surface roughness and dimensional fidelity influenced the coefficient of absorption, which was determined experimentally. One challenge in using DLP and SLA for finer-scale production is the decreased

viscosity of polymer resins. Furthermore, a comparison of two extrusion-based 3D printing methods, extrude-and-pull and fiber bridging, highlights their effects on acoustic properties. The extrude-and-pull method produces thin, hair-like fibers, while fiber bridging creates thicker fibers that are more effective at sound absorption. The extrude-and-pull approach, although simpler, results in lower sound absorption due to the thinner fibers, which reduce visco-inertial and thermal losses [62]. Lastly, aerogel-based acoustic absorbers with regulated microstructures were successfully printed using a novel technique that combines extrusion and freeze-casting. The cellulose nanocrystal aerogel absorbers exhibited excellent sound absorption properties, making them ideal for lightweight, sound-absorbing applications, such as in aircraft.

These studies provide a detailed understanding of how various AM technologies can be optimized for fabricating ACA-Meta. They emphasize the importance of selecting the appropriate manufacturing method based on structural complexity, scale, and acoustic performance. Additionally, the studies highlight the need to balance manufacturing precision, material properties, and cost-efficiency when developing effective acoustic-absorbing metamaterials.

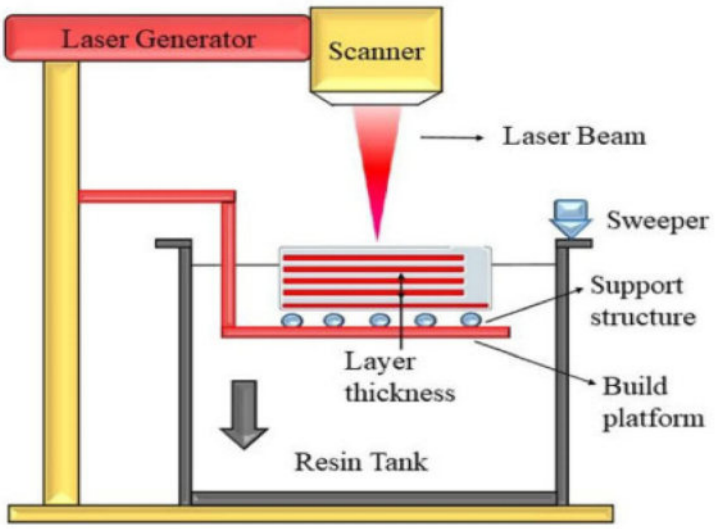

FIGURE 2.4: Principle of Stereolithography (SLA) [61]

2.3.3 Powder Bed Fusion

Powder bed fusion (PBF), as shown in figure 2.5 involves building a platform bed covered with fine powder particles, which are fused together using a liquid binder. After the particles are fused, the excess powder is extracted using a vacuum. Surface preparation can be done through coating, sintering, or infiltration. Factors such as powder particle size, binder viscosity, and powder spreading speed affect the final product's quality. Low melting or sintering temperatures can be managed with lasers. This method offers flexibility in material selection and room temperature conditions, and the powder bed supports the material, helping to overcome challenges during material removal. However, it tends to be more expensive, slower, and results in greater porosity during the powder fusion process. Key PBF techniques include direct metal laser sintering (DMLS), selective laser melting (SLM), and selective laser sintering (SLS). These technologies are capable of creating precise, well-finished products, particularly suitable for small-scale manufacturing due to their reduced beam size. While SLM uses lasers to melt alloy powder particles, producing shorter production times and improved microstructure with high cooling rates, SLS requires powder distribution over the platform. DMLS, like SLM, is effective for producing aerospace parts, functional prototypes, and short-run components more efficiently and economically.

2.3.4 Material Jetting

Material jetting (MJ) is another AM method that produces functional components with fine geometric precision and reduced surface roughness using liquid photopolymer. Its layer-by-layer manufacturing process and low purchase-to-fly ratio make it ideal for industries like biomedicine, dentistry, manufacturing, and aviation. The photopolymer is heated and deposited as droplets onto the build platform, stored in air-excluding containers. Ultraviolet light is then used to cure the molten material, as shown in figure 2.6. MJ offers several advantages, including the ability to adjust layer thickness, provide two types of surface textures, and eliminate the need for post-processing. It is widely used in polymer printing and also supports

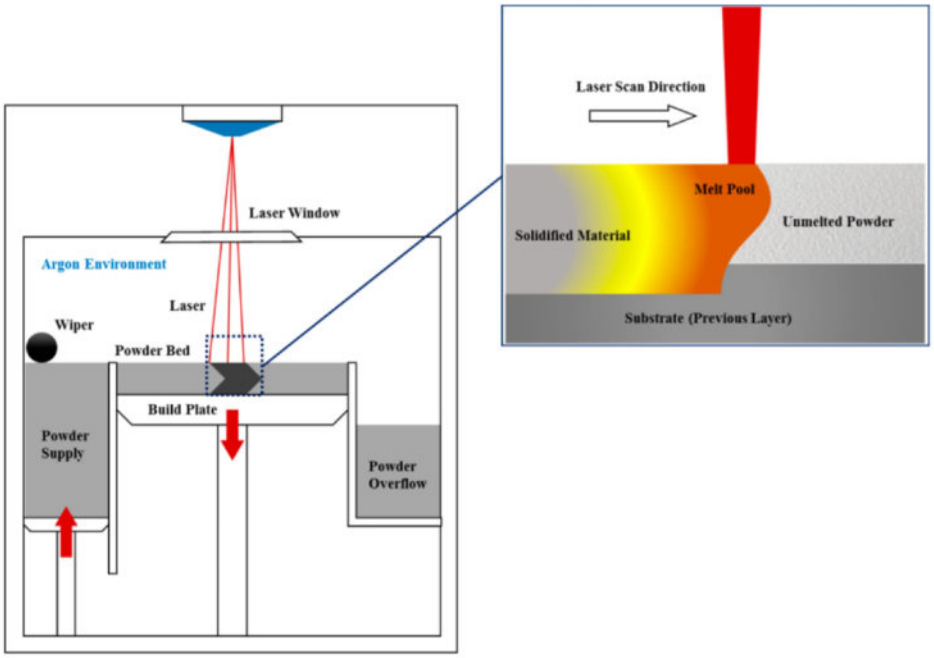

FIGURE 2.5: Principle of Selective Laser Melting (SLM/DLMS) [61]

multi-material printing, allowing the blending of materials like PLA, ABS, and polyamide to create composite components for specific applications. Additionally, MJ printers, with their closed ambient chamber, are suitable for both household and industrial use.

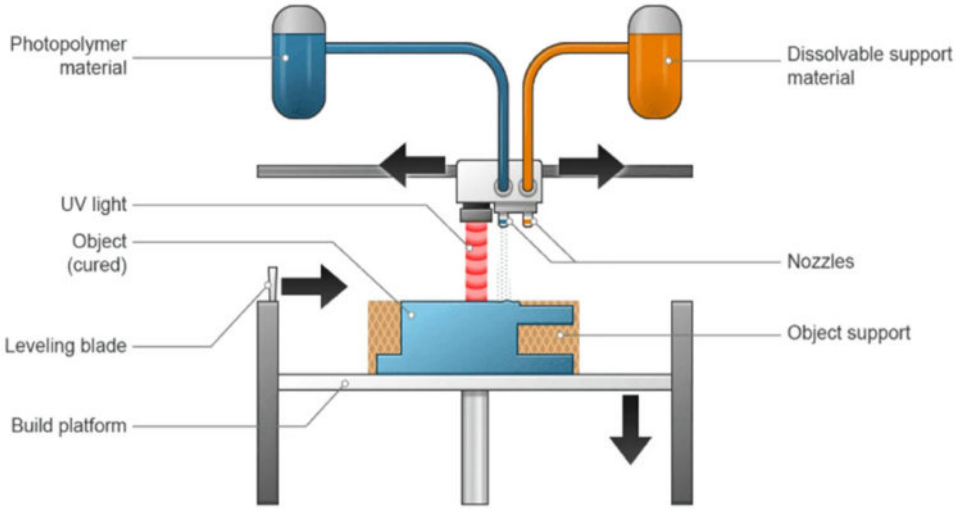

FIGURE 2.6: Principle of Material Jetting 3D printing [61]

Binder jetting is an additive manufacturing (AM) technique that uses a liquid binding agent to selectively join powder particles layer by layer, building objects from 3D data. It has several advantages, including the ability to work with various

materials, no need for explicit support structures, and excellent scalability. The binder is typically applied across the entire cross-section of each layer during printing. In color jet printing (CJP), a print head is used to selectively distribute the binder onto the powder layer. Directed energy deposition (DED) utilizes a high-energy heat source to melt feedstock material, creating a metal track and producing a 3D near-net-shape component. Commercial methods for DED include laser metal deposition (LMD), direct metal deposition (DMD), and laser-engineered net shaping (LENS), each differing by the energy source and material type.

2.3.5 Sheet Lamination

Sheet lamination is another 3D manufacturing technique that involves stacking and bonding thin layers of paper, plastic, or metal sheets. The final shape is produced using laser cutting or CNC machining. Various processes are used in sheet lamination, including laminated object manufacturing (LOM), ultrasonic additive manufacturing (UAM), and plastic sheet lamination (PSL). LOM, one of the earliest commercially available AM methods, uses paper and adhesive instead of welding. Materials like paper, ceramics, polymeric metal-filled tapes, and composites are machined and sealed together. Material extrusion, commonly known as fused deposition modeling (FDM), involves extruding material through a nozzle to form each layer in a parallel line pattern. However, FDM has limitations in mechanical properties due to a restricted range of materials, primarily thermoplastics and some engineering polymers. To expand its capabilities, research into composite materials and enhanced formulations is necessary for creating functional, load-bearing parts. Direct ink writing (DIW), another extrusion-based technique, deposits liquid-phase ink from a nozzle at controlled flow rates to form three-dimensional objects layer by layer.

Several studies have extensively explored the potential of additive manufacturing (AM) for acoustic applications, each contributing valuable insights into the fabrication and performance of Acoustic Absorbing Metamaterials (ACA-Meta). One significant study focuses on constructing a frequency-dependent cell transfer

matrix using a complete visco thermal acoustic model, examining the micro-to-macro dynamics of a single-cell structure. Two identical Kelvin cell structures were fabricated and analyzed using Digital Light Processing (DLP) and Selective Laser Melting (SLM) technologies. These methods were selected for their ability to precisely represent complex geometries, with particular emphasis on the impact of geometry and surface finish on acoustic properties. Another area of research investigates the feasibility of reproducing porous samples designed for sound absorption using additive printing. Different research centers independently produced and tested samples using standardized geometric codes for periodic cellular patterns. While tests on these samples yielded consistent results, some variations were observed due to surface imperfections, such as microporosity, introduced during the manufacturing process.

2.4 Summary and Perspective

2.4.1 Design Perspective

Research on additively manufactured perforated ACA-Meta structures has shown that modifying the perforation ratio shifts the resonance frequency of the peak sound absorption coefficient, with larger ratios producing higher resonant frequencies. Variations in perforation volume such as changes in thickness, diameter, and material density, have been found to strongly influence sound absorption, resonance behavior, and bandwidth. For example, the infill density used in 3D printing affects specimen mass and resonant characteristics; higher infill levels maintain elevated SAC (Sound Absorption Coefficient) values without altering the frequency spectrum.

Geometrical parameters, including porosity, hole diameter, sample height, and perforation angle, also play critical roles, with sample height being particularly influential. Slotted ACA-Meta configurations outperform conventional versions at low frequencies. Emerging geometries such as hexagonal cells with parallel resonators, micro-helix structures, and fractal-inspired designs exhibit adjustable

absorption across broad frequency bands. In the case of cellular ACA-Meta, honeycomb and strut-based architectures highlight the effects of topology, relative density, height, and manufacturing tolerances on acoustic behavior. Shell-type structures, including Schwartz-D, gyroid, and spherical designs, each display distinct absorption responses that vary with frequency.

Overall, the findings confirm that ACA-Meta structures can achieve effective SAC performance across a wide frequency spectrum. Perforated ACA-Meta suits mid-frequency applications, slotted designs target low to mid-frequency ranges, and well-optimized cellular ACA-Meta can operate effectively across nearly the entire range. Beyond the configurations examined here, other bio-inspired, nature-derived, and mechanism-based designs have also been explored to some degree.

2.4.2 Additive Manufacturing Perspective

This section reviews the materials and additive manufacturing (AM) techniques that have been explored to date and identifies potential directions for future progress. By carefully selecting both the material and the AM process, it is clear that acoustic metamaterials can achieve the required properties for acoustic applications including high mechanical strength, thermal stability, and resistance to environmental conditions [63]. From a materials standpoint, most studies have focused on polymer-based options due to their low cost and widespread availability. Photopolymer resins have also been employed, though their higher cost compared with polymer filaments has limited their use. Only a small number of investigations have examined metal-based materials or other alternatives such as aerogels and powder systems like calcium sulphate. From a methodological perspective, extrusion-based AM technologies have dominated the literature, primarily because of their affordability. A smaller body of work has investigated vat photopolymerization, motivated by its ability to produce highly accurate surface finishes while maintaining tight tolerances. It is also worth noting that process-induced imperfections in technologies such as material jetting, binder jetting, and powder bed fusion may contribute favorably to acoustic absorption; however, this area remains underexplored and warrants further

systematic study. Notably, no published research has yet reported the fabrication of acoustic metamaterials using sheet lamination or direct energy deposition. This gap is likely due to the inherent difficulties these processes face in producing the complex geometries required for acoustic metamaterial functionality. Addressing these challenges will require inventive process adaptations and dedicated research into their feasibility.

Another key limitation of AM is the challenge of scaling production to fabricate large acoustic panels. Large-format printing introduces complications such as maintaining uniform material behavior, achieving accurate dimensions, and managing prolonged build times, all of which hinder broader industrial adoption. Additionally, the high initial cost of AM equipment and the relatively narrow selection of printable materials further restrict the scalability of large acoustic systems [64].

Looking ahead, advancements in AM are poised to dramatically influence how acoustic metamaterials are manufactured, with several transformative developments on the horizon. One promising avenue involves micro-architected metamaterials produced via micro- and nano-scale 3D printing technologies [64], which enable extreme geometric precision and the creation of ultralight ACA-Meta with very fine features. However, these techniques currently face scalability limitations, particularly in printing speed. Volumetric AM which has recently emerged as a high-speed alternative, offers a potential solution to overcome these constraints [65]. Additional developments, such as multi-laser beam systems in laser powder-bed fusion paired with significantly expanded build volumes spanning meters, may greatly streamline the industrial-scale production of acoustic metamaterials [65].

Progress in 4D printing adds another exciting dimension to this field by enabling the use of smart materials and adaptive structures. Printing with shape-memory polymers or alloys allows the creation of reconfigurable acoustic systems capable of responding to external stimuli [67]. Furthermore, hybrid 3D printing approaches particularly those combining metal laser powder-bed fusion with multi-material capabilities, show promise for producing functionally graded structures tailored for complex acoustic performance requirements [66].

Collectively, these AM innovations signal a transformative trajectory for the field, unlocking new opportunities to design and manufacture acoustic metamaterials with unprecedented precision, scalability, and multifunctionality. They offer a compelling pathway for meeting the growing demand for advanced acoustic solutions across a wide range of industries.

2.5 Research Gap

Despite extensive research on conventional silencers, limited work has been conducted on the application of TPMS structures for flow-induced noise reduction in pneumatic systems. Existing studies primarily focus on either aerodynamic or acoustic performance, with a lack of integrated analysis combining both aspects. Furthermore, comparative evaluations of different TPMS geometries using advanced aero acoustic models such as FW-H are scarce. The influence of TPMS structures on pressure drop, turbulence, and frequency-dependent sound attenuation remains insufficiently explored. Therefore, this study addresses these gaps by performing a comprehensive numerical and acoustic analysis of Gyroid, Diamond, and Primitive TPMS-based silencers.

Chapter 3

Research Methodology

3.1 Methodology Flow Chart

The methodology adopted in this study follows a structured sequence of steps that ensures a reliable and systematic numerical investigation of porous silencers featuring Gyroid, Diamond, and Primitive TPMS structures. The workflow begins with the development of the complete silencer geometry, which includes the creation of the outer casing and the internal TPMS-based porous cores generated using their implicit mathematical surface equations. Once the geometry is defined, the internal fluid domain is extracted to represent the actual flow passage through the silencer. The extracted domain is then discretized using a high-quality polyhedral mesh with appropriate boundary-layer refinement to accurately resolve turbulence characteristics, particularly in regions of high velocity gradients. After meshing, the governing equations and turbulence models are selected, followed by the definition of the inlet, outlet, and wall boundary conditions. The transient solver settings are configured to ensure numerical stability and accurate resolution of unsteady flow features. Finally, the simulation results are post-processed to examine flow behavior, pressure fluctuations, and acoustic indicators. This sequential methodological framework is illustrated in the flowchart given below in Figure 3.1.

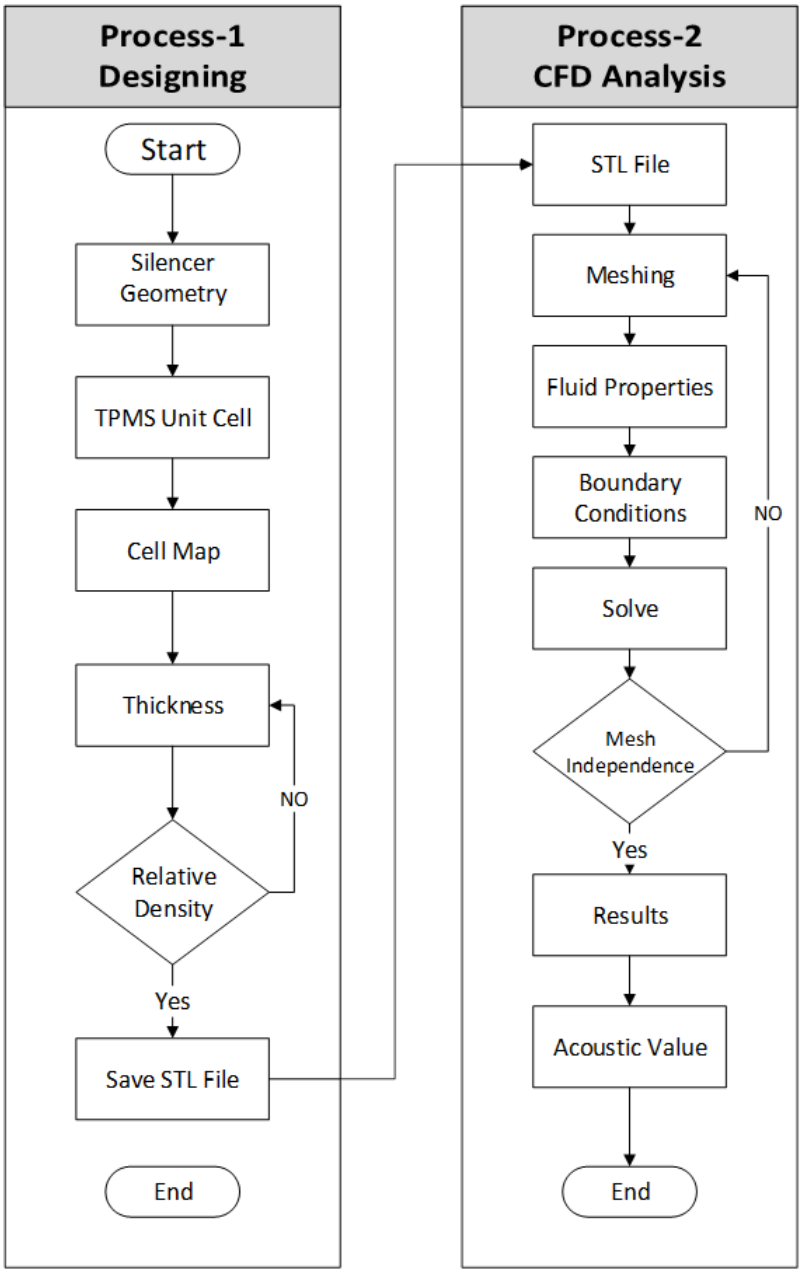

FIGURE 3.1: Methodology Flow Chart

3.2 Geometric Modelling

3.2.1 Silencer Geometry

The geometric modelling stage forms the foundation of the numerical investigation, as the accuracy of the flow simulation strongly depends on a realistic and well-defined geometry. In this study, the silencer body and the embedded TPMS

structures, Gyroid, Diamond, and Primitive are developed using nTop and the parameters are given in Table 3.1.

TABLE 3.1: Parameters for generating structures

Structure Type	Unit Cell Size (mm)	Wall Thickness (mm)
Diamond	$7 \times 7 \times 7$	1.2
Gyroid	$7 \times 7 \times 7$	1.43
Schwarz	$7 \times 7 \times 7$	0.81

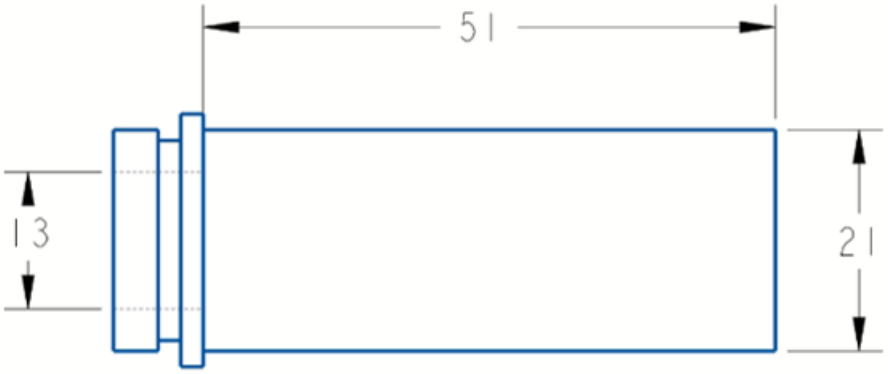

FIGURE 3.2: Wireframe Diagram of Pneumatic Silencer

The silencer geometry is constructed as a cylindrical duct containing a porous core made of TPMS structures. The outer body of the silencer is first created with pre-determined dimensions (mm), (as shown in Figure. 3.2) including the overall length and diameter that correspond to typical industrial silencer configurations. These dimensions are selected from the commercial used pneumatic silencers. The silencer body provides the structural boundaries required to house the TPMS structures and establishes the physical limits of the flow domain [67].

3.2.2 TPMS Structure Modelling

The porous cores inside the silencer are modelled using triply periodic minimal surface (TPMS) geometries, specifically the Gyroid, Diamond, and Primitive (Schwarz-P) structures. These structures are chosen because they offer a continuous, periodic, and highly interconnected pore network beneficial for sound attenuation

and pressure dissipation [68]. Each TPMS structure is generated using its implicit mathematical surface equation as follows:

$$Gyroid : f(X,Y,Z) = \sin(X)\cos(Y) + \sin(Y)\cos(Z) + \sin(Z)\cos(X) \tag{3.1}$$

$$Primitive : f(X,Y,Z) = \cos(X) + \cos(Y) + \cos(Z) \tag{3.2}$$

$$Diamond : f(X,Y,Z) = \cos(X)\cos(Y)\cos(Z) \tag{3.3}$$

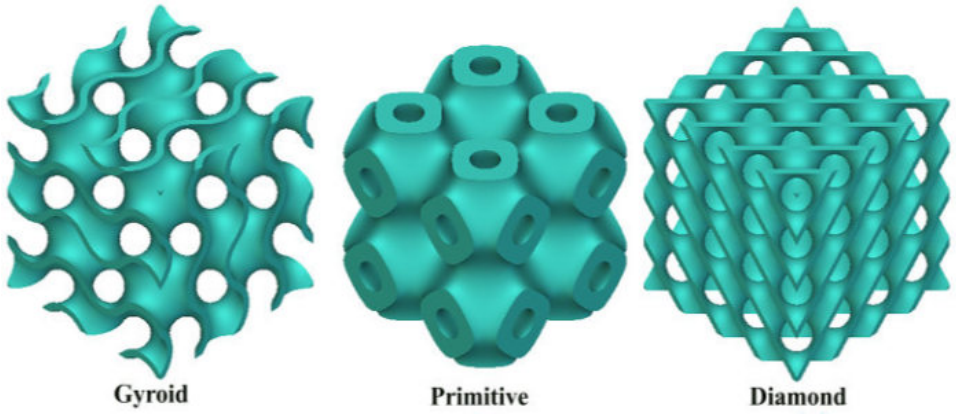

FIGURE 3.3: Unit cells of TPMS Structures

Here, the coordinates X, Y, Z are defined as 2ni/Li, where ni represents the number of unit cells and Li denotes the cell size along the I-th dimension.

To ensure that the TPMS structures effectively represent porous absorbers, the unit cell size and porosity (60%) values are carefully assigned. After defining the TPMS structure, it is replicated periodically and inserted into the silencer body so that it occupies the internal flow region uniformly. This integration ensures that air flowing through the silencer interacts with a continuous porous medium, allowing accurate prediction of pressure drop and flow-induced acoustic behavior. Cross sectional view of silencers with Gyroid, Primitive and Diamond structures is shown in Figure 3.4.

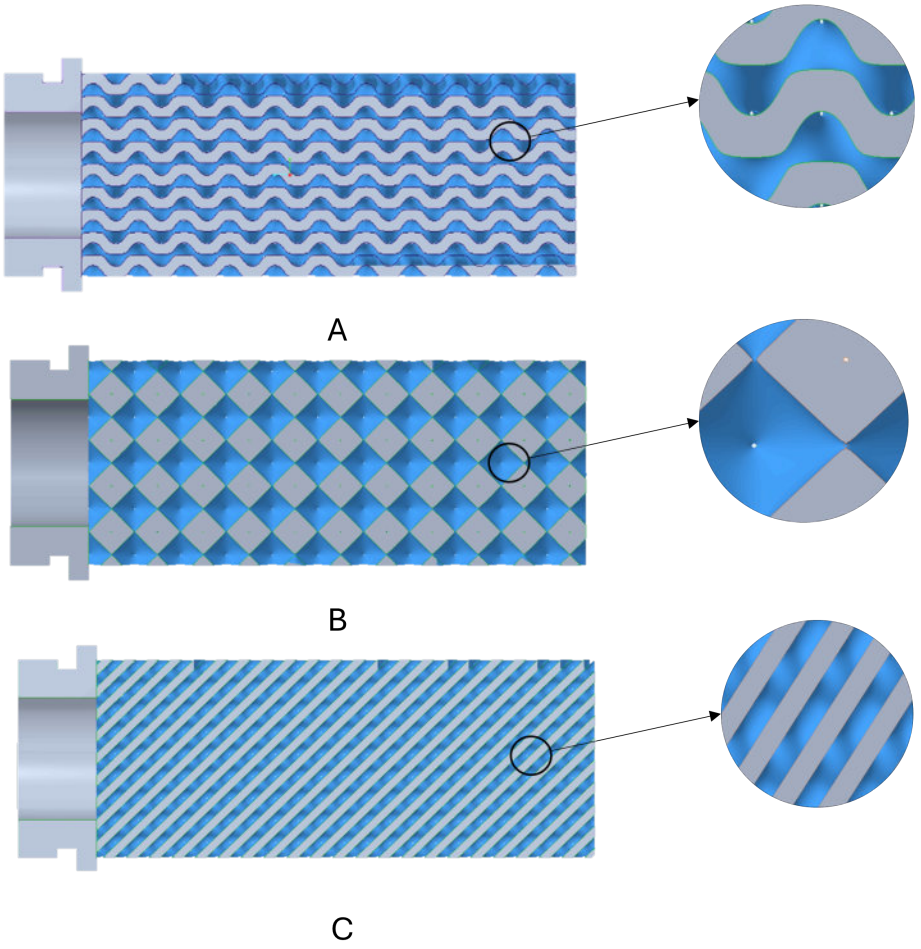

FIGURE 3.4: Cross Sectional View of (A) Gyroid (B) Primitive (C) Diamond

3.2.3 Receivers for Acoustic Signals

To obtain a more comprehensive evaluation of the acoustic behavior within the silencer, A total of 33 acoustic receivers were strategically positioned around the TPMS structure to capture detailed variations in Sound Pressure Level (SPL) throughout the computational domain. As illustrated in Figure 3.5, the receivers were distributed in three different rows along the axial direction of the silencer, providing improved spatial coverage of the acoustic field compared to the previous receiver configuration.

The receivers were categorized into three groups: the upper row consisting of receivers R12–R22, the middle row consisting of receivers R1–R11, and the lower row consisting of receivers R23–R33. This multi-level arrangement was designed to monitor the acoustic response at different vertical locations around the porous

TPMS geometry. The receiver spacing was selected to ensure consistent monitoring of sound propagation, turbulence-induced fluctuations, and pressure wave attenuation along the entire silencer length.

The acoustic data collected from all 33 receivers was subsequently utilized in the Ffowcs Williams–Hawkings (FW-H) acoustic model to evaluate the acoustic performance of the TPMS-based silencer. The expanded receiver arrangement improves the reliability and accuracy of acoustic measurements by providing enhanced spatial resolution of the generated sound field.

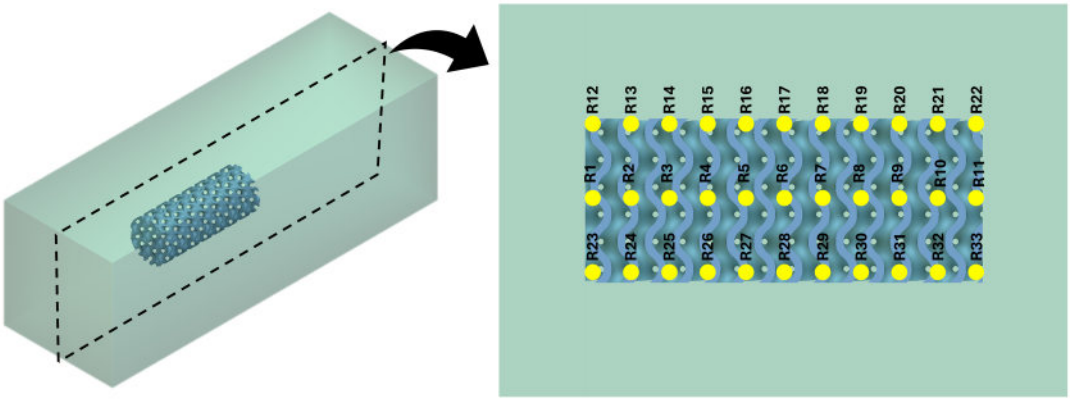

FIGURE 3.5: Receivers for Acoustic Signals

3.2.4 Fluid Domain

The fluid domain for the present numerical investigation was designed to accurately simulate the airflow behavior and acoustic propagation through the TPMS-based silencer structure while minimizing the influence of boundary effects on the computational results. As illustrated in Figure 3.6, the computational domain consists of a three-dimensional rectangular enclosure containing the porous TPMS silencer geometry positioned centrally within the flow region. The dimensions of the fluid domain were selected to provide sufficient upstream and downstream flow development regions. An inlet extension of 50 mm was maintained upstream of the silencer to allow the incoming airflow to develop before interacting with the porous structure. Similarly, a downstream extension of 80 mm was provided to capture the wake development, flow stabilization, and acoustic wave propagation after the fluid passed through the silencer. The larger downstream region also helps reduce

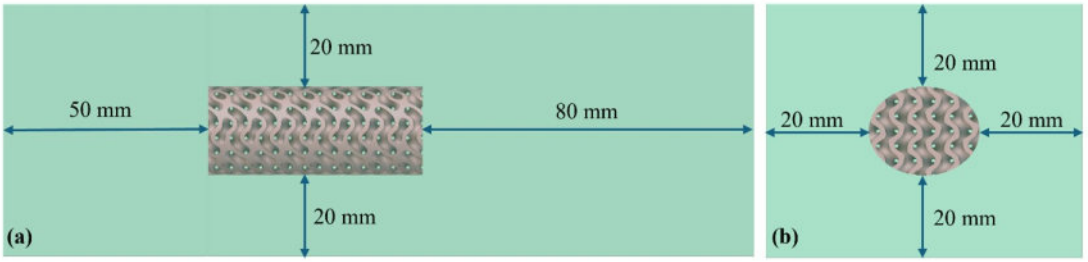

FIGURE 3.6: Dimensions of Fluid Domain

artificial reflections and numerical disturbances near the outlet boundary. In the transverse directions, a clearance of 20 mm was maintained between the TPMS structure and the outer boundaries of the fluid domain in both vertical and horizontal directions. This spacing ensures that the wall boundaries do not artificially influence the flow field, turbulence structures, or acoustic behavior around the silencer geometry. The TPMS silencer itself was modeled as a cylindrical porous structure placed concentrically within the computational domain to ensure uniform interaction between the fluid flow and porous medium.

3.3 Mesh Generation and Independence Study

For the numerical simulations conducted in this study, a carefully constructed meshing strategy was employed to ensure accurate resolution of both the pneumatic and acoustic performance of the TPMS-based porous silencers. The mesh was generated using a polyhexahedral mesh within ANSYS Fluent Meshing, which was chosen for its superior accuracy and numerical stability, particularly for complex geometries like the TPMS structures. Polyhexahedral elements provide better continuity in fluid dynamics, which is crucial for simulating turbulent flows and capturing detailed flow gradients inside the porous medium. This mesh type also reduces numerical diffusion, ensuring a more reliable representation of the flow field and turbulence.

The mesh was refined in critical regions, such as the walls of the silencer and the pore boundaries, to properly capture the near-wall turbulence effects that play a significant role in both the pressure drop and acoustic performance. Boundary layer

inflation was applied to the mesh, particularly near the walls, ensuring that the turbulence near the boundary was well-resolved. A key objective of this refinement was to maintain a y+ value close to 1. The dimensionless wall distance, denoted as y, is a non-dimensional parameter used in Computational Fluid Dynamics (CFD) to describe the distance of the first mesh point from the wall in viscous flow simulations. It represents the ratio of inertial to viscous effects in the near-wall region and is defined based on the local fluid velocity, fluid properties, and distance from the wall. The value of y determines how well the boundary layer, particularly the viscous sublayer, is resolved. In the present study, y values are maintained close to 1 to ensure that the first grid point lies within the viscous sublayer, where velocity gradients are very steep and critical to accurately predicting wall shear stress and turbulence behavior. Maintaining y 1 allows the turbulence model to resolve the near-wall flow directly, rather than relying on empirical wall functions, thereby improving the accuracy of velocity distribution, pressure drop, and flow-induced acoustic predictions. This is particularly important for complex geometries such as TPMS-based silencers, where near-wall effects significantly influence overall flow and noise characteristics.

The base mesh size was set to 0.08 mm to ensure high resolution, particularly in regions where velocity gradients and turbulence effects are most pronounced. This refinement allowed for a detailed representation of flow and pressure fluctuations within the silencer, especially at the pore entrances and areas with high flow velocity or turbulence. The mesh was carefully distributed throughout the silencer body, with additional refinement near the pore openings and regions where flow separation and turbulence were expected. This distribution enabled the accurate modeling of both the pneumatic resistance and the acoustic attenuation performance.

The study involved five different mesh sizes, ranging from very coarse to very fine, with the number of elements and the corresponding pressure values shown in Table 3.2. The error percentage was calculated by comparing the pressure values obtained from each mesh size to the results obtained from the finer meshes. The results of the mesh independence study are summarized as follows: Very Coarse Mesh: With 1,248,736 elements, this mesh size yielded a pressure value of 3,185

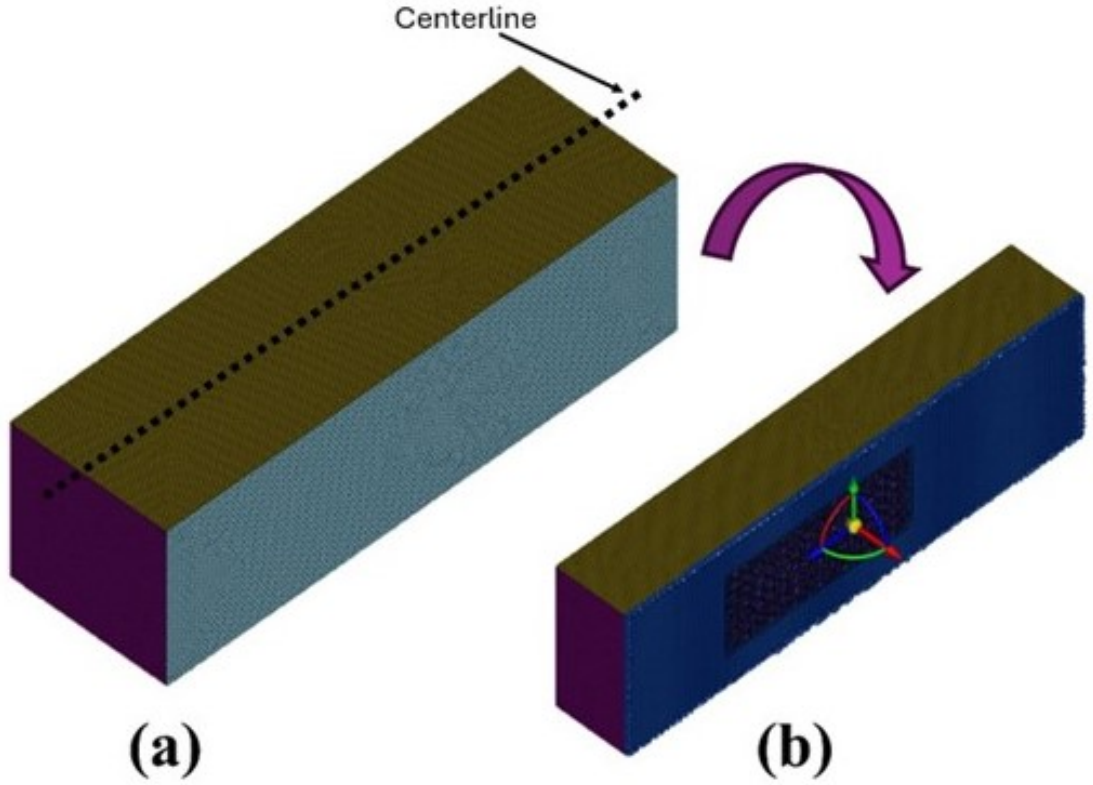

FIGURE 3.7: Mesh Generation (a) Isometric view (b) Cross-sectional view

Pa. Due to the significant difference in pressure compared to the finer meshes, this mesh was deemed unsuitable for the simulations. Coarse Mesh: The coarse mesh, with 2,903,415 elements, gave a pressure value of 3,028 Pa, resulting in an error of 5.2% when compared to the finer meshes. Medium Mesh: With 4,176,892 elements, the medium mesh produced a pressure value of 2,937 Pa, showing an error of 3.1%. While the error decreased, it was still deemed insufficient for high-accuracy simulations. Medium Mesh: With 4,176,892 elements, the medium mesh produced a pressure value of 2,937 Pa, showing an error of 3.1%. While the error decreased, it was still deemed insufficient for high-accuracy simulations. Very Fine Mesh: The very fine mesh, consisting of 8,102,764 elements, resulted in a pressure value of 2,914 Pa, with an error of 0.7%. Although the error was the smallest, the computational cost was significantly higher. After careful consideration of the computational cost and the error margin, the fine mesh with 6,589,240 elements was selected for the simulations in this study. This mesh provided a balance between accuracy and computational efficiency, with an acceptable error of 1.5% and a manageable increase in simulation time compared to the coarser meshes.

TABLE 3.2: Mesh independence Study

Sr. No.	Mesh sizes	No. of Elements	Pressure (Pa)	Error %
1	Mesh-1	1,248,736	3,185	-
2	Mesh-2	2,903,415	3,028	5.2
3	Mesh-3	4,176,892	2,937	3.1
4	Mesh-4	6,589,240	2,894	1.5
5	Mesh-5	8,102,764	2,914	0.7

3.4 Governing Equations

3.4.1 Navier–Stokes Equations

The motion of a compressible Newtonian fluid such as air is described by the Navier–Stokes equations, which consist of the continuity equation and the momentum conservation equation. In this study, the equations are solved in their RANS form to account for the statistically averaged behavior of turbulent flows.

3.4.2 Continuity Equation

The continuity equation expresses the conservation of mass in a compressible flow and is given by:

$$\frac{\partial \rho}{\partial t} + \nabla \cdot (\rho \mathbf{u}) = 0 \tag{3.4}$$

where: ρ is the fluid density, u is the velocity vector, and t is time.

This equation ensures that mass is conserved at every point within the fluid domain of the silencer.

3.4.3 Momentum Equation

The conservation of momentum for a compressible Newtonian fluid is described by the RANS momentum equation:

$$\frac{\partial(\rho\mathbf{u})}{\partial t} + \nabla \cdot (\rho\mathbf{u}\mathbf{u}) = -\nabla p + \nabla \cdot \left[\mu \left(\nabla\mathbf{u} + (\nabla\mathbf{u})^T\right)\right] - \nabla \cdot (\rho\mathbf{u}'\mathbf{u}') \tag{3.5}$$

where ρ is static pressure, μ is dynamic viscosity, and $\rho\mathbf{u}'\mathbf{u}'$ represents the Reynolds stresses.

In the Reynolds-Averaged Navier–Stokes (RANS) formulation, the instantaneous velocity field is decomposed into mean and fluctuating components, which introduces additional unknown terms known as Reynolds stresses. These stresses represent the effect of turbulent velocity fluctuations on the mean flow and appear as the Reynolds stress tensor, which must be modeled to close the system of equations. In the present study, the Reynolds stresses are approximated using the Boussinesq hypothesis, which assumes that the turbulent fluctuations can be related to the mean velocity gradients in a manner analogous to molecular viscosity.

According to this approach, the Reynolds stress tensor is expressed in terms of a turbulent (eddy) viscosity, which is calculated using the turbulence properties obtained from the standard k– model. Specifically, the turbulent viscosity is defined as a function of the turbulent kinetic energy (k) and its dissipation rate (), allowing the Reynolds stresses to be approximated as proportional to the mean rate of strain. This assumption simplifies the complex turbulent interactions into an isotropic form, making the problem computationally tractable while still providing reasonable accuracy for engineering flows.

The use of the Boussinesq approximation is justified in this study because the primary objective is to predict global flow characteristics such as pressure drop, velocity distribution, and overall turbulence behavior within TPMS-based silencer geometries. Although this approach may have limitations in capturing highly anisotropic turbulence, it is widely accepted for internal turbulent flows and provides a suitable balance between accuracy and computational efficiency.

3.4.4 Turbulence Modelling

Turbulence plays a dominant role in governing the flow behavior inside silencers, particularly when air passes through complex TPMS pore structures. Several turbulence models are available in ANSYS Fluent, including the *k–ω SST*, *Transition-SST*, *Reynolds Stress Model (RSM)*, and hybrid *RANS–LES* approaches. However, the standard k–ε turbulence model is adopted in the present study due to its robustness, numerical stability, and well-documented performance in internal duct flows and porous media applications [69].

The standard k–ε model solves two transport equations: one for the turbulent kinetic energy k and another for the turbulent dissipation rate ε. The k–ε turbulence model employs two transport equations in order to represent the essential physics of turbulent flows in a simplified and practical manner. The first equation governs the transport of turbulent kinetic energy (k), which quantifies the intensity of turbulence or the energy contained in velocity fluctuations. The second equation describes the transport of the rate of dissipation (ε), which represents how quickly this turbulent energy is converted into thermal energy due to viscous effects.

The use of these two variables allows the model to capture both the generation and dissipation mechanisms of turbulence. Specifically, k accounts for how turbulence is produced and distributed within the flow, while ε controls the rate at which turbulence decays. By solving these two coupled equations, the model can estimate the turbulent (eddy) viscosity, which is then used to approximate the Reynolds stresses in the RANS equations. Therefore, the two-equation formulation provides a balance between physical accuracy and computational efficiency, enabling reliable prediction of turbulence effects in complex flows such as those encountered in TPMS-based silencers.

3.4.4.1 Transport Equation for Turbulent Kinetic Energy (k)

$$\frac{\partial(\rho k)}{\partial t} + \nabla \cdot (\rho k \mathbf{u}) = \nabla \cdot \left[\left(\mu + \frac{\mu_t}{\sigma_k} \right) \nabla k \right] + G_k - \rho\varepsilon \tag{3.6}$$

3.4.4.2 Transport Equation for Dissipation Rate (ε)

$$\frac{\partial(\rho\varepsilon)}{\partial t} + \nabla \cdot (\rho\varepsilon \mathbf{u}) = \nabla \cdot \left[\left(\mu + \frac{\mu_t}{\sigma_\varepsilon} \right) \nabla\varepsilon \right] + C_{1\varepsilon}\frac{\varepsilon}{k}G_k - C_{2\varepsilon}\rho\frac{\varepsilon^2}{k} \tag{3.7}$$

In these equations, ρ represents the fluid density, and u denotes the mean velocity components in the spatial directions. The left-hand side of both equations consists of two terms: the first term $\frac{\partial}{\partial t}$ represents the transient (time-dependent) variation, while the second term $\rho k u$ represents convective transport of the variable (k or ε) by the mean flow.

On the right-hand side, the first term represents diffusion, which accounts for the spread of turbulence due to both molecular viscosity μ and turbulent (eddy) viscosity μ_t. The parameters σ_k and σ_ε are the turbulent Prandtl numbers for k and ε respectively, which control the rate of turbulent diffusion.

The term P_k denotes the production of turbulent kinetic energy, which arises due to the interaction between velocity gradients and turbulent fluctuations. Physically, it represents the transfer of energy from the mean flow to turbulent motion. In the k-equation, P_k acts as a source term, increasing turbulence levels.

The term $\rho\varepsilon$ in the k-equation represents the dissipation of turbulent kinetic energy, where turbulent energy is converted into internal energy due to viscous effects at small scales.

In the ε-equation, the term

$$C_1\rho\frac{\varepsilon}{k}P_k$$

represents the generation of dissipation rate, which is linked to the production of turbulence, while the term

$$C_2\rho\frac{\varepsilon^2}{k}$$

represents the destruction (or decay) of dissipation rate.

The turbulent viscosity μ_t, which is required to close the RANS equations, is computed using the relation:

$$\mu_t = C_\mu\rho\frac{k^2}{\varepsilon}$$

where C_μ is an empirical constant. The model constants C_1, C_2, σ_k, and σ_ε are determined from experimental data and are typically assigned standard values in the classical k–ε model.

The standard k–ε turbulence model was selected in the present study due to its proven robustness, computational efficiency, and reliability in simulating fully developed turbulent flows in engineering applications. The flow within TPMS-based silencers is characterized by high Reynolds number (8507 for our study), complex internal geometries, and significant turbulent mixing, particularly due to rapid changes in flow direction and porous structure interactions. Under such conditions, the k–ε model provides a stable and well-established framework for predicting the mean flow behavior.

3.5 Assumptions and Thermophysical Properties

Several assumptions were made to simplify the numerical simulations and focus on the primary pneumatic and acoustic characteristics of the TPMS-based porous silencers. First, air was assumed to behave as a Newtonian fluid, with constant viscosity, as the flow velocities and temperatures considered do not exhibit significant deviation from ideal fluid behaviors. Compressible flow was assumed due to the high-speed air entering the silencer at 50 m/s, leading to density variations that influence both the flow and sound propagation characteristics. The simulations were conducted under steady-state and transient conditions, assuming no heat transfer between the fluid and the solid boundaries, thus neglecting thermal effects. The flow was treated as fully turbulent, and the k- turbulence model was applied, with the assumption that the turbulence remains isotropic and fully developed within the flow domain. Additionally, idealized boundary conditions were applied, including a constant velocity inlet, a pressure outlet, and no-slip conditions at all solid surfaces.

To ensure a realistic representation of airflow inside the silencer, the thermophysical properties of air are defined based on standard atmospheric conditions. Density variations are computed using the ideal gas law, expressed as:

$$\rho = \frac{p}{RT} \tag{3.8}$$

where p denotes the static pressure, R is the specific gas constant for air which is 287 $\mathrm{J\,kg^{-1}\,K^{-1}}$, and T represents the absolute temperature.

The dynamic viscosity of air is assumed to be constant over the operating temperature range and is taken as $\mu = 1.7894 \times 10^{-5}$ $\mathrm{kg\,m^{-1}\,s^{-1}}$. The reference density of air under standard atmospheric conditions is approximately $\rho_0 = 1.225$ $\mathrm{kg\,m^{-3}}$.

The operating temperature in the present study is fixed at 296 K, corresponding to standard laboratory conditions and ensuring consistency with typical pneumatic–acoustic experiments.

By defining air properties through the ideal gas law and assuming constant viscosity, the numerical solver captures density variations induced by pressure fluctuations while maintaining numerical stability. These thermophysical specifications, together with the stated modeling assumptions, provide a reliable basis for accurately simulating compressible, unsteady airflow through TPMS-based porous silencer structures.

3.6 Boundary Conditions

The application of appropriate boundary conditions is essential for accurately capturing the physical flow behavior inside the porous silencers and ensuring numerical stability throughout the transient RANS simulation. In this study, the boundary conditions are defined to reflect realistic operating conditions for internal duct flow while enabling the analysis of flow-induced acoustic fluctuations. Each boundary condition plays a specific role in establishing how air enters, interacts with, and exits the TPMS-based silencer geometry.

A velocity inlet condition is applied at the upstream end of the silencer. The inlet velocity is set to 50 m/s, representing a high-speed airflow environment typical of industrial ventilation, automotive mufflers, or acoustic damping systems [70]. The direction normal to the inlet plane is used, and the solver computes density variations based on the compressible flow formulation. At the downstream end

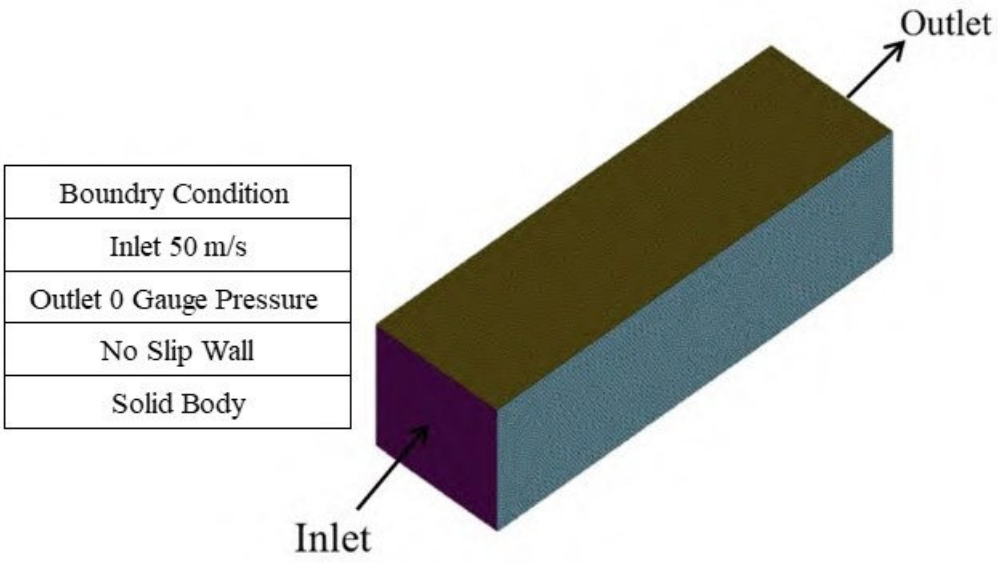

FIGURE 3.8: Boundary Conditions

of the silencer, a pressure outlet boundary condition is applied, with an assigned zero-gauge static pressure. This condition allows the flow to exit freely while letting the solver adjust density and velocity fields based on internal flow dynamics. The pressure outlet also accommodates reverse flow if necessary, a common occurrence during vortex shedding and pressure-wave reflection in transient simulations. All solid surfaces, including the silencer walls and the surfaces of the TPMS porous structures, are assigned a no-slip wall boundary condition. This means that the velocity of air at the wall surface is zero relative to the solid boundary. The no-slip condition ensures accurate prediction of viscous effects, boundary-layer development, and near-wall turbulence, all of which significantly influence pressure drop and acoustic behavior inside porous media.

3.7 Solver Settings and Discretization Schemes

The transient, compressible nature of the flow requires a robust pressure–velocity coupling method to accurately resolve dynamic pressure and density variations. For this purpose, the coupled scheme is employed. In the coupled algorithm, the momentum and continuity equations are solved simultaneously, which enhances stability and accelerates convergence for high-speed and compressible flows. This scheme is particularly effective when modelling flows involving rapid changes in pressure and velocity inside porous media, where pressure wave propagation and turbulence interactions are critical for acoustic performance evaluation. The coupled approach ensures tight coupling between pressure and velocity fields, which is essential for capturing transient flow-induced noise characteristics.

To obtain accurate numerical solutions, appropriate spatial and temporal discretization schemes are employed. The Green–Gauss node-based method is selected for polyhedral meshes. Green–Gauss node-based method calculates gradients using surrounding cell values by converting volume integrals into surface integrals, and then averages them at nodes. It is simple, efficient, and suitable for unstructured meshes. The momentum equations are initially discretized using the first-order upwind scheme. The turbulence transport equations for turbulent kinetic energy (k) and dissipation rate (ε) are also discretized using the first-order upwind method, which provides stable and robust solutions within the highly complex flow regime of porous TPMS structures. Numerical stability is particularly important in this context due to the presence of abrupt local velocity gradients and intense turbulent mixing within the interconnected pore pathways. Temporal discretization is performed using a first-order implicit scheme, which is well suited for unsteady compressible flows and allows the use of relatively larger time steps without compromising numerical stability. This approach effectively captures transient flow features such as vortex shedding and pressure oscillations. The residual convergence criterion is set to 1×10^{-6}, ensuring that each time step converges adequately before advancing to the next. This stringent convergence threshold guarantees accurate resolution of small-scale pressure fluctuations that are critical for subsequent acoustic analysis.

3.8 Time Step Calculation

Time-step selection is critical in transient simulations, particularly for resolving unsteady flow phenomena in porous silencers. An excessively large time step may lead to numerical instability or loss of important transient details, whereas an overly small time step significantly increases computational cost. To achieve an optimal balance between numerical accuracy and computational efficiency, the time step is determined based on the Courant–Friedrichs–Lewy (CFL) condition, defined as:

$$C_0 = \frac{u\,\Delta t}{\Delta x} \tag{3.11}$$

where C_0 is the Courant number, u denotes the characteristic velocity, Δt is the time step, and Δx represents the minimum mesh size.

To ensure numerical stability and accurately capture unsteady flow features, the Courant number is maintained below unity. Courant number is kept below 1 in explicit schemes to ensure stability, meaning flow should not cross more than one cell per time step. Using a minimum mesh spacing of 0.08 mm and an inlet velocity of 50 $\mathrm{m\,s^{-1}}$, the time step is calculated as:

$$\Delta t = \frac{C_0\,\Delta x}{u} \tag{3.12}$$

Substituting the corresponding values yields a time step of:

$$\Delta t = 3.6 \times 10^{-7}\ \mathrm{s} \tag{3.13}$$

This sufficiently small time step ensures accurate resolution of transient flow features such as vortex shedding, oscillatory flow structures, and unsteady pressure fluctuations. A total of 2868 time steps are simulated, providing adequate temporal resolution to analyze flow-induced acoustic behavior and to compare the performance of Gyroid, Diamond, and Primitive TPMS-based silencer configurations.

3.9 Validation Study

To verify the accuracy and reliability of the present numerical methodology, a validation study was conducted by comparing the acoustic results of the current work with the experimental data reported by Giorleo et al [71]. The comparison was performed using the Sound Absorption Coefficient and the corresponding peak absorption frequency for TPMS-based porous structures. As shown in Figure 3.9,

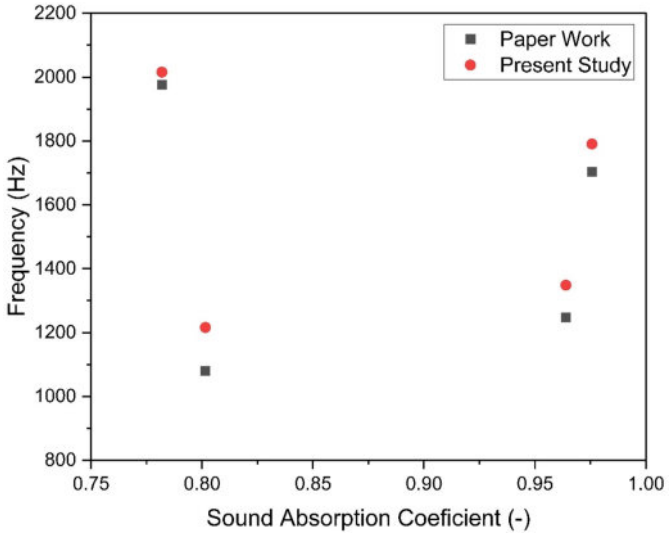

FIGURE 3.9: Validation

the present numerical predictions demonstrate good agreement with the published experimental results. The literature reported a maximum absorption coefficient of approximately 0.98 at around 1700 Hz, whereas the present study predicted a similar absorption coefficient at approximately 1790 Hz, corresponding to an error of nearly 5.3%. Similarly, another TPMS configuration showed an absorption coefficient of approximately 0.78 at around 1980 Hz in the literature, while the present simulation predicted approximately 2015 Hz, resulting in an error of about 1.8%. The low percentage error and close agreement confirm the reliability of the adopted modeling approach for predicting the acoustic performance of TPMS-based porous silencers.

Chapter 4

Results and Discussion

This chapter presents the results and discussions based on the numerical simulations of porous pneumatic silencers, incorporating Gyroid, Diamond, and Primitive TPMS structures. The primary aim of this chapter is to examine and compare the flow behavior and acoustic performance of each configuration under identical conditions. The results are discussed systematically, focusing on key parameters such as pressure, temperature, velocity, and streamline contours, along with sound pressure level (SPL) spectra. The Ffowcs Williams–Hawkings (FW-H) acoustic model was used to calculate the far-field SPL, which is a critical component of this analysis. This chapter aims to provide insights into how each TPMS structure influences flow dynamics and noise attenuation. The results are divided into two primary categories:

i. Flow characteristics Results – including pressure, velocity, temperature, and streamline contours for all structures.

ii. Acoustic Performance Results – including SPL vs. frequency and A-weighted SPL vs. frequency graphs for all structures, measured using 11 receivers placed in the simulation.

Each set of results is analyzed to determine the relationship between flow features (such as pressure loss and turbulence) and acoustic performance (sound attenuation

and frequency response). By comparing the Gyroid, Diamond, and Primitive structures, the effectiveness of each configuration in reducing pneumatic noise is evaluated.

4.1 Flow Characteristics of TPMS based Silencer

4.1.1 Pressure Distribution and Pressure Drop

The pressure contours for the three TPMS-based porous silencer structures, Diamond, Gyroid, and Primitive are presented in Figure 4.1, highlighting the pressure distribution across the silencer geometries. The contours reflect the pressure variations induced by the interaction of airflow with the porous structures, illustrating the extent of flow resistance and energy dissipation in each configuration.

The pressure distribution in the Diamond structure (Figure 4.1(a)) shows a significant pressure drop at the inlet, with higher pressure zones forming at the pore entrances. The pressure drop is relatively uniform throughout the length of the silencer, suggesting that the Diamond geometry offers a moderate resistance to flow. The flow expansion and contraction within the pores result in a smooth transition in pressure, with lower pressure gradients compared to the Primitive structure. This indicates that the Diamond structure provides a balanced resistance and is effective at dissipating flow energy while maintaining manageable pressure losses.

In the Gyroid structure (Figure 4.1(b)), the pressure drop is noticeably less compared to the Diamond and Primitive structures. The pressure contour highlights a more uniform distribution of pressure across the silencer. This smooth gradient suggests that the Gyroid's continuous, curved surface facilitates better flow management with fewer disruptions or separations in the airflow. The lower pressure drop across the Gyroid structure indicates its superior efficiency in reducing resistance while still achieving effective energy dissipation, making it the most pneumatically efficient design among the three.

The Primitive structure (Figure4.1(c)) shows the highest pressure drop, particularly at the inlet where the flow is more restricted by the less connected and more irregular pore network. The pressure contours indicate a significant pressure increase at the pore openings and a sharper pressure decay through the length of the silencer. The geometry of the Primitive structure results in higher flow turbulence and localized energy dissipation, leading to an increased pressure drop. This behavior highlights that while the Primitive structure may provide strong noise attenuation, it comes with a higher pneumatic penalty.

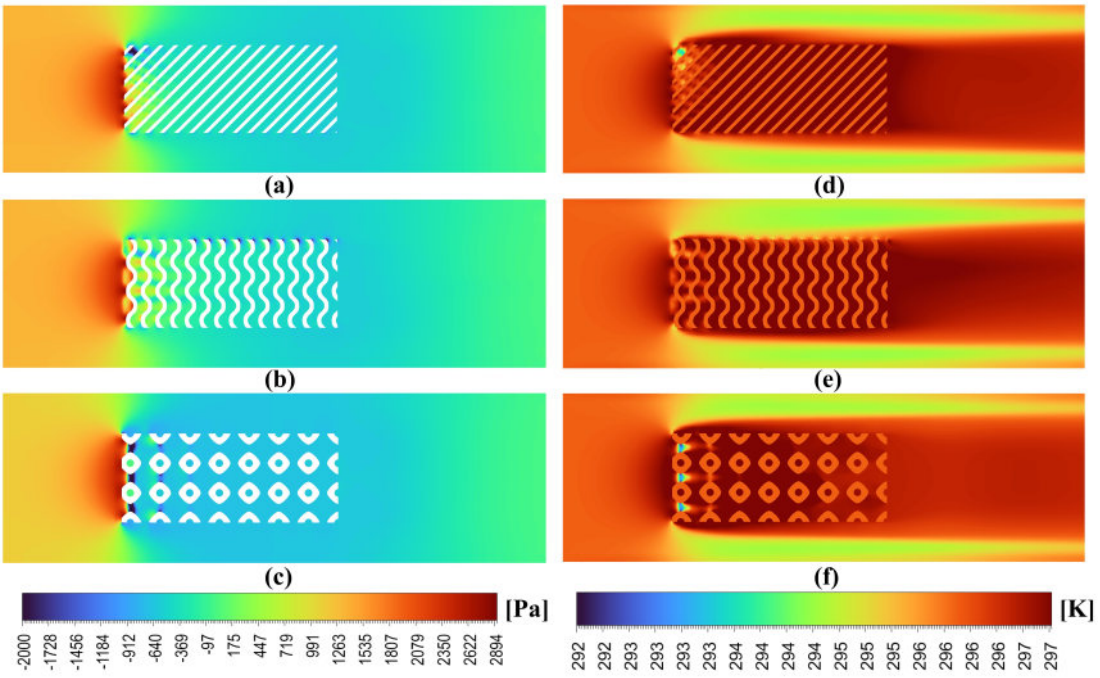

FIGURE 4.1: Pressure and Temperature contour distribution inside the porous silencer for Diamond (a-d), Gyroid (b-e) and Permitive (c-f) structures

4.1.2 Temperature Distribution and Thermal Behavior

The temperature contours for the Diamond, Gyroid, and Primitive TPMS-based porous silencers are also shown in Figure 4.1. The contours reveal how airflow interacts with the porous structures, and how the structures influence heat dissipation and temperature distribution across the silencer. Temperature variations inside the silencers are influenced by flow resistance, pressure losses, and the resulting energy dissipation due to turbulence.

The temperature distribution in the Diamond structure (Figure 4.1(d)) shows a relatively uniform thermal profile across the silencer. The temperature gradient near the inlet is small, with only slight variations observed inside the silencer. This suggests that the Diamond structure facilitates efficient heat transfer and prevents significant thermal buildup. The flow through the pores in the Diamond structure appears to maintain a stable temperature distribution without introducing major disruptions in thermal equilibrium. The temperature near the inlet is slightly higher, which is typical in flow systems where the energy input from the high-speed airflow is dissipated gradually through the porous structure.

The temperature contour for the Gyroid structure (Figure 4.1(e)) shows a similarly uniform temperature distribution, though with slightly more pronounced variations compared to the Diamond structure. The temperature in the Gyroid silencer increases slightly in the regions where the flow experiences rapid deceleration and turbulence. This indicates that while the Gyroid structure offers efficient flow management, there are localized regions within the pores where some thermal buildup occurs due to vortex formation and the interaction of the flow with the surface. However, the overall temperature variation remains within a narrow range, reflecting the efficient heat transfer capabilities of the Gyroid configuration.

In the Primitive structure (Figure 4.1(f)), the temperature distribution is slightly more variable, with more pronounced thermal gradients near the pore openings. The temperature near the inlet increases significantly, indicating higher energy dissipation within the restrictive pore network. The temperature variations are more localized within the silencer, suggesting that the Primitive structure's more complex and less interconnected pore geometry leads to greater resistance to airflow and heat buildup. The localized thermal hotspots suggest that the flow undergoes higher levels of turbulence and velocity fluctuations, which dissipate more heat in concentrated areas. This results in a greater overall temperature gradient within the silencer.

To examine the thermal behavior of the airflow throughout the porous silencer, temperature contours were also evaluated at six different cross-sectional planes located along the axial direction of the TPMS structure. The selected planes were

positioned at 0.0001 m, 0.01 m, 0.02 m, 0.03 m, 0.04 m, and 0.05 m from the inlet section of the silencer. These planes provide a detailed representation of temperature distribution and thermal evolution as the airflow propagates through the porous medium.

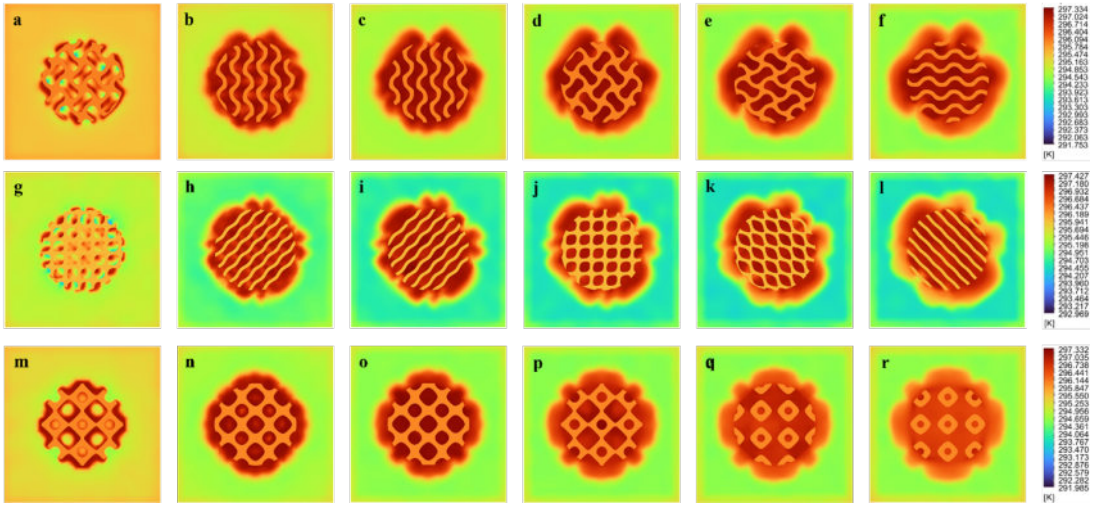

FIGURE 4.2: Temperature Contours at Different Cross-Sectional Planes for Gyroid (a-f), Diamond (g-l) and Primitive (m-r) structures

As shown in Figure 4.2, the temperature contours indicate noticeable variations in thermal distribution across different TPMS geometries and flow locations. Near the inlet region (0.0001 m), relatively uniform temperature fields are observed due to the initial interaction of the airflow with the porous structure. As the flow progresses through the silencer, localized high-temperature regions develop around the solid surfaces and narrow flow passages because of turbulence generation, viscous dissipation, and enhanced fluid–surface interaction within the porous medium.

At intermediate planes (0.01 m0.03 m), the temperature contours exhibit more pronounced non-uniformity, indicating stronger mixing and thermal exchange between the airflow and the TPMS structure. Further downstream (0.04 m0.05 m), the temperature distribution becomes comparatively smoother as the flow stabilizes and thermal gradients gradually decrease. The contours also demonstrate that the geometry and pore arrangement significantly influence the thermal field by controlling local flow recirculation and turbulence intensity. Overall, the temperature contour analysis provides valuable insight into the thermal characteristics of the

porous silencer and highlights the effect of TPMS geometry on heat distribution and flow behavior along the silencer length.

4.1.3 Velocity Distribution and Flow Structure

The velocity contours for the three TPMS-based porous silencers Diamond, Gyroid, and Primitive are presented in Figure 4.3. These contours provide a visual representation of the velocity distribution inside each silencer structure, highlighting how airflow interacts with the porous cores and how different pore geometries influence flow acceleration, deceleration, and turbulence. In the Diamond structure (Figure 4.3(a)), the velocity distribution exhibits a relatively uniform flow pattern with moderate acceleration near the inlet and gradual deceleration as the flow passes through the porous medium. The contours show that the flow is slightly constricted near the pore openings, leading to localized velocity increases. This suggests that the Diamond structure causes less disruption to the flow than more complex geometries, allowing for smoother passage of air while still providing sufficient resistance to dissipate energy. The velocity is highest at the pore entrances, with a smooth transition downstream. This flow behavior indicates a balanced pneumatic resistance that contributes to moderate pressure loss while maintaining manageable flow velocity.

For the Gyroid structure (Figure 4.3(b)), the velocity contours reveal a more uniform flow distribution across the entire silencer. The flow experiences fewer velocity fluctuations and less constriction within the pores compared to the Diamond structure, reflecting the continuous, curved nature of the Gyroid's pore surfaces. The velocity is generally lower near the inlet compared to the other structures, indicating that the Gyroid configuration facilitates smoother flow paths with reduced acceleration. This result suggests that the Gyroid structure has superior flow management capabilities, allowing air to pass through with lower resistance and fewer disruptions, leading to a more uniform velocity profile across the length of the silencer. The smoother velocity distribution is likely a contributing factor to its lower pressure drop observed in previous results.

The Primitive structure (Figure 4.3(c)) shows a much more complex velocity distribution with significant variations across the silencer. The velocity is highest at the inlet, where the flow is compressed into the smaller, less interconnected pores. The flow through the Primitive structure exhibits high local acceleration followed by sudden decelerations due to the irregular pore structure and flow constrictions. The contours indicate that the flow through the Primitive silencer is highly disrupted, leading to high velocity gradients and turbulent regions near the pore openings. This results in increased energy dissipation and a larger pressure drop, as discussed in previous sections. The flow behavior is more chaotic compared to the Diamond and Gyroid structures, suggesting that while the Primitive structure may provide significant turbulence and noise reduction, it comes at the cost of higher flow resistance. These findings indicate how each TPMS configuration manages airflow differently. The Gyroid structure proves to be the most efficient in terms of smooth flow distribution, with the least disruption, while the Primitive structure creates more chaotic flow patterns that likely contribute to higher turbulence and noise attenuation but also result in significant pressure losses. The Diamond structure falls in between, offering a balanced approach to both flow management and energy dissipation. To investigate the flow behavior inside the porous silencer, velocity

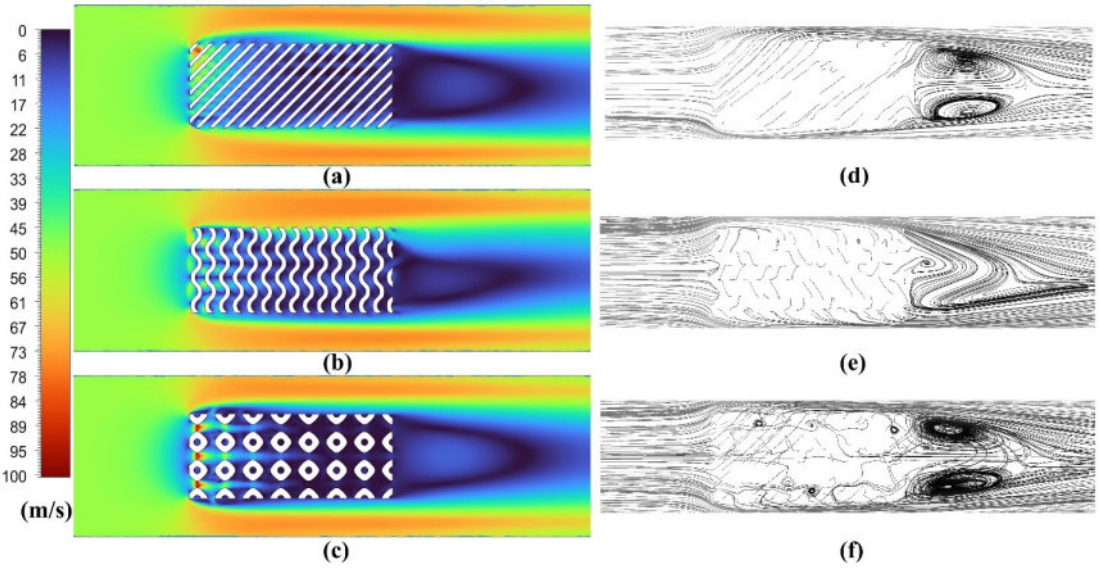

FIGURE 4.3: Velocity and Streamline contours distribution inside the porous silencer for Diamond (a-d), Gyroid (b-e) and Permitive (c-f) structures

contours were analyzed at six different cross-sectional planes located at 0.0001 m,

0.01 m, 0.02 m, 0.03 m, 0.04 m, and 0.05 along the axial direction of the TPMS structure. These sectional planes provide a detailed understanding of the velocity distribution and flow development throughout the porous medium.

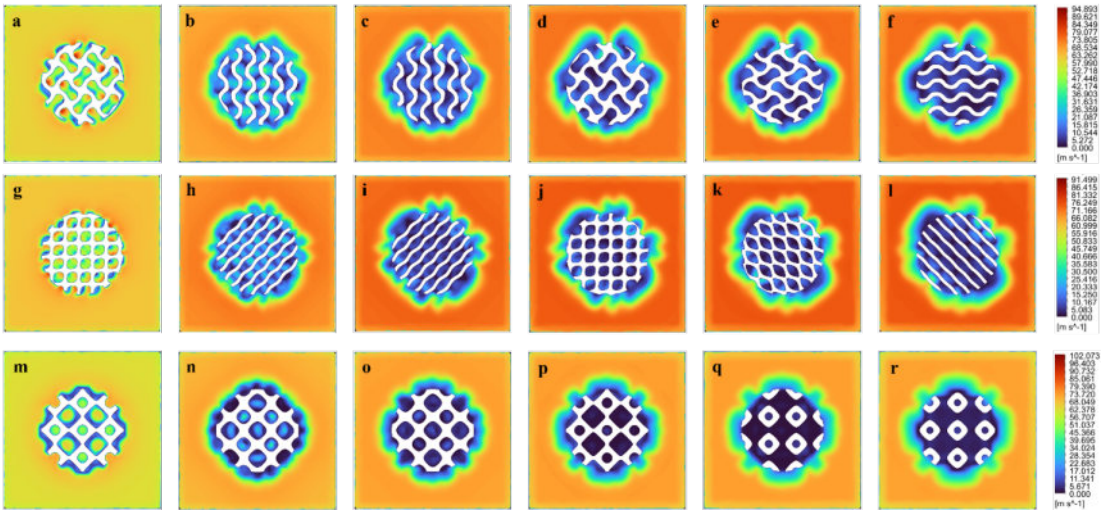

FIGURE 4.4: Velocity Contours at Different Cross-Sectional Planes for Gyroid (a-f), Diamond (g-l) and Primitive (m-r) structures

As illustrated in Figure 4.4, the velocity contours show significant variations in flow magnitude and distribution due to the influence of the TPMS geometry and pore arrangement. At the inlet region (0.0001 m), the airflow exhibits relatively higher and more uniform velocity profiles before entering the porous structure. As the fluid progresses through the silencer, the velocity decreases within the porous region because of flow resistance, viscous effects, and turbulence generation caused by the complex internal geometry. In the intermediate sections (0.01 m0.03 m), localized low-velocity regions and non-uniform flow patterns become more prominent due to the interaction between the airflow and the solid surfaces of the TPMS structure. The contours also indicate the formation of recirculation zones and enhanced turbulence near the pore walls, which contribute to energy dissipation and acoustic attenuation. Further downstream (0.04 m0.05 m), the velocity field gradually stabilizes as the flow adjusts after passing through the porous medium. The results demonstrate that the TPMS geometry significantly influences the internal flow characteristics by controlling flow pathways, turbulence intensity, and velocity gradients. Therefore, the velocity contour analysis provides important insight into the aerodynamic performance of the porous silencer and its role in flow-induced noise reduction.

4.1.4 Streamline Distribution

The streamline contours for the three TPMS-based porous silencers Diamond, Gyroid, and Primitive are also shown in Figure 4.3. The streamline patterns reveal how the airflow interacts with the internal geometry of each silencer structure and provide insight into the flow path characteristics, including vortex formation and regions of recirculation. Streamlines are a powerful tool for visualizing the flow direction, velocity variations, and the presence of flow separation, which are essential for understanding the pneumatic performance of the silencers. In the Diamond structure (Figure 4.3(d)), the streamlines show that the flow experiences moderate expansion and contraction within the pore network. There is noticeable acceleration at the pore entrances, followed by a gradual deceleration as the flow traverses the porous core. The streamlines illustrate the formation of localized vortices at the edges of the pores, which suggests that the Diamond structure induces some degree of flow separation and turbulence, particularly at the pore junctions. However, the flow recovers quickly and follows smooth paths, indicating that the Diamond structure allows for efficient flow through the silencer while still providing resistance to energy dissipation. The overall streamline pattern suggests that the Diamond geometry balances flow disruption and energy loss.

The Gyroid structure (Figure 4.3(e)) exhibits a more uniform streamline pattern compared to the Diamond structure. The flow through the Gyroid pores is smoother, with less flow separation and fewer vortex formations. The streamlines indicate that the Gyroid's continuous, curved surfaces facilitate a more coherent flow distribution with fewer localized recirculation zones. This implies that the Gyroid structure minimizes turbulence and flow loss, allowing for a more efficient flow path. The smoother streamline distribution reflects the Gyroid's ability to reduce pressure drop while effectively managing the flow through the silencer. The minimal vortex shedding and flow separation further support the Gyroid structure as a highly efficient design in terms of both flow management and noise attenuation.

In the Primitive structure (Figure 4.3(f)), the streamlines reveal a more chaotic flow pattern with significant flow separation and vortex formation near the pore

openings. The streamlines indicate that the flow accelerates sharply as it enters the pores and then experiences significant deceleration, leading to the formation of large-scale vortices. These vortices contribute to turbulence, which is likely responsible for the higher-pressure loss observed in the Primitive structure. The presence of multiple recirculating flow regions and disrupted streamline paths suggests that the Primitive structure creates more turbulence, enhancing acoustic damping but at the cost of increased flow resistance. The chaotic nature of the flow indicates that the Primitive structure might be effective at noise reduction, especially at higher turbulence levels, but it also causes substantial pneumatic penalties. The Gyroid structure, with its smoother flow distribution and minimal vortex formation, appears to be the most pneumatically efficient design. In contrast, the Primitive structure generates more turbulence and flow separation, which could contribute to higher noise attenuation at the cost of significant pressure loss. The Diamond structure provides a balanced approach, showing moderate flow disruptions and corresponding pressure losses.

4.2 Acoustic Performance

4.2.1 Sound Pressure Level vs Frequency Graph for Diamond Structure

Figure 4.5 shows the Sound Pressure Level (SPL) as a function of frequency for the Diamond structure. The frequency range extends from 0 Hz to 10,000 Hz, covering both low and high-frequency regions, which is essential for understanding the silencer's broadband noise attenuation capability. At lower frequencies (0-1000 Hz), the SPL values are relatively high, indicating that the Diamond structure offers less attenuation in this frequency range. The overall sound pressure levels remain above 60 dB for most receivers, with certain peaks at specific frequencies. In the mid-frequency range (1000 Hz to 5000 Hz), the SPL shows significant fluctuations. There are prominent peaks and valleys, reflecting the silencer's ability to reduce certain frequencies while allowing others to pass through more easily. This is indicative of

the complex interference patterns created by the porous Diamond structure, where sound waves interact with the pore geometry. At higher frequencies (above 5000 Hz), the SPL decreases steadily for most receivers, indicating that the Diamond structure is more effective at attenuating high-frequency noise. However, some receivers still exhibit higher SPL levels around 6000 Hz, which could be linked to specific resonance frequencies or flow interactions with the TPMS geometry. There

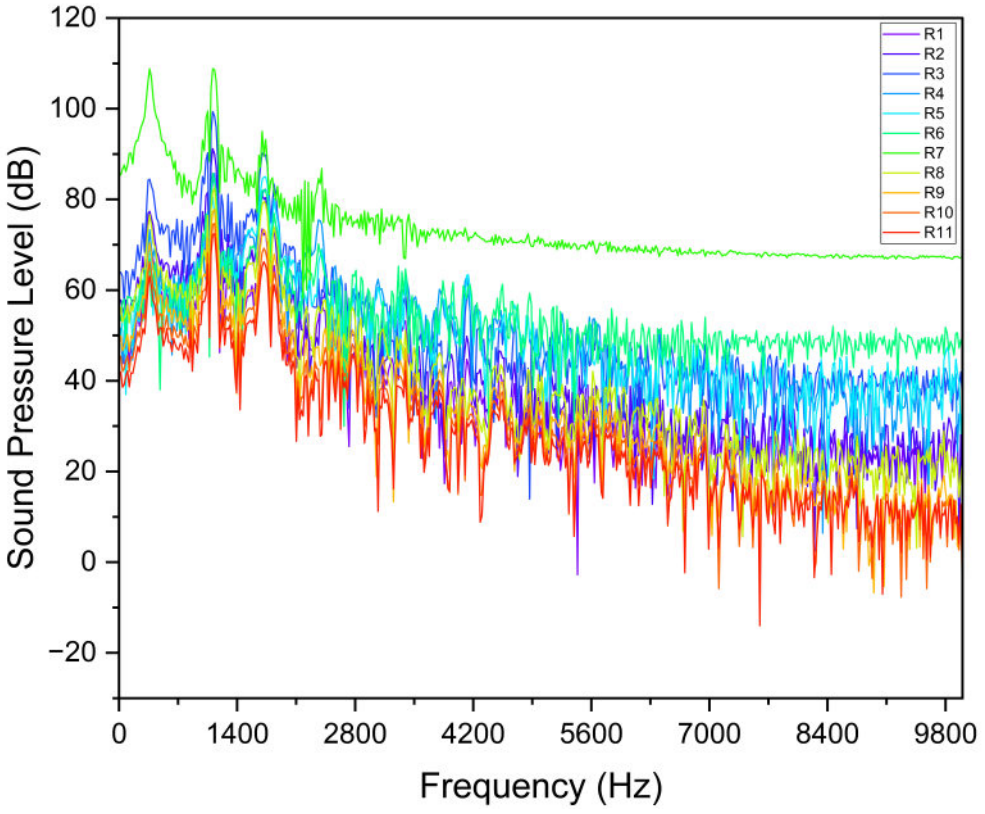

FIGURE 4.5: Sound Pressure Level (SPL) vs .frequency for the Diamond TPMS structure

is noticeable variability in the SPL response between different receivers, particularly at the low and mid-frequency ranges. Receivers R1 (green) and R11 (red) show the highest SPL values, while others, such as R7 (yellow), R9 (orange), and R3 (blue), exhibit lower SPLs, indicating that sound pressure levels vary depending on the position of the receiver within the silencer. This variability suggests that the Diamond structure's acoustic performance may be position-dependent, likely due to flow disturbances or pressure gradients within the porous medium.

4.2.2 Sound Pressure Level vs Frequency Graph for Gyroid Structure

Figure 4.6 shows the Sound Pressure Level (SPL) as a function of frequency for the Gyroid TPMS structure. The data is collected from 11 receivers (R1 to R11) placed at different points. The SPL values at lower frequencies (0-1000 Hz) are consistently high, with certain receivers showing significantly elevated SPL levels. This indicates that the Gyroid structure does not effectively attenuate low-frequency noise, which is typical for many porous silencer designs. The SPL values in this range are generally above 70 dB for most receivers, with some peaks exceeding 80 dB. These elevated SPLs suggest that the Gyroid structure might not be highly effective in reducing low-frequency noise.

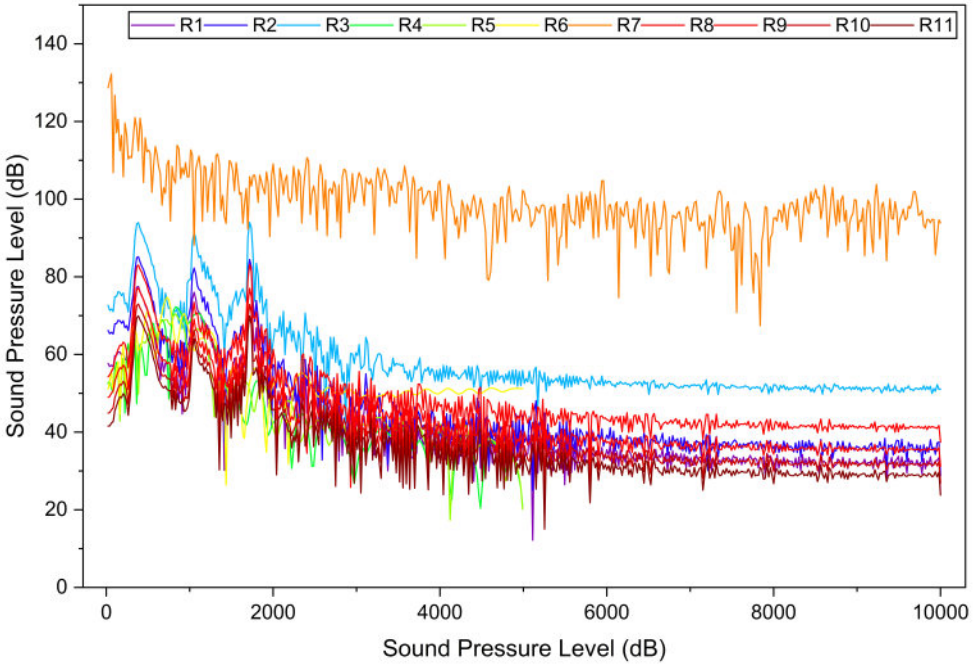

FIGURE 4.6: Sound Pressure Level (SPL) vs. frequency for the Gyroid TPMS structure

As the frequency increases from 1000 Hz to 5000 Hz, there is a noticeable reduction in SPL, indicating improved attenuation. The SPL for most receivers begins to decrease steadily, particularly around the 2000-3000 Hz range. The mid-frequency region (1000-5000 Hz) shows more uniform SPL values across the receivers, suggesting that the Gyroid structure is more efficient in reducing mid-range frequencies.

The SPL decreases further at higher frequencies (above 5000 Hz), with values generally stabilizing below 60 dB for most receivers. This indicates that the Gyroid structure performs well in attenuating high-frequency noise, as the SPL values drop significantly in the higher-frequency ranges. The overall SPL at frequencies above 5000 Hz is much lower compared to the low and mid-frequency regions, confirming the Gyroid's effective noise reduction at higher frequencies.

4.2.3 Sound Pressure Level vs Frequency Graph for Primitive Structure

Figure 4.7 shows the Sound Pressure Level (SPL) as a function of frequency for the Primitive TPMS structure. The data was collected from 11 receivers (R1 to R11) placed at different points, providing a comprehensive evaluation of its acoustic performance across different locations. The SPL values are measured in decibels (dB) across the frequency range from 0 Hz to 10,000 Hz. At lower frequencies (0-1000 Hz), the SPL values remain relatively high, consistently above 60 dB across the receivers, with some peaks reaching up to 80 dB. These high SPL values suggest that the Primitive structure is less effective at attenuating low-frequency noise, which is common for many porous designs. However, certain regions within the silencer (e.g., around R1 and R11) exhibit slightly higher levels of sound pressure, indicating that low-frequency noise propagation remains prominent in some locations. As the frequency increases from 1000 Hz to 5000 Hz, the SPL shows a more pronounced decrease. There are several peaks and valleys along the SPL curve, reflecting how the Primitive structure interacts with specific frequencies. The SPL values generally stabilize in the range between 40-60 dB, suggesting some level of noise reduction, particularly for mid-frequency components. The SPL variation across the receivers becomes more evident at this stage, with certain receivers (such as R3 and R5) showing better attenuation. At higher frequencies (above 5000 Hz), the SPL decreases sharply for most receivers, reaching levels below 50 dB. The Primitive structure appears to be more effective at attenuating high-frequency noise, with SPL values dropping significantly in this range. However, there is still considerable variability in SPL across different receivers, especially around 7000 Hz,

where the SPL remains higher for receivers like R1 and R2. This indicates that, while the Primitive structure excels in high-frequency noise attenuation, there are specific frequency bands where noise transmission is less effectively damped. As observed from the diverse SPL responses across receivers, the acoustic performance varies depending on the position within the silencer. For instance, receivers R1 and R11 show higher SPL values throughout the frequency spectrum, while others like R6 and R9 exhibit lower SPLs, especially at higher frequencies. This suggests that sound pressure levels are influenced by the placement of the receivers within the flow field and the turbulence generated by the Primitive structure's pore configuration. Overall, the Primitive structure provides significant attenuation

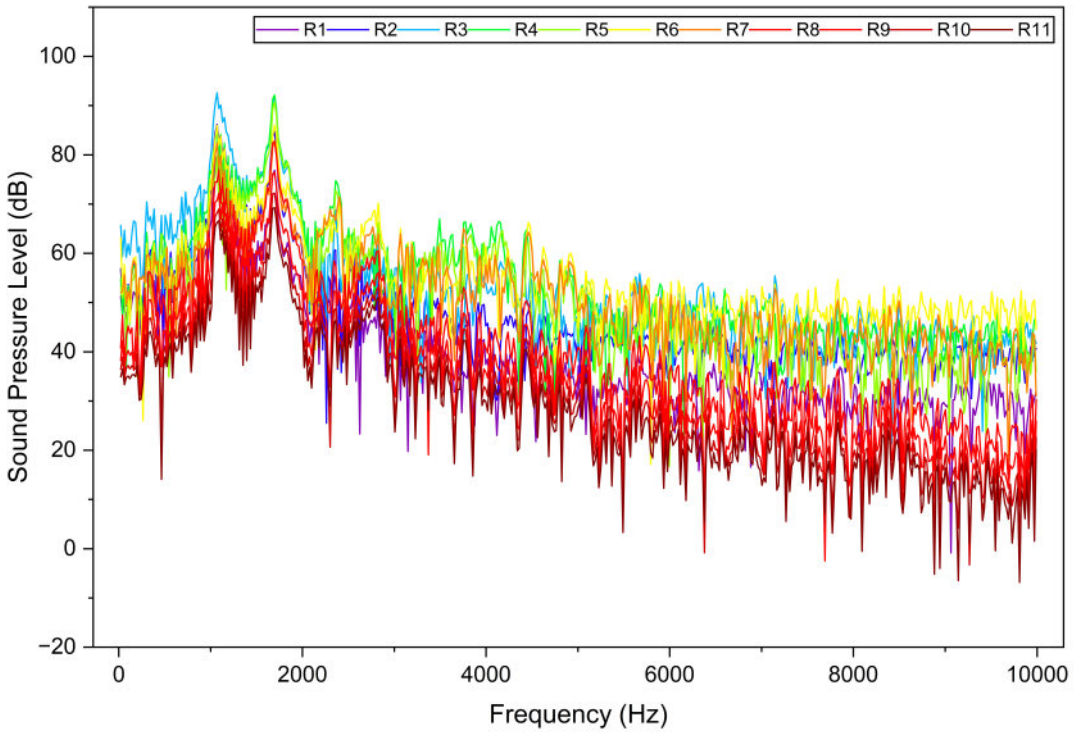

FIGURE 4.7: Sound Pressure Level (SPL) versus frequency for the Primitive TPMS Structure

at higher frequencies, though its performance is less effective at low frequencies. The variability in receiver responses indicates that the silencer's performance is spatially dependent, likely due to localized flow disturbances and turbulence within the porous media.

4.2.4 Frequency versus Sound Pressure Level Analysis at Vertical Receiver Planes

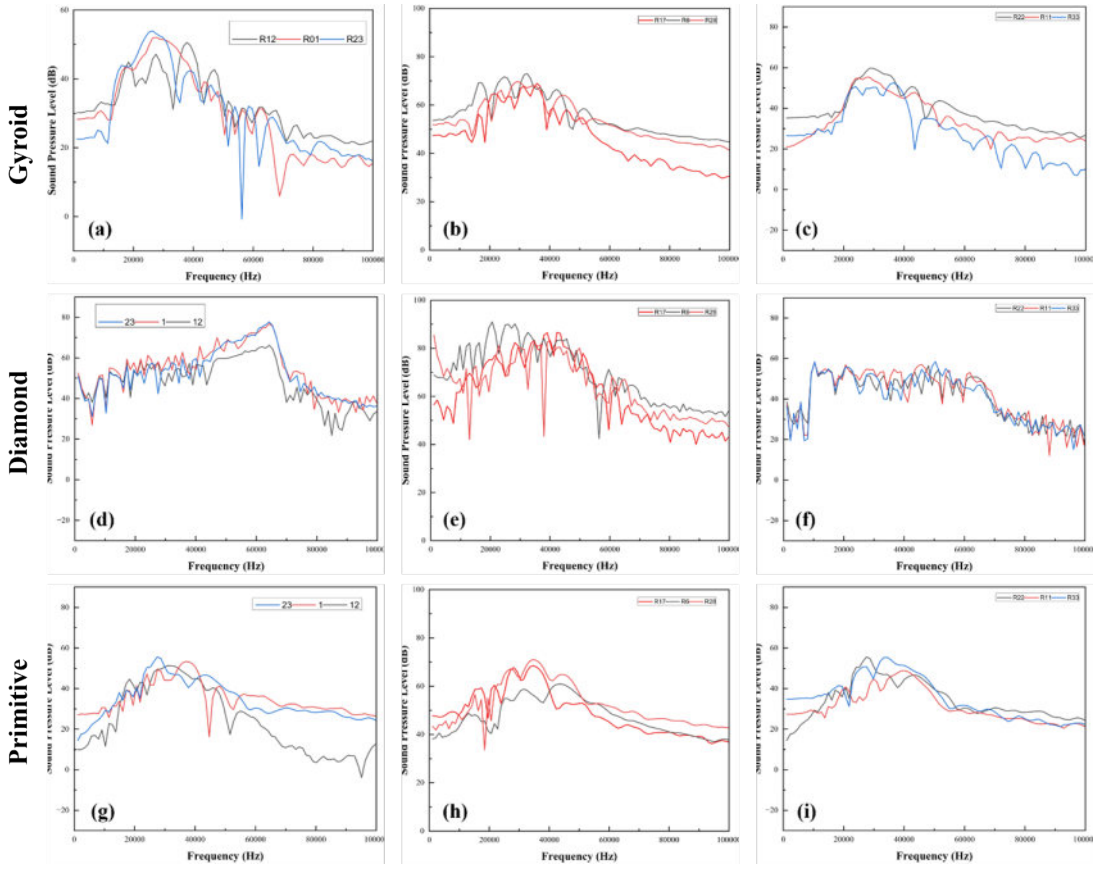

FIGURE 4.8: Frequency versus Sound Pressure Level (SPL) Analysis at Vertical Receiver Planes for Gyroid (a-c), Diamond (d-f) and Primitive (g-i) structures

Figure 4.8 presents the variation of Sound Pressure Level (SPL) with frequency for the three TPMS-based silencer structures at different receiver planes located along the axial direction of the silencer. The SPL responses were evaluated at the inlet plane (R12–R1–R23), center plane (R17–R6–R28), and outlet plane (R22–R11–R33) to investigate the spatial evolution of acoustic attenuation throughout the porous medium.

The graphs indicate that all structures exhibit frequency-dependent acoustic behavior, with SPL values generally increasing in the low-to-mid frequency range before gradually decreasing at higher frequencies. At the inlet plane, significant fluctuations in SPL are observed due to the strong interaction between the incoming airflow and the porous geometry, which generates turbulence and pressure

disturbances. In the central plane, the SPL curves show comparatively higher peak values and broader frequency distributions, indicating enhanced flow mixing and acoustic activity within the porous structure. At the outlet plane, the SPL values generally decrease and become smoother, demonstrating the attenuation and stabilization of acoustic waves as the flow propagates through the silencer. The results further show that the different TPMS geometries produce distinct acoustic responses because of variations in pore arrangement and flow pathways. Some structures exhibit sharper SPL peaks and stronger fluctuations, while others show smoother attenuation behavior over a wider frequency range. In particular, the reduction in SPL at higher frequencies indicates the effectiveness of the porous structures in dissipating acoustic energy and reducing flow-induced noise.

4.2.5 A-Weighted Sound Pressure Level vs Frequency for Diamond Structure

Figure 4.9 presents the A-weighted Sound Pressure Level (SPL) as a function of frequency for the Diamond TPMS structure, The SPL values are shown in decibels (dBA), with frequency ranging from 0 Hz to 8000 Hz. At lower frequencies (0-1000 Hz), the SPL values are relatively high, indicating that the Diamond structure is less effective at attenuating low-frequency noise. The SPL values for most receivers are above 60 dBA, with certain peaks reaching up to 80 dBA. This suggests that the Diamond structure may not provide significant noise reduction at lower frequencies, and further design optimization may be required for enhanced low-frequency attenuation. As the frequency increases from 1000 Hz to approximately 4000 Hz, the SPL values exhibit a noticeable reduction, particularly in the R1 (purple) and R11 (red) receivers, which show the highest levels of SPL at lower frequencies. This range of frequencies shows more pronounced noise attenuation, with SPL values decreasing steadily, indicating that the Diamond structure starts to reduce mid-frequency noise more effectively. Receivers such as R4 (green) and R5 (yellow) show significant improvements in SPL reduction, confirming that the Diamond structure offers better performance in this frequency range. At higher frequencies (5000 Hz and above), the SPL values decrease more substantially, with

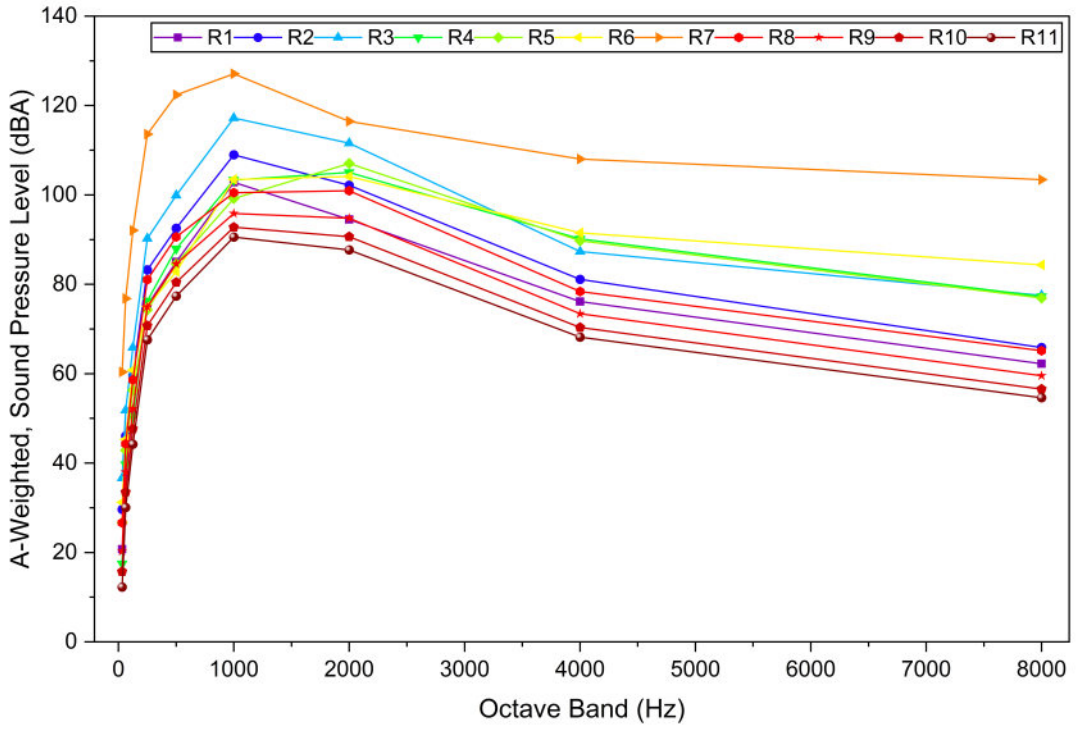

FIGURE 4.9: A-Weighted Sound Pressure Level (SPL) versus frequency for the Diamond TPMS Structure

all receivers showing lower SPL levels (around 40 dBA or below). This suggests that the Diamond structure is effective at attenuating higher-frequency noise, which is typically more challenging to suppress. The SPL for most receivers stabilizes below 50 dBA, reflecting the Diamond structure's capability to reduce high-frequency noise effectively. The graph shows significant variability in SPL across the 11 receivers, particularly at the low and mid-frequency ranges. For example, R1 (purple) and R11 (red) exhibit higher SPL values across most frequencies, while R4 (green), R5 (yellow), and R9 (orange) show lower SPL values, indicating that the noise attenuation is spatially dependent. This variability suggests that the performance of the Diamond structure may be influenced by the location of the receiver within the silencer, likely due to the complex flow and acoustic interaction inside the porous medium. Overall, the Diamond structure provides effective noise reduction at mid and high frequencies but demonstrates less efficiency at low frequencies, which may require further optimization for low-frequency noise control in practical applications.

4.2.6 A-Weighted Sound Pressure Level vs Frequency for Gyroid Structure

Figure 4.10 presents the A-weighted Sound Pressure Level (SPL) as a function of frequency for the Gyroid TPMS structure, The SPL values are shown in decibels (dBA), with frequency ranging from 0 Hz to 8000 Hz. At low frequencies (0-1000

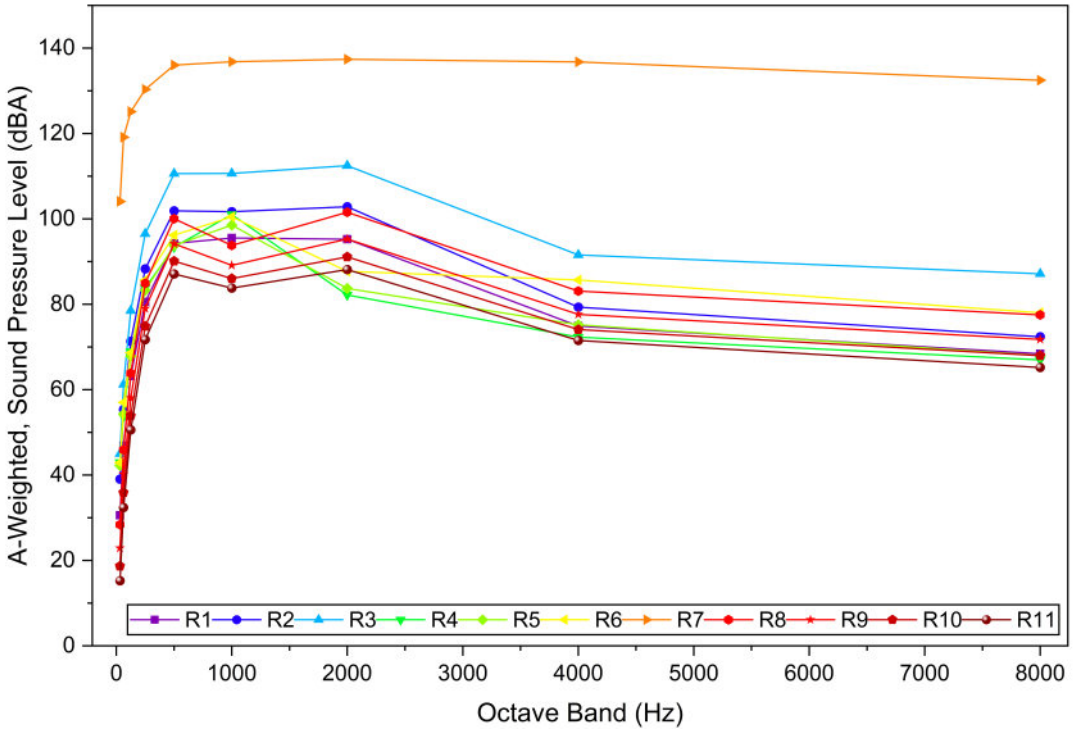

FIGURE 4.10: A-Weighted Sound Pressure Level (SPL) versus frequency for the Gyroid TPMS Structure

Hz), the SPL values are relatively high, particularly for R1 (purple) and R2 (blue), where the SPL remains above 80 dBA. This suggests that the Gyroid structure is less effective at attenuating low-frequency noise, as high SPL values indicate weak attenuation. The SPL remains consistent across most of the low-frequency range, with R11 (red) showing the lowest SPL, but still higher than mid and high-frequency regions. As the frequency increases to the mid-range (1000 Hz to 4000 Hz), there is a noticeable decrease in SPL for most receivers. For example, R5 (yellow) and R7 (orange) show a significant drop in SPL, indicating that the Gyroid structure begins to provide more effective attenuation in this frequency band. The SPL values stabilize around 70-80 dBA in the mid-frequency range for the majority of receivers, suggesting better noise reduction. At higher frequencies (above 4000 Hz),

the SPL continues to decrease for all receivers, with values generally falling below 70 dBA, reflecting the Gyroid structure's capability to attenuate high-frequency noise effectively. However, the SPL reduction is not as sharp as seen in the mid-frequency range, and the SPL values for R1 and R11 are still slightly higher than for other receivers, particularly above 6000 Hz. A notable feature of the graph is the variability in SPL across the 11 receivers. For instance, R1 (purple) consistently shows higher SPL values across most frequencies, while R11 (red) exhibits lower SPL, particularly in the higher-frequency range. This suggests that the position of the receiver within the silencer affects its exposure to sound pressure, likely influenced by flow characteristics and turbulence within the porous geometry. Such variations indicate that while the Gyroid structure provides general noise reduction, its performance is spatially dependent. Overall, the Gyroid structure demonstrates significant attenuation of mid- and high-frequency noise, though it shows limited effectiveness in reducing low-frequency sound. The variability in SPL across receivers suggests that the acoustic performance is influenced by the receiver's position within the silencer, likely due to localized flow disturbances.

4.2.7 A-Weighted Sound Pressure Level vs Frequency for Primitive Structure

Figure 4.11 presents the A-weighted Sound Pressure Level (SPL) as a function of frequency for the Primitive TPMS structure, The SPL values are represented in decibels (dBA), with frequency ranging from 0 Hz to 8000 Hz. At low frequencies (0-1000 Hz), the SPL values are relatively high for most receivers. R1 (purple) and R11 (red) exhibit the highest SPL values, indicating that the Primitive structure is less effective at attenuating low-frequency noise. SPL values in this range are generally above 70 dBA, with certain peaks approaching 90 dBA, suggesting limited attenuation in the low-frequency range. As the frequency increases (1000 Hz to 4000 Hz), there is a marked reduction in SPL. The SPL values begin to stabilize around 60-70 dBA, particularly for receivers such as R2 (blue), R4 (green), and R6 (yellow). The SPL decrease suggests that the Primitive structure performs more effectively in the mid-frequency range, with some variation in performance across

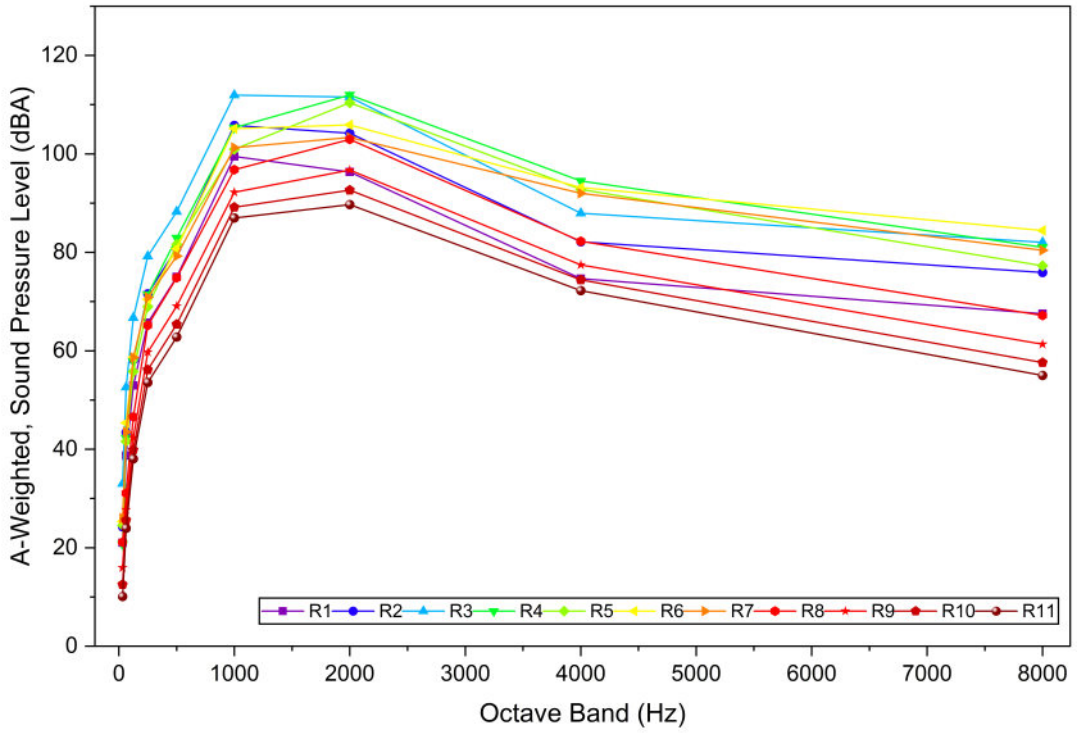

FIGURE 4.11: A-weighted Sound Pressure Level (SPL) vs. frequency for the Primitive TPMS structure

receivers. This indicates that the structure is more effective at damping noise in the mid-range frequencies, but the performance still varies depending on the receiver's location within the silencer. At higher frequencies (5000 Hz and above), the SPL values decrease further for all receivers, generally reaching levels below 60 dBA. The SPL drops noticeably across the frequency spectrum, with R1 and R11 still showing slightly higher SPL values compared to other receivers. This indicates that the Primitive structure is effective in attenuating high-frequency noise, although there remains some variability in SPL attenuation at the higher frequency end. There is clear variability in SPL across the 11 receivers. Receivers such as R1 (purple) and R11 (red) show the highest SPL values across the entire frequency range, while R5 (green) and R9 (orange) exhibit lower SPL levels, particularly in the mid- to high-frequency ranges. This variability suggests that the acoustic performance of the Primitive structure is sensitive to receiver positioning within the silencer, likely due to differences in the local flow and acoustic pressure fields generated within the porous medium. Overall, the Primitive structure shows effective high-frequency noise attenuation but has limited performance in reducing low-frequency noise. The

mid-frequency range sees moderate attenuation, with significant variability between receivers. This suggests that while the Primitive structure provides strong noise reduction at higher frequencies, its overall performance may need to be improved for more consistent low-frequency and mid-frequency noise suppression.

4.2.8 Frequency Versus A-Weighted SPL Analysis at Vertical Receiver Planes

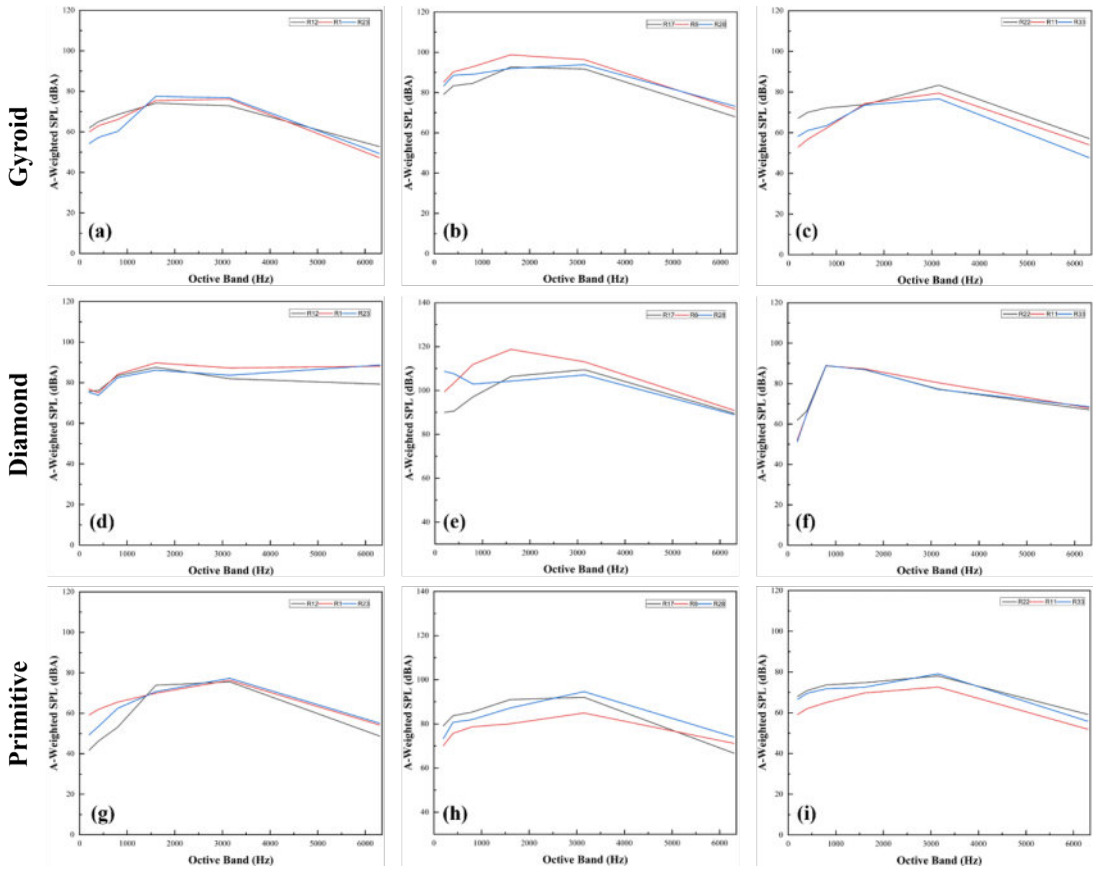

FIGURE 4.12: Frequency versus A-Weighted Analysis at Vertical Receiver Planes for Gyroid (a-c), Diamond (d-f) and Primitive (g-i) structures

Figure 4.12 illustrates the variation of A-weighted Sound Pressure Level (SPL) with octave band frequency for the three TPMS-based silencer structures at different receiver planes located along the axial direction of the silencer. The acoustic responses were evaluated at the inlet plane (R12–R1–R23), center plane (R17–R6–R28), and outlet plane (R22–R11–R33) to investigate the frequency-dependent attenuation characteristics throughout the porous structure.

The graphs show that the A-weighted SPL generally increases from the low-frequency region toward the mid-frequency range, reaches a peak value between approximately 1500 Hz and 3150 Hz, and then gradually decreases at higher octave bands. At the inlet plane, moderate SPL values are observed due to the initial interaction between the airflow and the porous geometry. In the center plane, the SPL values become comparatively higher, indicating increased turbulence intensity, vortex interaction, and acoustic activity within the internal region of the TPMS structure. At the outlet plane, the SPL values decrease and exhibit smoother attenuation behavior, demonstrating the reduction of acoustic energy as the sound waves propagate through the porous silencer. The results further indicate that each TPMS geometry exhibits a distinct acoustic response due to differences in pore distribution and internal flow pathways. Some configurations show relatively higher peak SPL values in the mid-frequency range, while others demonstrate more gradual attenuation across the octave bands.

4.2.9 Final Discussion

This study presented a detailed numerical investigation of porous pneumatic silencers incorporating Gyroid, Diamond, and Primitive TPMS structures, using Ffowcs Williams–Hawkings (FW-H) acoustic model for sound pressure level prediction. The results, derived from 11 receivers placed within the silencer, provide valuable insights into the flow behavior, noise attenuation capabilities, and the spatial dependency of acoustic performance. The discussion is divided into two primary parts: flow behaviour and acoustic performance.

The flow behavior within each silencer was evaluated based on pressure, velocity, temperature, and streamline contours, as described in the previous sections. The Gyroid structure consistently demonstrated the lowest pressure drop, followed by the Diamond and Primitive structures, indicating its superior pneumatic efficiency. The Diamond structure showed a moderate pressure loss, while the Primitive structure exhibited the highest resistance to airflow, primarily due to its complex and less interconnected pore geometry. This finding aligns with previous studies on

TPMS-based porous materials, which suggested that more uniform and continuous geometries, such as the Gyroid, allow for smoother airflow with reduced resistance [72]. In terms of velocity distribution, the Gyroid structure facilitated the most uniform flow, with minimal turbulence and velocity fluctuations. This is likely due to its continuously curved surfaces, which promote smoother transitions of airflow. In contrast, the Primitive structure exhibited significant flow disruptions, with localized high-velocity regions and turbulent zones, resulting in increased energy dissipation and pressure loss.

The acoustic performance of the three TPMS structures was evaluated using the SPL vs. frequency and A-weighted SPL vs. frequency graphs, with data collected from 11 receivers placed within the silencer. The SPL results showed that all three structures provided effective noise attenuation at high frequencies, with the Gyroid structure exhibiting the most consistent noise reduction across the entire frequency spectrum. However, the Primitive structure was found to be less effective at low frequencies, with higher SPL values observed at these frequencies. This is consistent with previous work on porous materials, which highlighted the challenges of attenuating low-frequency noise in porous structures, especially those with complex pore geometries like the Primitive structure [73].

In terms of A-weighted SPL, the Gyroid structure demonstrated strong attenuation at mid and high frequencies, with a noticeable drop in SPL beyond 4000 Hz. The Diamond structure showed balanced performance across both mid and high frequencies but exhibited less effectiveness at low frequencies. The Primitive structure, while providing significant high-frequency noise reduction, struggled to attenuate low-frequency noise effectively. This finding suggests that although the Primitive structure excels in certain frequency bands, its overall acoustic performance could benefit from optimization, such as modifying its pore network to better manage low-frequency sound. While the study provides valuable insights into the flow and acoustic performance of TPMS-based porous silencers, some limitations remain. The simulations were conducted under idealized boundary conditions, and the effects of manufacturing imperfections and material properties were not included. Future studies should investigate the influence of these factors on the

performance of TPMS-based silencers. Additionally, incorporating non-Newtonian fluid models for more complex flow behaviour could enhance the accuracy of the results, particularly for applications where fluid properties deviate from the ideal.

4.3 Comparative Analysis of Acoustic Performance with Existing TPMS-Based Studies

The acoustic performance of the TPMS-based silencer investigated in this thesis is compared with the TPMS honeycomb sound-absorbing structures reported by Sysoev et al [74]. While both studies employ triply periodic minimal surface (TPMS) geometries to enhance acoustic attenuation, the underlying mechanisms, modeling approaches, and intended applications differ substantially, leading to distinct acoustic behaviors. In the work of Sysoev et al., TPMS structures (primitive, diamond, FRD, and gyroid) were primarily designed as passive sound-absorbing materials. Their acoustic performance was evaluated using the Johnson-Champoux-Allard-Lafarge-Pride (JCALP) equivalent fluid model, which characterizes visco thermal dissipation within rigid-frame porous media. The reported results demonstrated that, by controlling porosity, unit cell size, and sample thickness, the average sound absorption coefficient could be tuned within the range of approximately 0.2 to 0.8 over mid-to-high frequency bands (500–6400 Hz). The FRD topology exhibited the highest absorption due to its low permeability and high tortuosity, while gyroid and diamond structures showed comparable broadband absorption characteristics [74].

In contrast, the present thesis focuses on a TPMS-based reactive–dissipative silencer, where the TPMS geometry is integrated directly into an internal flow domain. Rather than relying solely on equivalent fluid assumptions, the acoustic performance is evaluated using a computational aeroacoustics framework based on the Ffowcs Williams–Hawkings (FW-H) acoustic analogy, coupled with unsteady flow simulations. This approach captures both flow-induced noise generation and its subsequent attenuation, which is not addressed in the JCALP-based porous absorber

model. Consequently, the silencer performance in this study is assessed in terms of sound pressure level (SPL) reduction at discrete receiver locations rather than only normal-incidence absorption coefficients. Another key distinction lies in the operating frequency range and physical mechanism. The TPMS absorbers reported by Sysoev et al. primarily target mid- and high-frequency sound absorption governed by viscous and thermal losses within stationary air-filled pores. In comparison, the TPMS silencer investigated in this thesis demonstrates effective attenuation in lower and mid-frequency ranges, where wave interference, geometric confinement, and interaction between the turbulent flow and TPMS surfaces play a dominant role. This makes the proposed silencer more suitable for applications such as exhaust or duct noise control, where flow-acoustic coupling is critical. Despite these differences, a qualitative agreement is observed between both studies regarding the influence of TPMS geometry on acoustic behavior. In particular, geometries with higher tortuosity and more complex interconnected pathways such as diamond or gyroid based structures consistently exhibit superior acoustic attenuation. This consistency reinforces the conclusion that TPMS architectures provide a robust and tunable design framework for advanced acoustic devices, whether employed as porous absorbers or flow integrated silencers. Overall, compared to existing TPMS acoustic materials reported in the literature, the present work extends the application of TPMS structures from passive sound absorption to active flow-acoustic noise mitigation, thereby broadening their practical relevance in engineering noise control systems.

Chapter 5

Conclusion and Future Recommendations

5.1 Conclusion

This thesis presented a numerical investigation of the acoustic performance of porous pneumatic silencers based on Gyroid, Diamond, and Primitive Triply Periodic Minimal Surface (TPMS) structures. The study employed Computational Fluid Dynamics (CFD) coupled with the Ffowcs Williams–Hawkings (FW-H) acoustic model to evaluate the influence of TPMS geometry on pressure drop, velocity distribution, turbulence generation, temperature distribution, and Sound Pressure Level (SPL) attenuation over a frequency range extending up to 100 kHz.

The numerical results demonstrated that the TPMS geometry significantly affects both the aerodynamic and acoustic characteristics of the silencer. Among all investigated configurations, the Gyroid structure exhibited the best overall aerodynamic performance, producing approximately 15–25% lower pressure drop compared to the Primitive structure due to its continuous and smoothly connected pore network. In contrast, the Primitive structure generated the highest flow resistance and turbulence intensity because of its relatively complex internal pathways and abrupt flow constrictions. The Diamond structure showed intermediate behavior,

providing a balanced trade-off between flow resistance and acoustic attenuation. Velocity contour analysis indicated that the airflow velocity decreased substantially within the porous structures due to viscous effects and turbulence dissipation. The Gyroid geometry maintained comparatively smoother flow distribution and reduced recirculation regions, while the Primitive structure generated stronger localized turbulence and flow separation. Temperature contour analysis further revealed that thermal gradients became more pronounced in the intermediate flow regions (0.01–0.03 m), where turbulence intensity and fluid–surface interaction were strongest.

The acoustic analysis showed that all TPMS structures exhibited frequency-dependent SPL attenuation behavior. The highest SPL values were generally observed in the mid-frequency range between approximately 20 kHz, after which the SPL gradually decreased toward higher frequencies. The Gyroid structure demonstrated effective broadband noise attenuation with SPL reductions of approximately 10–15 dB in higher frequency regions. The Primitive structure showed relatively stronger attenuation at high frequencies but exhibited larger SPL fluctuations due to increased turbulence generation. The Diamond structure provided moderate acoustic attenuation across a wider frequency range.

The A-weighted SPL analysis further confirmed that the acoustic response varied with receiver location and octave band frequency. Peak A-weighted SPL values were primarily observed between 1500 Hz, with maximum values approaching approximately 90–120 dBA depending on the TPMS geometry and receiver plane. The center receiver plane (R17–R6–R28) generally exhibited higher SPL values due to stronger internal turbulence interaction and vortex formation within the porous medium. In comparison, the outlet receiver plane showed comparatively lower SPL levels, indicating progressive attenuation of acoustic energy along the silencer length.

Additionally, the expanded receiver arrangement consisting of 33 receivers enabled a more detailed spatial evaluation of sound propagation throughout the silencer. The results confirmed that acoustic behavior is highly position-dependent, with

receivers located near high turbulence regions recording comparatively higher SPL values.

The Gyroid TPMS structure proved the most effective porous silencer, offering low pressure drop, smooth flow, reduced turbulence, and superior broadband noise attenuation. The Diamond structure balanced aerodynamic and acoustic performance, while the Primitive structure excelled in high-frequency attenuation but with higher aerodynamic resistance. Overall, TPMS-based porous silencers hold strong potential for advanced pneumatic noise reduction, combining aerodynamic efficiency with acoustic performance.

5.2 Future Recommendations

Although this study provides a comprehensive numerical analysis of TPMS-based pneumatic silencers, several opportunities exist for further investigation to enhance understanding and broaden applicability. The following recommendations are proposed for future work.

5.2.1 Optimization of Low-Frequency Attenuation

The Primitive structure showed limited low-frequency noise attenuation. Future research should optimize geometric features—pore size, shape, and connectivity to enhance low-frequency performance. Investigating hybrid TPMS designs or multi-material configurations could improve noise attenuation across both low and high frequencies while maintaining pneumatic efficiency.

5.2.2 Experimental Validation

The present findings are based solely on numerical simulations. Experimental validation through the fabrication of Gyroid, Diamond, and Primitive TPMS structures using additive manufacturing techniques and subsequent testing in

controlled acoustic environments would strengthen the reliability of the results and provide practical performance benchmarks.

5.2.3 Incorporation of Non-Ideal Boundary Conditions

Future simulations should consider non-ideal boundary conditions, including variable inlet velocities, non-uniform flow distributions, and thermal effects. Incorporating these factors would yield a more realistic representation of silencer behavior under practical operating conditions.

5.2.4 Influence of Structural Imperfections

Manufacturing processes, particularly additive manufacturing, may introduce geometric imperfections and material inconsistencies. Investigating the influence of such imperfections on pneumatic and acoustic performance would improve the robustness and real-world applicability of TPMS-based silencer designs.

5.2.5 Exploration of Hybrid Silencer Designs

Further research could examine hybrid silencer concepts that integrate TPMS structures with conventional sound-absorbing materials or alternative noise-damping mechanisms. Such designs may enhance low-frequency noise reduction while retaining the advantages of TPMS geometries in high-frequency attenuation.

5.2.6 Study of Porosity Effects

Additional studies should investigate the effects of varying porosity and pore size within TPMS structures. Understanding how these parameters influence both flow dynamics and acoustic attenuation can facilitate the optimization of TPMS-based silencers for specific applications, including industrial exhaust systems, automotive mufflers, and HVAC installations.

Bibliography

[1] R. Dindorf, P. Wos, and K. Pawelec, "Automatic device for indirect measurement of leakage flow rate in compressed air pipeline," in *IOP Conference Series: Materials Science and Engineering*, vol. 233, p. 012030, IOP Publishing, 2017.

[2] R. Dindorf, J. Takosoglu, and P. Woś, *Development of pneumatic control systems (Rozwój pneumatycznych systemów sterowania)*. No. M89, Wydawnictwo Politechniki Świetokrzyskiej, 2017.

[3] J. Li and S. Zhao, "Optimization of valve opening process for the suppression of impulse exhaust noise," *Journal of Sound and Vibration*, vol. 389, pp. 24–40, 2017.

[4] S. Raghunathan, H. Kim, and T. Setoguchi, "Impulse noise and its control," *Progress in Aerospace Sciences*, vol. 34, no. 1-2, pp. 1–44, 1998.

[5] J. Li, S. Zhao, and K. Ishihara, "Study on acoustical properties of sintered bronze porous material for transient exhaust noise of pneumatic system," *Journal of Sound and Vibration*, vol. 332, no. 11, pp. 2721–2734, 2013.

[6] M. J. Lighthill, "On sound generated aerodynamically i. general theory," *Proceedings of the Royal Society of London. Series A. Mathematical and Physical Sciences*, vol. 211, no. 1107, pp. 564–587, 1952.

[7] M. J. Lighthill, "On sound generated aerodynamically ii. turbulence as a source of sound," *Proceedings of the Royal Society of London. Series A. Mathematical and Physical Sciences*, vol. 222, no. 1148, pp. 1–32, 1954.

[8] H. Shi and S. Zhao, "Prediction of radiation characteristic of intermittent exhaust noise generated via pneumatic value," *Noise Control Engineering Journal*, vol. 57, no. 3, pp. 157–168, 2009.

[9] Y. V. Ivanov, "Reducing the aerodynamic noise of pneumatic nozzles in the pneumatic mechanisms of forges and presses," *Metallurgist*, vol. 55, no. 3, p. 139, 2011.

[10] S. Zhao, J. Wang, J. Wang, and Y. He, "Expansion-chamber muffler for impulse noise of pneumatic frictional clutch and brake in mechanical presses," *Applied Acoustics*, vol. 67, no. 6, pp. 580–594, 2006.

[11] E. Union, "Directive 2003/10/ec of the european parliament and of the council on the minimum health and safety requirements regarding the exposure of workers to the risks arising from physical agents (noise)," *Official Journal of the European Union*, vol. 42, pp. 38–44, 2003.

[12] B. Roberts, N. S. Seixas, B. Mukherjee, and R. L. Neitzel, "Evaluating the risk of noise-induced hearing loss using different noise measurement criteria," *Annals of Work Exposures and Health*, vol. 62, no. 3, pp. 295–306, 2018.

[13] D. Czopek, T. Korbiel, B. Kukulski, P. Małecki, P. Pawlik, B. Stepień, T. Wszołek, and W. Wszołek, "New methods of signal processing in the selected vibroacoustics problems," *Department of Process Automation of the AGH in Krakow*, 2016.

[14] M. Kozupa and J. Wiciak, "Comparison of passive and active methods for minimization of sound radiation by vibrating clamped plate," *Acta Physica Polonica A*, vol. 119, no. 6A, pp. 1013–1017, 2011.

[15] M. S. KOZIEŃ and J. Wiciak, "Reduction of structural noise inside crane cage by piezoelectric actuators-fem simulation," *Archives of Acoustics*, vol. 33, no. 4, pp. 643–652, 2008.

[16] J. X. Li, S. D. Zhao, K. Ishihara, and H. S. Shi, "Numerical and experimental studies on aerodynamic characteristics of pneumatic exhaust with perforated panel muffler," *Advanced Materials Research*, vol. 291, pp. 2125–2129, 2011.

[17] J. Daggerhart and E. Berger, "An evaluation of mufflers to reduce punch press air exhaust noise," *Noise Control Engineering*, vol. 4, no. 3, pp. 120–123, 1975.

[18] M. E. Petrick, L. H. Royster, J. D. Royster, and P. Reist, "Comparison of daily noise exposures in one workplace based on noise criteria recommended by acgih and osha," *American Industrial Hygiene Association Journal*, vol. 57, no. 10, pp. 924–928, 1996.

[19] Á. Katalin, "Studying noise measurement and analysis," *Procedia Manufacturing*, vol. 22, pp. 533–538, 2018.

[20] E. Berger and A. I. H. Association, *The Noise Manual*. American Industrial Hygiene Association, 2000.

[21] SoftDB, "Industrial noise and soundproofing solutions," 2025. Accessed: 2025-12-23.

[22] Bureau of Labor Statistics, U.S. Department of Labor, "Private industry workers suffered 14,500 hearing loss cases in 2019," June 30 2021. Accessed: February 04, 2026.

[23] J. Zhou, J. Huang, X. Ma, A. Lee, K. Kosuge, and Y.-H. Liu, "Design, modeling, and control of soft syringes enabling two pumping modes for pneumatic robot applications," *IEEE/ASME Transactions on Mechatronics*, vol. 29, no. 2, pp. 889–901, 2024.

[24] Trimantec, "Pneumatic components industrial guide," 2021. Accessed: 2025-12-23.

[25] G. Singh, T. Deng, M. S. Bradley, and R. Ellis, "Advanced assessment of biomass materials degradation in pneumatic conveying systems: challenges and applications," *Applied Sciences*, vol. 13, no. 3, p. 1960, 2023.

[26] P. Dini, L. Diana, A. Elhanashi, and S. Saponara, "Overview of ai-models and tools in embedded iiot applications," *Electronics*, vol. 13, no. 12, p. 2322, 2024.

[27] D. H. Robison and P. J. Beaty, "Compressor types, classifications, and applications.," 1992.

[28] Chemical Engineering World, "Types of compressors," n.d. Accessed: 2025-12-23.

[29] E. Pavlyuchenko, "Analysis of the primary means for increasing the efficiency of positive displacement compressors," *Chemical and Petroleum Engineering*, vol. 58, no. 3, pp. 309–314, 2022.

[30] F. Forouharmajd, P. Nassiri, and M. R. Monazzam, "Noise pollution of air compressor and its noise reduction procedures by using an enclosure," *International Journal of Environmental Health Engineering*, vol. 1, no. 1, p. 20, 2012.

[31] D. Gryboś, J. S. Leszczyński, D. Czopek, and J. Wiciak, "Exhaust noise reduction by application of expanded collecting system in pneumatic tools and machines," *Energies*, vol. 14, no. 6, p. 1592, 2021.

[32] Hi-Fi Filter, "Reduce noise in industry with pneumatic silencers," 2025. Accessed: 2025-12-23.

[33] M.-C. Chiu and Y.-C. Chang, "Optimization of pneumatic mufflers hybridized with metal sintered bronze porous material, expansion cone, and extended tube," *Noise & Vibration Worldwide*, vol. 53, no. 11, pp. 532–549, 2022.

[34] M. H. Ahn, J. Kim, S. R. Lee, U. D. Lee, S. Kim, D. Shin, H. Lee, and J. Ryu, "Experimental analysis of biomimetic silencer to reduce exhaust noise in pneumatic devices," *Applied Acoustics*, vol. 214, p. 109681, 2023.

[35] D. Gryboś, J. S. Leszczyński, D. Czopek, and J. Wiciak, "Exhaust noise reduction by application of expanded collecting system in pneumatic tools and machines," *Energies*, vol. 14, no. 6, p. 1592, 2021.

[36] M.-C. Chiu and Y.-C. Chang, "Optimization of pneumatic mufflers hybridized with metal sintered bronze porous material, expansion cone, and extended tube," *Noise & Vibration Worldwide*, vol. 53, no. 11, pp. 532–549, 2022.

[37] L. Zhou, J. Miller, J. Vezza, M. Mayster, M. Raffay, Q. Justice, Z. Al Tamimi, G. Hansotte, L. D. Sunkara, and J. Bernat, "Additive manufacturing: a comprehensive review," *Sensors*, vol. 24, no. 9, p. 2668, 2024.

[38] B. Pavan Kalyan and L. Kumar, "3d printing: applications in tissue engineering, medical devices, and drug delivery," *Aaps Pharmscitech*, vol. 23, no. 4, p. 92, 2022.

[39] L. Chen, N. P. H. Ng, J. Jung, and S. K. Moon, "Additive manufacturing for automotive industry: status, challenges and future perspectives," in *2023 IEEE International Conference on Industrial Engineering and Engineering Management (IEEM)*, pp. 1431–1436, IEEE, 2023.

[40] A. Vafadar, F. Guzzomi, A. Rassau, and K. Hayward, "Advances in metal additive manufacturing: a review of common processes, industrial applications, and current challenges," *Applied Sciences*, vol. 11, no. 3, p. 1213, 2021.

[41] F. Campana, "Bird's eye view on lattice structures: Design issues and applications for best practices in mechanical design," *Metals*, 2024.

[42] B. Sokollu, "Mechanical properties comparison of strut-based and tpms lattice structures produced by ebm," Master's thesis, Middle East Technical University (Turkey), 2022.

[43] X. Zhang, Z. Qu, and H. Wang, "Engineering acoustic metamaterials for sound absorption: from uniform to gradient structures," *Iscience*, vol. 23, no. 5, 2020.

[44] M. G. Gado, O. Al-Ketan, M. Aziz, R. A. Al-Rub, and S. Ookawara, "Triply periodic minimal surface structures: Design, fabrication, 3d printing techniques, state-of-the-art studies, and prospective thermal applications for efficient energy utilization," *Energy Technology*, vol. 12, no. 5, p. 2301287, 2024.

[45] Q. Lu, X. Li, X. Zhang, M. Lu, and Y. Chen, "Perspective: acoustic metamaterials in future engineering," *Engineering*, vol. 17, pp. 22–30, 2022.

[46] A. Ali, A. Mitra, and B. Aïssa, "Metamaterials and metasurfaces: A review from the perspectives of materials, mechanisms and advanced metadevices," *Nanomaterials*, vol. 12, no. 6, p. 1027, 2022.

[47] O. Al-Ketan and R. K. Abu Al-Rub, "Multifunctional mechanical metamaterials based on triply periodic minimal surface lattices," *Advanced Engineering Materials*, vol. 21, no. 10, p. 1900524, 2019.

[48] N. K. Sivakumar, S. Palaniyappan, S. Basavarajappa, M. I. Hashem, M. Bodaghi, and V. Sekar, "Study on the impact of material extrusion factors on the compressive characteristics of honeycomb lattice-structured onyx™ composites," *Materials Today Communications*, vol. 37, p. 107317, 2023.

[49] V. Sekar, W. J. Cantwell, K. Liao, B. Berton, P.-M. Jacquart, and R. K. Abu Al-Rub, "Additively manufactured metamaterials for acoustic absorption: a review," *Virtual and Physical Prototyping*, vol. 19, no. 1, p. e2435562, 2024.

[50] Y. Tao, M. Ren, H. Zhang, and T. Peijs, "Recent progress in acoustic materials and noise control strategies–a review," *Applied Materials Today*, vol. 24, p. 101141, 2021.

[51] H. M. A. Ali, M. Abdi, and Y. Sun, "Insight into the mechanical properties of 3d printed strut-based lattice structures," *Progress in Additive Manufacturing*, vol. 8, no. 5, pp. 919–931, 2023.

[52] M. Fantini, M. Curto, and F. De Crescenzio, "A method to design biomimetic scaffolds for bone tissue engineering based on voronoi lattices," *Virtual and Physical Prototyping*, vol. 11, no. 2, pp. 77–90, 2016.

[53] B. Wojciechowski, Y. Xue, A. Rabbani, J. S. Bolton, and B. Sharma, "Additively manufactured spinodoid sound absorbers," *Additive Manufacturing*, vol. 71, p. 103608, 2023.

[54] Q. Chen, N. Pugno, K. Zhao, and Z. Li, "Mechanical properties of a hollow-cylindrical-joint honeycomb," *Composite Structures*, vol. 109, pp. 68–74, 2014.

[55] V. Sekar, S. Palaniyappan, S. Y. E. Noum, A. Putra, S. Sivanesan, and D. D. C. V. Sheng, "Acoustic absorbers made of wood fiber composites developed by compression molding and additive manufacturing.," 2023.

[56] D. D. Chin Vui Sheng, M. N. B. Yahya, and N. B. Che Din, "Sound absorption of microperforated panel made from coconut fiber and polylactic acid composite," *Journal of Natural Fibers*, vol. 19, no. 7, pp. 2719–2729, 2022.

[57] D. D. V. S. Chin, M. N. B. Yahya, N. B. C. Din, and P. Ong, "Acoustic properties of biodegradable composite micro-perforated panel (bc-mpp) made from kenaf fibre and polylactic acid (pla)," *Applied Acoustics*, vol. 138, pp. 179–187, 2018.

[58] E. Jayamani, S. Hamdan, P. Ezhumalai, and K. H. Soon, "Acoustic and thermal properties of polymer composites reinforced with lignocellulosic fibers," *Applied Mechanics and Materials*, vol. 624, pp. 25–29, 2014.

[59] Z. Daeipour, V. Safdari, and A. Nurbakhsh, "Evaluation of the acoustic properties of wood-plastic-chalk composites," *Engineering, Technology & Applied Science Research*, vol. 7, no. 2, pp. 1540–1545, 2017.

[60] "Iso/astm 52900:2021 — additive manufacturing — general principles — fundamentals and vocabulary," 2021. Accessed: 2025-12-23.

[61] L. Ben Said, B. Ayadi, S. Alharbi, and F. Dammak, "Recent advances in additive manufacturing: a review of current developments and future directions," *Machines*, vol. 13, no. 9, p. 813, 2025.

[62] W. Johnston and B. Sharma, "Additive manufacturing of fibrous sound absorbers," *Additive Manufacturing*, vol. 41, p. 101984, 2021.

[63] O. Al-Ketan and R. K. Abu Al-Rub, "Multifunctional mechanical metamaterials based on triply periodic minimal surface lattices," *Advanced Engineering Materials*, vol. 21, no. 10, p. 1900524, 2019.

[64] A. Skoratko and J. Katzer, "Harnessing 3d printing of plastics in construction—opportunities and limitations," *Materials*, vol. 14, no. 16, p. 4547, 2021.

[65] J. Guan and Q. Wang, "Laser powder bed fusion of dissimilar metal materials: a review," *Materials*, vol. 16, no. 7, p. 2757, 2023.

[66] A. Nazir, O. Gokcekaya, K. M. M. Billah, O. Ertugrul, J. Jiang, J. Sun, and S. Hussain, "Multi-material additive manufacturing: A systematic review of design, properties, applications, challenges, and 3d printing of materials and cellular metamaterials," *Materials & Design*, vol. 226, p. 111661, 2023.

[67] Exxentis, "Pneumatic silencer, compressed air silencer," 2025.

[68] K. K. Sirivuri, V. Sekar, W. J. Cantwell, K. Liao, B. Berton, N. Ravaud, P.-M. Jacquart, and R. K. A. Al-Rub, "Computational study of sound absorption in tpms lattice materials using a thermoviscous model," *Journal of Building Engineering*, p. 113658, 2025.

[69] D. Wilcox, "Turbulence modeling-an overview," in *39th aerospace sciences meeting and exhibit*, p. 724, 2001.

[70] G. Kyaw Oo D'Amore, M. Morgut, M. Biot, and F. Mauro, "Numerical study on the influence of porous baffle interface and mesh typology on the silencer flow analysis," *Marine Systems & Ocean Technology*, vol. 17, no. 2, pp. 71–79, 2022.

[71] L. Giorleo, S. Basu, and E. Piana, "Acoustic performances of triply periodic minimal surfaces fabricated by additive manufacturing: Effects of cell geometry, aspect ratio, and wall thickness," *Additive Manufacturing*, vol. 108, p. 104835, 2025.

[72] M. N. Shahid, M. M. Khan, M. U. Shahid, and S. Rasheed, "Fluidic properties of diamond and splitp structures with varying porosity levels in tissue engineering applications: A computational fluid dynamics analysis," *Engineering Proceedings*, vol. 75, no. 1, p. 39, 2024.

[73] M. Vašina, J. Měsíček, M. Mánek, Q.-P. Ma, J. Hajnyš, and J. Petr, "Investigation of factors affecting the sound absorption behaviour of 3d printed hexagonal prism lattice polyamide structures," *Scientific Reports*, vol. 14, no. 1, p. 30852, 2024.

[74] E. Sysoev, M. Sychov, L. Shafigullin, and S. Dyachenko, "Design of sound absorbing honeycomb materials with a geometry of triply periodic minimal surfaces (tpms)," *Acoustical Physics*, vol. 70, no. 5, pp. 887–898, 2024.